UNIVERSITÉ DU QUÉBEC EN OUTAOUAIS

Characterization and Stochastic Modeling of MIMO-WBAN Channels in an Underground Mine

par

Moulay El Hassan El Azhari

Thèse présentée au

Département d'informatique et d'ingénierie

pour l'obtention du grade de

Philosophiae Doctor (Ph.D.)

en Sciences et technologies de l'information

Membres du jury :	*Président*	*Prof. Ahmed Lakhssassi, UQO*
	Examinateur externe	*Dr. Liang Zhang, CRC - Ottawa*
	Examinateur interne	*Prof. Tinko Eftimov, UQO*
	Directeur de thèse	*Prof. Larbi Talbi, UQO*
	Codirecteur	*Prof. Nedil Mourad, UQAT*

This thesis is dedicated to

My Mother

My Wife

My lovely Daughter

And

My dear Brothers

Abstract

Recently, the rising accident rates in the underground mining field pushed toward exploring new communication schemes destined to the safety of the miners. Indeed, the WBAN technology has emerged as a promising communication scheme dedicated to the miners safety. The first contribution of this PhD Thesis consists in characterizing the WBAN channel under different channel conditions. Valuable channel measurements data are processed and reported in the open literature.

The second contribution of this thesis consists in statistical and empirical modeling of the WBAN channels within an underground mine. This step allows predicting the propagation characteristics of a certain underground WBAN channel based on the entered parameters (which could be determined empirically from measurements or estimated from published results in similar environments). These stochastic and empirical methods have proven to be suitable for the studied environment with encouraging results approaching the measurements. This study opens the door for wider investigation of novel modeling methods, consisting in empirically modeling the multipath amplitudes as an exponentially decaying PDP, while arrival times are stochastically modeled by comparing the measurements to different random distributions from the literature. Hence, the impulse response model is generated, which completely characterizes the WBAN channel.

The significance of this PhD thesis is that it would provide a tool for communication system designers to understand the underground WBAN propagation mechanism and take economic design decisions (without the need of extensive underground measurements campaigns).

Acknowledgements

First and the foremost, I praise Almighty Allah, the Compassionate and Merciful, and thank Him for bestowing His blessings upon me and enabling me to complete this work. He blessed me with his bounties. May the peace and blessing be upon the prophet Muhammad, and his noble family.

I would like to express my high gratitude to my advisors Larbi Talbi and Mourad Nedil for their precious support and guidance during this work. It was delighted to work closely with them and thereby benefit from their knowledge and expertise.

I would like to thank my mother, my wife, and my brothers for their continuous support during my educational endeavor. Without their support, this dissertation could not have been achieved.

My friends (Mejdi Laribi, Abdennour Benterki, Hamid Ait Taleb and Seddiki Mohamed Lamine) have always been supporting, helpful and kind. I am especially grateful to Mejdi and Abdennour for spending much of their valuable time to help me perform the measurements and provide their well-appreciated opinions.

Last, but not the least, I am very grateful to the Natural Sciences and Engineering Research Council of Canada (NSERC) for providing me with the postgraduate scholarships, which helped me pursue my Ph.D. degree.

List of Acronyms and Abbreviations

AWGN Additive White Gaussian Noise

CDF Cumulative Distribution Function

CIR Circular

CP Co-positioned

CSI Channel State Information

dB Decibel (ratio in log scale)

dBm Decibel relative to 1 milliwatt

FFT Fast Fourier Transform

IEEE Institute of Electrical and Electronics Engineers

i.i.d. Independent Identically Distributed

IFFT Inverse Fast Fourier Transform

ISM Industrial Scientific and Medical

K Rician factor

Lin Linear

LNA Low Noise Amplifier

LoS Line-of-Sight

MPC Multi-Path Component

MIMO Multiple-Input Multiple-Output

NLoS Non-Line-Of-Sight

PA Power amplifier

PDF Probability Density Function

PDP Power Delay Profile

PL Path Loss

RF Radio Frequency

RMS Root Mean Square

Rx Receive

SISO Single-Input Single-Output

SNR Signal-to-Noise Ratio

Tx Transmit

UWB Ultra-Wideband

VNA Vector Network Analyzer

WLAN Wireless Local Area Network

90R 90degrees rotated

Content

Résumé de la thèse 13

Introduction 13

Caractérisation et modélisation du canal de propagation 15

Caractérisation et modélisation des canaux corporels (B2B) 17

i. Description de la mine souterraine 18

ii. Configuration de mesure 18

iii. Système de communication MIMO 19

iv. Résumé des résultats 20

a. Réponse impulsionnelle du canal 20

b. Affaiblissement de parcours 22

c. Matrices de corrélation spatiale 23

d. L'étalement efficace du délai de propagation et la bande de cohérence 26

e. Facteur de Rice K 27

f. Capacité du canal 28

g. Modélisation du canal 32

h. Discussion des résultats 34

Caractérisation des canaux corporels « on-body » 36

i. Caractérisation du canal corporel « on-body » 36

ii. Modélisation stochastique-empirique pour le canal corporel « on-body » 37

Caractérisation des canaux corporels « off-body » 39

Références 39

Chapter 1 Introduction 42

1.1 Motivation 47

1.2 Research problems and objectives 48

1.3 Thesis Contribution 49

1.4 Thesis Structure 50

1.5 Publications 51

1.5.1 Papers published or accepted in peer-reviewed journals 51

1.5.2 Conference Papers 52

1.6 References 54

Chapter 2 Overview of channel characterization 58

2.1 Large-scale channel characterization 60

2.1.1 Path loss 61

2.2 Small-scale channel characterization 61

2.2.1 Rican K-Factor 63

2.2.2 Time dispersion parameters 64

2.3 References 64

Chapter 3 Overview of MIMO systems and diversity schemes 66

3.1 Diversity techniques 67

3.2 Antenna diversity 69

3.3 Diversity Gain 71

3.4 Multiplexing gain 72

3.5 MIMO matrix 72

3.6 Correlation of the branch signals 73

3.7 MIMO channel capacity 73
3.8 References 74
Chapter 4 WBAN systems 76
4.1 Application areas of WBAN 76
4.2 WBAN studies in underground mines 77
4.3 Measurement techniques 78
4.3.1 Time domain measurement methods-impulse response 78
4.3.2 Frequency-domain measurement methods 79
4.4 References 81
Chapter 5 Body-to-Body Channel Characterization and Modeling Inside an Underground Mine 83
5.1 Abstract 83
5.2 Introduction 84
5.3 Measurement procedure 88
5.3.1 Description of the Underground Mine 88
5.3.2 Measurement setup 90
5.4 Measurement results 91
5.4.1 Channel impulse response 91
5.4.2 Path loss 94
5.4.3 Spatial Correlation Matrices 97
5.4.4 RMS delay spread and coherence bandwidth 101
5.4.5 Rican K-factor 103
5.4.6 Channel Capacity 104

5.4.6.1 Capacity at a constant SNR 105
5.4.6.2 Capacity at a constant transmit power 106
5.4.7 Channel modeling 110
5.4.7.1 Path amplitude modeling 110
5.4.7.2 Time of arrival modeling 111
5.5 Conclusion 113
5.6 References 115
Chapter 6 Characterization of MIMO point-to -point systems inside a mine..... 119
6.1 Channel impulse response and path loss 123
6.2 RMS delay spread, coherence bandwidth and Rican K-Factor 125
6.3 Channel Capacity 128
6.4 References 131
Chapter 7 Performance evaluation of on-body systems in a mine environment. 133
7.1 Measurements procedure 133
7.2 Channel impulse response 136
7.3 Rican K-Factor 138
7.4 RMS delay spread and Coherence bandwidth 139
7.5 Channel Capacity at a Constant Transmission Power 139
7.6 Channel Capacity for a constant SNR 141
7.7 Dynamic channel parameters results 143
7.8 Stochastic-empirical modeling for the on-body channel 144
7.9 Conclusion 145
7.10 References 146

Chapter 8 Characterization of off-body systems inside a mine 148

8.1 Effect of human obstruction on the MIMO-off-body link 149

8.2 Effect of directivity on the MIMO-off-body link 152

8.3 UWB measurements results for an off-body channel inside a mine 155

8.3.1 Impulse response and path loss 155

8.3.2 RMS delay spread 156

8.3.3 Channel Capacity 157

8.4 References 158

Chapter 9 Discussion and conclusion 160

9.1 Application based discussion 160

9.2 Conclusion 163

9.2.1 Summary 163

9.2.2 Future work 164

9.3 References 165

Appendix: Stochastic processes 166

Rayleigh distribution 167

Rice distribution 167

Nakagami distribution 169

Weibull distribution 170

Gaussian or normal distribution 170

Lognormal distribution 171

References 172

Résumé de la thèse

Caractérisation et modélisation des canaux MIMO-WBAN dans une mine souterraine

Introduction

Au cours de la dernière décennie, la communauté des chercheurs a multiplié les efforts pour étudier les communications sans fil dans les mines souterraines. Ces études ont été motivées par une pression croissante pour améliorer les conditions de travail dans mines souterraines en appliquant des systèmes de communication fiables [1]. Les liaisons sans fil sont essentielles pour surveiller les mines souterraines et lancer les opérations de secours en cas d'accident, ce qui améliore la sécurité dans la mine et réduit les coûts [1]. L'effet de cet environnement particulier (mine souterraine) sur les performances des liaisons réseau corporel sans fil (« Wireless Body Area Network » ou bien « WBAN ») ainsi que les liaisons point à point est évalué. Par conséquent, les études de caractérisation ont rapporté les propriétés des canaux de propagation pour différentes bandes de fréquences, diversité et propriétés des antennes [1-17].

Concernant cette thèse de doctorat (PhD), la première contribution consiste à caractériser le canal WBAN sous différents scénarios tels que la ligne de vue directe (« line of sight » ou bien « LOS ») et la ligne de vue indirecte (« none line of sight » ou bien NLOS), les caractéristiques de l'antenne (telles que le gain et la polarisation) et la diversité (telle que

la diversité spatiale pour les systèmes MIMO). Les données mesurées sont traitées et les paramètres de canal sont rapportées dans la littérature [1-17]. À notre connaissance, aucune étude basée sur des mesures expérimentales de ce type n'a été réalisée auparavant dans les mines souterraines pour les systèmes WBAN.

La deuxième contribution consiste en une modélisation des canaux WBAN au sein d'une mine souterraine (publiés dans [4], [6] et [8]). Elle permet de prédire les caractéristiques de propagation d'un certain canal WBAN souterrain sur la base des paramètres saisis (qui pourraient être déterminés empiriquement à partir de mesures ou estimés à partir de résultats publiés dans des environnements similaires). La modélisation déterministe, qui nécessite l'étude des phénomènes physiques affectant la propagation des ondes électromagnétiques (à savoir la réflexion et la diffraction) sur la base de la géométrie de l'environnement, s'est avérée fastidieuse pour l'environnement de la mine étudiée. Les méthodes stochastiques et empiriques nous ont donné des résultats encourageants (tel que quantifié par l'étude d'erreur quadratique minimale). Cette étude consiste à modéliser empiriquement les amplitudes des multi trajets comme un profil de retard de puissance (PDP) en décroissance exponentielle, tandis que le temps d'arrivée est modélisé de façon stochastique en comparant les mesures à différentes distributions aléatoires de la littérature (telles que Poisson, gaussien et Weibull) [4]. Cette nouvelle méthode a abouti à la modélisation de la réponse impulsionnelle du canal WBAN, qui la caractérise complètement.

L'importance de cette méthode innovante est qu'elle fournit un outil permettant (aux concepteurs de systèmes de communication) de comprendre les mécanismes de

propagation et de prendre des décisions de conception économiques (sans avoir recours aux campagnes de mesures expérimentales souterraines).

Caractérisation et modélisation du canal de propagation

Lorsqu'une onde électromagnétique se propage à travers un canal radio, elle est affectée par des phénomènes divers, dégradant sa qualité et nuisant au lien de communication. Ces problèmes de propagation sont généralement attribués à la réflexion, la diffraction et la diffusion de cette onde électromagnétique. Dans un environnement complexe et confiné, tel qu'une galerie minière, la ligne de vue directe est parfois obstruée par les différents objets et obstacles de l'entourage pouvant alors entraîner une perte de puissance considérable. En conséquence à ces phénomènes, de multiples rayons ayant des parcours de propagation différents (différentes longueurs) relient l'émetteur au récepteur. Ces rayons se superposent de façon constructive ou destructive formant ainsi un profil de puissance reçue avec un évanouissement multitrajet.

La caractérisation des canaux est un processus qui étudie les propriétés d'un lien de communication. Il s'agit d'une étude de la propagation du signal entre l'émetteur et récepteur qui représente l'effet combiné de différents phénomènes tels que la diffusion, la diffraction, la réflexion et la dégradation de la puissance du signal avec la distance. Les paramètres de canal importants sont l'étalement efficace du délai de propagation, la bande de cohérence, l'affaiblissement de parcours et la capacité du canal. Cette connaissance du canal de transmission dans un environnement minier souterrain est essentiel pour la conception de systèmes de communication répondant aux besoins du milieu miner.

Différents modèles de propagation sont disponibles pour prédire la propagation des ondes. Les modèles de propagation à grande échelle prédisent la puissance moyenne du signal en fonction de la séparation Tx-Rx. D'autre part, les modèles de propagation à petite échelle prédisent les fluctuations rapides du signal reçu sur de courtes distances (quelques longueurs d'onde). Le modèle PL (« affaiblissements de parcours » ou bien « path loss »), fréquemment utilisé, vise à dériver l'exposant PL à travers l'analyse de la régression linéaire des résultats de PL en fonction du logarithme de la distance.

En ce qui concerne la modélisation des canaux, elle vise à développer des modèles mathématiques qui pourraient être utilisés dans les simulations pour générer les réponses impulsionnelles d'un canal donné sans avoir à réaliser des campagnes de mesure. Un bon modèle de canal radio (qui prédit étroitement des environnements de propagation réels) peut fournir un aperçu détaillé des mécanismes complexes de propagation des ondes radio. La génération d'un modèle précis peut être très complexe et difficile. Cependant, dans la plupart des applications, un modèle suffisamment acceptable est un modèle qui capture les effets clés du canal, en gardant à l'esprit le compromis entre simplicité et précision. Il existe deux grandes catégories de modèles de propagation : déterministes et stochastiques. La modélisation déterministe vise généralement à étudier l'effet de la réflexion et de la diffraction et à construire des modèles mathématiques complexes qui décrivent avec précision ces effets sur le signal reçu.

Cependant, en raison de la nature de l'environnement minier, qui est très complexe et irrégulier, et du système WBAN, installé sur le corps ayant des propriétés électriques différentes pour la peau, les muscles et les os, la réflexion et la diffraction ne peuvent être modélisées avec précision à l'aide de méthodes déterministes [4]. Au lieu de compromettre

la précision avec une modélisation déterministe, qui néglige entre autres les ondes rampantes sur le corps humain, des modèles basés sur des mesures expérimentales, à savoir, les modèles stochastiques-empiriques, sont adoptés dans cette thèse de doctorat.

Caractérisation et modélisation des canaux corporels (B2B)

Dans [4], l'utilisation d'un système d'antennes à entrées multiples et sorties multiples à polarisation circulaire (MIMO) est proposé comme une nouvelle solution pour les futurs systèmes de communication corps à corps (B2B). Quatre canaux B2B ont été caractérisés à l'intérieur d'une mine. Les paramètres statistiques des canaux B2B, utilisant des antennes co-positionnées (CP) et déviées à 90 degrés (90R), ont été déterminés. Les valeurs de l'exposant des affaiblissements de parcours (PL) varient entre 2.33 et 1.26. Les paramètres de dispersion temporelle et les capacités des canaux sont calculés pour les scénarios CP et 90R. De plus, les matrices de corrélation des canaux et le facteur de Rice K ont été déterminés et discutés en fonction de l'étalement efficace du délai de propagation ainsi que de la capacité du canal. En général, la configuration à polarisation circulaire présente des performances mieux que celles de la configuration à polarisation linéaire, en termes de PL, d'étalement efficace du délai de propagation et de capacité de canal. La situation NLOS a provoqué une baisse significative de la capacité du canal, une augmentation significative du PL et une augmentation de l'étalement efficace du délai de propagation, en raison de la richesse du milieu en trajets multiples. Le scénario MIMO-NLOS présente le gain de débit le plus élevé (comparé à SISO) équivalent à 1.752 (pour un SNR de 20 dB), en raison de la faible corrélation entre les antennes. Un modèle de la réponse impulsionnelle B2B a été

créé sur la base d'une approche statistique-empirique, pour déterminer les amplitudes optimales des trajets et leurs temps d'arrivée.

i. Description de la mine souterraine

Dans une mine d'or actuellement non exploitée, située dans la ville de Val d'Or (dans le nord du Québec), une galerie à une profondeur de 90 m sous terre est utilisée pour effectuer des campagnes de mesures autour de la fréquence de 2.4 GHz. Cette galerie se caractérise par des surfaces très rugueuses, une humidité proche de 100%, une température d'environ 8°C et une ambiance pleine de poussière. La gallerie s'étend sur une longueur de 20 m, une hauteur d'environ 2.45 m et une largeur d'environ 5 m. Des flaques d'eau, des machines d'extraction et des tiges et grillage métalliques (implantés au plafond) sont présents le long de la galerie. Cet environnement minier habituel (représenté à la Fig. 5.1) favorise le phénomène de trajets multiples dû à la réflexion et à la diffraction sur les surfaces rugueuses.

ii. Configuration de mesure

Deux systèmes d'antennes MIMO, à savoir, un système d'antennes patch 2×2 MIMO à polarisation circulaire (Cir) et un système d'antennes patch 2×2 MIMO à polarisation linéaire (Lin), sont utilisés durant les compagnes de mesures. Les deux types d'antennes ont un gain de 6.6 dBi (dBi étant le gain de l'antenne par rapport au gain d'une antenne isotrope) et un rapport axial (AR) inférieur à 3 dB à 2,4 GHz. La séparation des antennes MIMO est égale à la moitié de la longueur d'onde ($\lambda/2$). Un analyseur de réseau vectoriel (VNA) est utilisé pour mesurer les paramètres S dans la bande 2.3 GHz – 2.5 GHz. Pendant les mesures, les antennes d'émission (Tx) et de réception (Rx) sont fixées sur la poitrine de

deux étudiants portant une tenue de mineur. Le sujet humain récepteur se déplaçait à des pas de 1 m d'une position de départ de 1 m à une distance finale de 10 m pour les mesures LOS. Dans le scénario NLOS, les sujets humains récepteurs et émetteurs se positionnaient dans deux tunnels miniers différents. L'émetteur est placé à 4 m de distance de l'origine et le récepteur est positionné à différentes distances de l'origine, à partir de 2 m jusqu'à une distance finale de 10 m (comme illustré sur Fig. 5.2). Dans le traitement des résultats, les distances NLOS sont représentées par la notation: 4m / xm, où xm est la distance (en mètres) de Rx depuis l'origine. 10 fichiers de mesures (chacun avec 2049 points de fréquence) sont enregistrés à chaque position.

iii. Système de communication MIMO

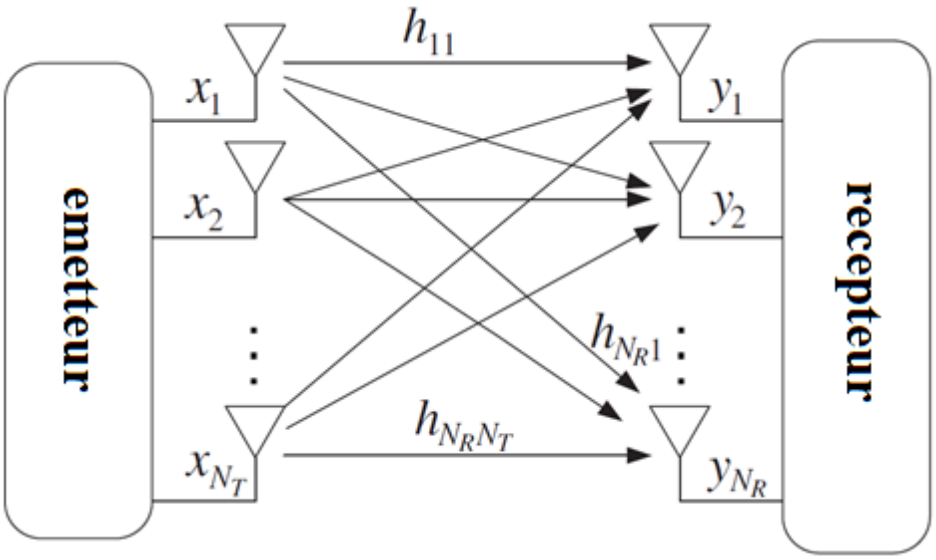

Fig. 1 Système MIMO T×R [18]

Fig. 1 illustre un système MIMO à N_T antennes émettrices et N_R antennes réceptrices. Il peut être présenté par une matrice ***H*** comme suit :

$$Y = \boldsymbol{H} \times X + N \quad (1)$$

où X est le vecteur transmis (de dimension $N_T \times 1$), Y est le vecteur reçu (de dimension $N_R \times 1$), N est le vecteur de bruit gaussien blanc additif (AWGN) et $\boldsymbol{H}$ est la matrice de canal (de dimension $N_T \times N_R$) qui, dans le cas où $N_T = N_R = 2$, s'écrit comme suit :

$$\boldsymbol{H} = \begin{bmatrix} h_{11} & h_{12} \\ h_{21} & h_{22} \end{bmatrix} \quad (2)$$

Sachant que h_{ij} est une variable aléatoire complexe qui représente le gain du sous-canal complexe de la ième antenne d'émission à la jième antenne de réception. Dans les mesures RF, les valeurs des paramètres S_{21} (coefficients de transmission directs) correspondent aux différentes valeurs de h_{ij}.

iv. Résumé des résultats

a. Réponse impulsionnelle du canal

La réponse impulsionnelle de canal *h(t)* est acquise en utilisant la transformée de Fourier inverse (IFT) de la fonction de transfert du canal mesuré donnée par le paramètre de diffusion S_{21}.

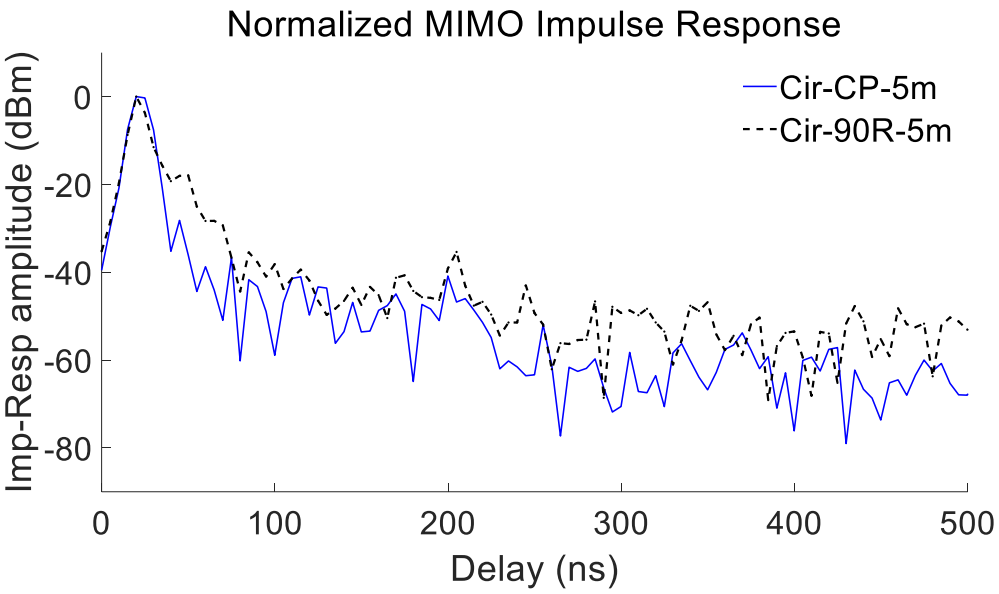

Fig. 2. Réponses impulsionnelles normalisées des canaux MIMO-B2B pour les configurations Cir-CP et Cir-90R, à une distance de 5 m en LOS.

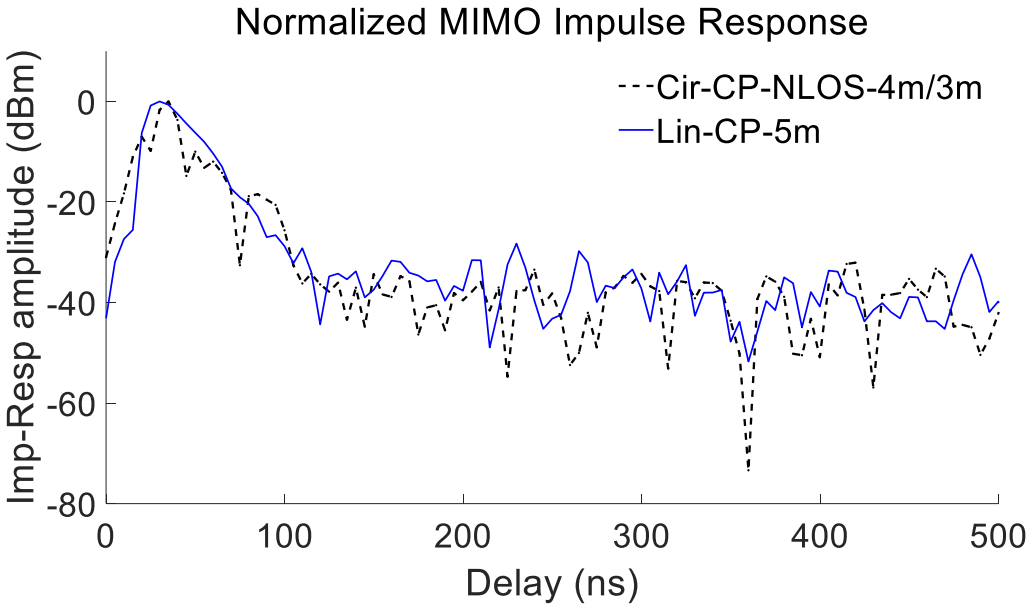

Fig. 3. Réponses impulsionnelles normalisées des canaux MIMO-B2B pour la configuration Cir-CP en NLOS et la configuration Lin-CP en LOS à une distance de 5 m.

À partir de ces réponses impulsionnelles, on remarque que le profil de puissance des composantes multitrajets (MPCs) pour Cir-MIMO-CP est similaire à celui du Cir-MIMO-

90R. En fait, en LOS, le Cir-MIMO-CP et le Cir-MIMO-90R présentent tous deux des MPCs à faibles puissances comparées à celle de la composante directe, importante, dont la puissance est déterministe. Cela est attendu car l'antenne à polarisation circulaire est capable de recevoir simultanément de façon efficace des signaux dans les deux directions, horizontale et verticale ; certaines des composantes multitrajets sont filtrées [4]. En ce qui concerne la situation NLOS, il est clair que la réponse impulsionnelle Cir-CP-NLOS présente un MPC dominant et d'autres MPCs moins importants. En comparant le Cir-CP au Lin-CP, on constate que la configuration linéaire reçoit mieux les puissances multitrajets. Cela est dû au fait que la configuration linéaire est capable de recevoir efficacement les signaux réfléchis des parois de la mine et des surfaces du corps. Ces signaux multitrajets atteignent le récepteur avec différents déphasages et se superposent souvent de manière destructrice, comme le montrent les résultats PL.

b. Affaiblissement de parcours

L'affaiblissement sur le trajet est défini comme le rapport entre la puissance transmise et une moyenne locale de la puissance reçue, et est généralement calculé à l'aide de l'équation suivante [4]:

$$PL_{dB} = 20Log10\ (\xi\ \{H_{x,y,f}\}) \quad (2)$$

où PL_{dB} est le PL à une certaine position, $H_{x,y,f}$ est le gain de sous-canal de l'antenne d'émission *x* à l'antenne de réception *y* à une fréquence *f*. ξ est l'opérateur de moyenne sur toutes les antennes de réception, les antennes d'émission et les fréquences [4].

Habituellement, le PL est modélisé en fonction de la distance *d*, Tx-Rx, comme suit [4]:

$$PL_{dB}(d) = PL_{dB}(d_0) + 10.\alpha.log_{10}\left(\frac{d}{d_0}\right) + X \quad (3)$$

où PL_{dB} (d_0) est l'affaiblissement de parcours moyen à la distance de référence d_0, d est la distance où les pertes de chemin sont calculées, α est l'exposant de l'affaiblissement de parcours (déterminé à l'aide d'une analyse de régression linéaire) et X est une variable gaussienne de moyenne nulle (en dB) représentant l'ombrage [4].

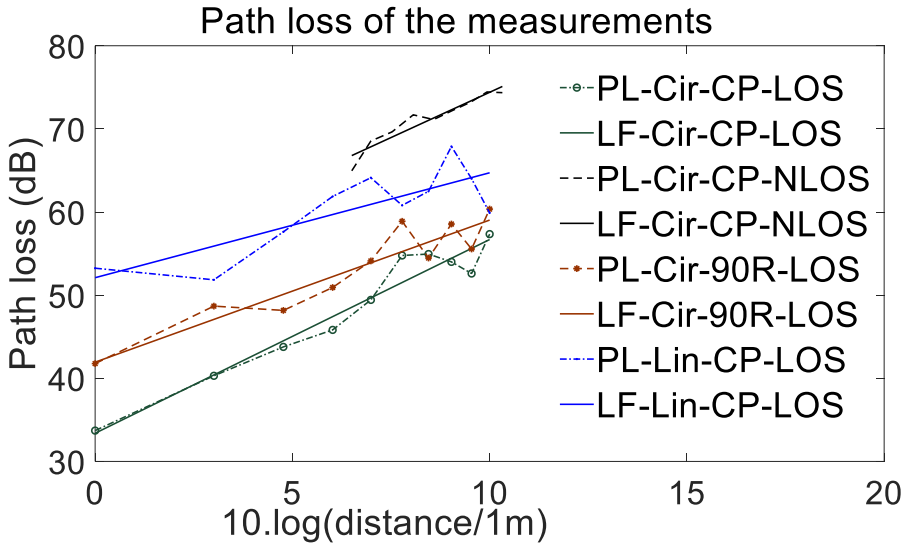

Fig. 4. PL pour les polarisations Cir et Lin ainsi que la régression linéaire (LF) pour les systèmes MIMO-CP et MIMO-90R pour les scénarios LOS et NLOS.

Tableau 1. Valeurs d'exposant de PL pour les différentes configurations de canaux.

Polarisation	**Circulaire**			**Linéaire**
Paramètres	CP-LOS	90R-LOS	CP-NLOS	CP
Exposant de PL	2.33	1.71	2.18	1.26
RMSE (dB)	1.84	2.10	1.01	3.10
Ombrage- STD σ (dB)	1.73	1.98	0.946	2.92
Ombrage - moyen (dB)	-0.0038	-0.0036	-0.0035	-0.0018

c. Matrices de corrélation spatiale

La matrice de corrélation spatiale est constituée des coefficients de corrélation entre les sous-canaux du système MIMO. Il est rapporté que la présence d'un rayon fort augmente

la corrélation entre les sous-canaux [4]. Le coefficient de corrélation entre les sous-canaux h_{AB} et h_{CD} est représenté par [4]:

$$\rho_{AB}^{CD} = \frac{cov(h_{AB},h_{CD})}{\sigma_{AB} \times \sigma_{CD}} \quad (4)$$

où cov (.) est l'opérateur de covariance et σ_{AB} et σ_{CD} représentent respectivement les écarts-types des signaux complexes h_{AB} et h_{CD}.

La matrice de corrélation spatiale du canal 2×2 MIMO-B2B, que nous nommons R, peut s'écrire comme suit [4]:

$$\mathbf{R} = \begin{bmatrix} 1 & \rho_{11}^{12} & \rho_{11}^{21} & \rho_{11}^{22} \\ \rho_{12}^{11} & 1 & \rho_{12}^{21} & \rho_{12}^{22} \\ \rho_{21}^{11} & \rho_{21}^{12} & 1 & \rho_{21}^{22} \\ \rho_{22}^{11} & \rho_{22}^{12} & \rho_{22}^{21} & 1 \end{bmatrix} \quad (5)$$

où ρ_{CD}^{AB} est le coefficient de corrélation entre les sous-canaux h_{AB} et h_{CD}.

Les matrices de corrélation spatiale des canaux MIMO 2 × 2 B2B sont dérivées à l'aide de (5) et représentées dans le **Erreur ! Source du renvoi introuvable.**.

Tableau 2. Matrices de corrélation pour différentes configurations à une distance de 5 m.

Cir-CP-LOS
$\begin{bmatrix} 1 & 0.46-0.51i & 0.39-0.37i & 0.35-0.44i \\ 0.46+0.51i & 1 & 0.8674 & 0.83-0.07i \\ 0.39+0.37i & 0.8674 & 1 & 0.92+0.04i \\ 0.35+0.44i & 0.83+0.07i & 0.92-0.04i & 1 \end{bmatrix}$
Cir-90R-LOS
$\begin{bmatrix} 1 & 0.84-0.06i & 0.44-0.51i & 0.53-0.66i \\ 0.84+0.06i & 1 & 0.59-0.36i & 0.64-0.64i \\ 0.44+0.51i & 0.59+0.36i & 1 & 0.73 \\ 0.53+0.66i & 0.64+0.64i & 0.73 & 1 \end{bmatrix}$

Cir-CP-NLOS
$\begin{bmatrix} 1 & 0.11-0.18i & 0.31-0.21i & 0.02-0.16i \\ 0.11-0.18i & 1 & 0.26-0.22i & 0.271-0.13i \\ 0.31-0.21i & 0.26-0.22i & 1 & 0.34-0.13i \\ 0.02-0.16i & 0.271-0.13i & 0.34-0.13i & 1 \end{bmatrix}$
Lin-CP-LOS
$\begin{bmatrix} 1 & 0.06-0.46i & 0.59-0.41i & 0.72-0.13i \\ 0.06-0.46i & 1 & -0.25-0.45i & 0.04-0.49i \\ 0.59-0.41i & -0.25-0.45i & 1 & 0.69-0.30i \\ 0.72-0.13i & 0.04-0.49i & 0.69-0.30i & 1 \end{bmatrix}$

À partir des matrices de corrélation spatiale, la corrélation de transmission (entre les deux signaux de transmission) est déterminée. Elle est égale à ρ_{11}^{12} à l'antenne de réception 1 et à ρ_{21}^{22} à l'antenne de réception 2. De même, la corrélation de réception (entre deux signaux reçus) est déterminée (en supposant que le signal transmis par l'antenne d'émission 1) comme ρ_{11}^{21}, et (en supposant que signal transmis par l'antenne d'émission 2) comme ρ_{22}^{12}. L'opérateur | . | désigne le module du nombre complexe.

Tableau 3. Corrélation entre deux signaux transmis à une certaine antenne réceptrice (Rx) et corrélation entre deux signaux reçus provenant d'une certaine antenne de transmission (Tx) à 5 m de distance.

	Correlation entre 2 signaux transmis		Correlation entre 2 signaux reçus	
	$\lvert\rho_{11}^{12}\rvert$	$\lvert\rho_{21}^{22}\rvert$	$\lvert\rho_{11}^{21}\rvert$	$\lvert\rho_{22}^{12}\rvert$
Cir-CP-LOS	0.68	0.92	0.54	0.84
Cir-XP-LOS	0.69	0.73	0.68	0.85
Cir-CP-NLOS	0.21	0.37	0.37	0.30

Lin-CP-LOS	0.46	0.75	0.72	0.49

d. L'étalement efficace du délai de propagation et la bande de cohérence.

L'étalement efficace du délai de propagation est égal à la racine carrée du deuxième moment central du profil de retard de puissance (PDP) [4], et est dérivé à l'aide des équations suivantes [4]:

$$\tau_{RMS} = \sqrt{\overline{\tau^2} - \bar{\tau}^2} \tag{6}$$

où $\bar{\tau}$ et $\overline{\tau^2}$ représentent le premier et le deuxième moment du PDP.

$\bar{\tau}$ s'exprime comme suit [4]:

$$\bar{\tau} = \frac{\sum_k p(t_k) t_k}{\sum_k p(t_k)} \tag{7}$$

où p (t_k) désigne la puissance du kième multi trajet et t_k son retard correspondant.

La bande de cohérence (Bc) est dérivée de l'étalement efficace du délai de propagation et est donné par [4]:

$$B_c \simeq \frac{1}{5\tau_{RMS}} \tag{8}$$

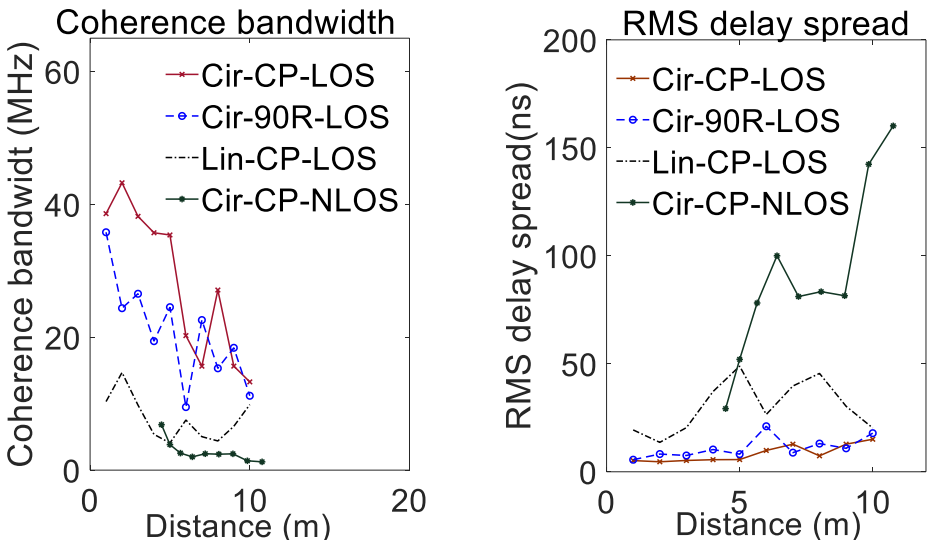

Fig. 5. Étalement efficace du délai de propagation et bande de cohérence, comparés pour les polarisations Cir vs Lin, les scénarios MIMO-CP vs MIMO 90R et LOS vs NLOS.

e. Facteur de Rice K

Le facteur de Rice (K) est défini par rapport suivant [4]:

$$K = \frac{P_D}{2P_R} \tag{9}$$

où P_D correspond à la puissance de la composante dominante et $2P_R$ est la puissance des composantes réfléchies, diffractées ou diffusées.

On peut le déduire directement à partir de la réponse impulsionnelle comme suit [4]:

$$K = \frac{|V_D|^2}{\sum_{m=1}^{M}|a_m|^2} \tag{10}$$

où M est le nombre de composantes multitrajets (MPCs), a_m est l'amplitude aléatoire du MPC et V_D est l'amplitude de la composante dominante (équivalente généralement à la composante LOS déterministe). Le facteur K ne diminue pas systématiquement avec la distance en raison de la structure aléatoire de la rugosité des murs de la galerie, ce qui affecte la richesse des trajets multiples.

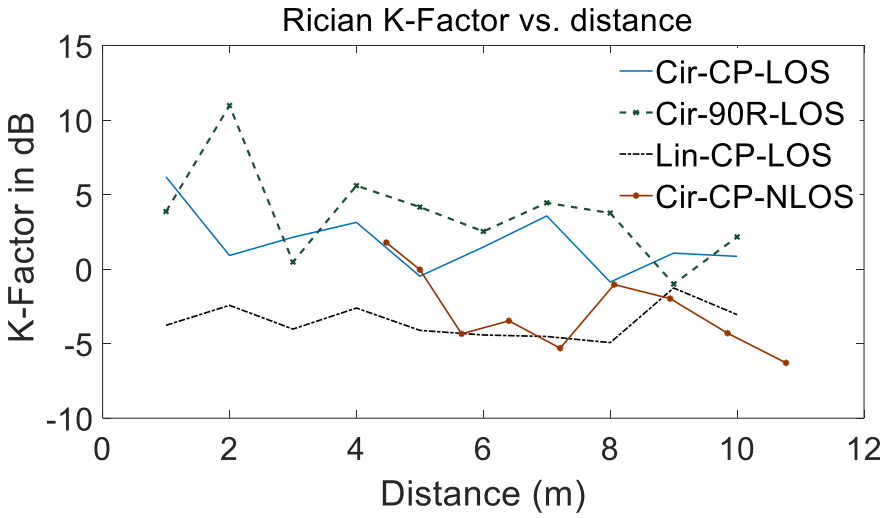

Fig. 6. Facteur de Rice K pour les canaux B2B

f. Capacité du canal

L'étude sur la capacité a pour objectif de montrer l'effet du PL, d'une part, et celui du multi-trajets, d'autre part, sur les différents canaux. Ceci est réalisé avec la supposition que la puissance transmise est constante et que le SNR est variable dans le premier cas, ensuite constant dans le deuxième cas [3].

La capacité du canal MIMO est dérivée en utilisant la formule suivante [4]:

$$C_{MIMO}[bps/Hz] = log_2(\det[\boldsymbol{I}_n + \frac{SNR_{av}}{m}\boldsymbol{H}\boldsymbol{H}^*]) \quad (11)$$

Où $\boldsymbol{I}_n$ est la matrice d'identité, SNR_{av} est le rapport signal sur bruit (SNR) moyen, $\boldsymbol{H}$ est la réponse normalisée du canal MIMO (de dimension m×n) et * représente l'opérateur de transposition conjugué.

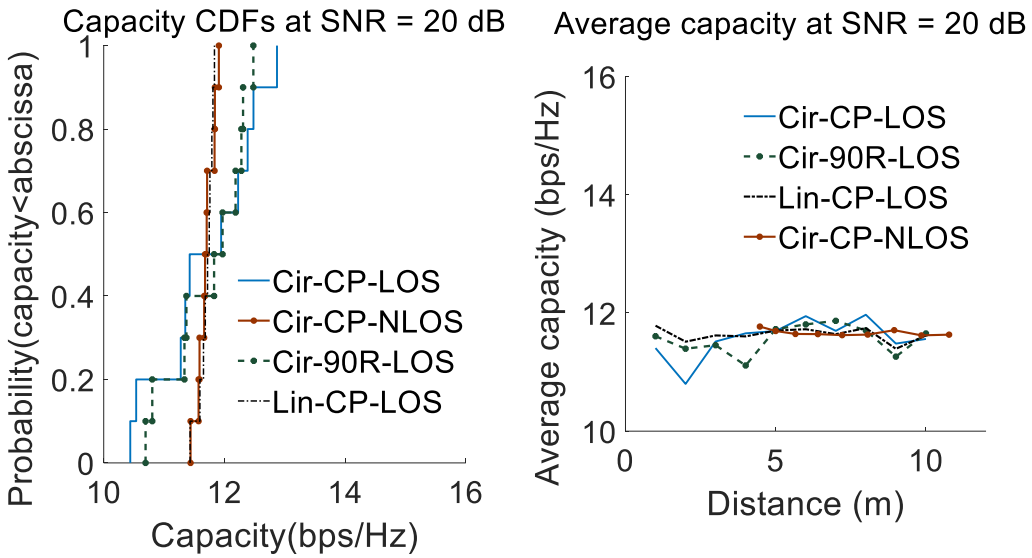

Fig. 7. Capacités moyennes des canaux MIMO des polarisations Cir et Lin et CDF de capacité (distance de 5 m) aux scénarios CP et 90R, en supposant un SNR fixe de 20 dB.

Tableau 4. Gain en capacité du système MIMO (comparé à SISO) pour les canaux B2B lorsque SNR = 20 dB

Canal	**Gain en capacité**
Cir-CP-LOS	1.738
Cir-90R-LOS	1.736
Cir-CP-NLOS	1.752
Lin-CP-LOS	1.748

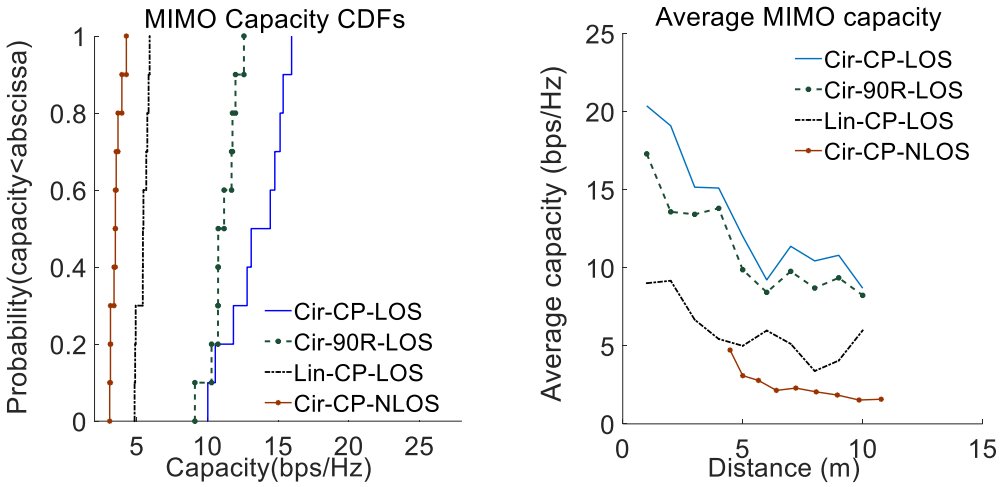

Fig. 8. Capacités moyennes des canaux MIMO pour les polarisations circulaires et linéaires et CDF de capacité (distance de 5 m) dans les scénarios CP et 90R et une puissance de transmission constante.

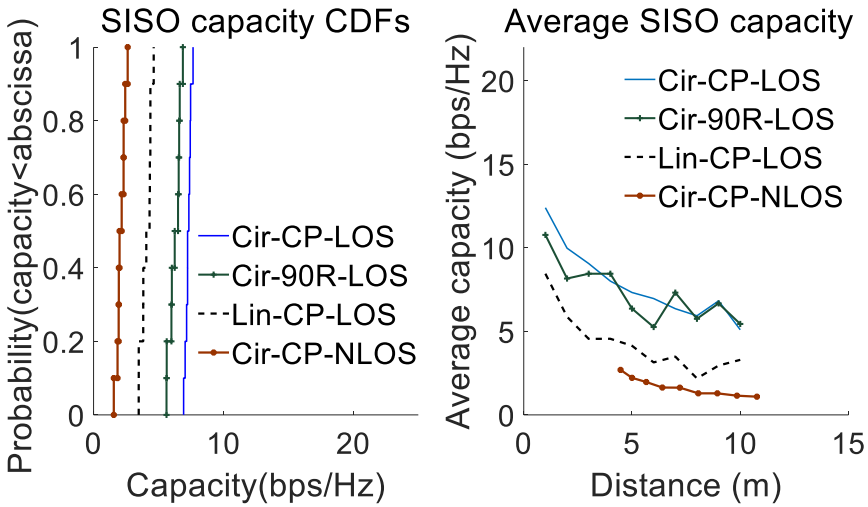

Fig. 9. Capacités moyennes des canaux MIMO pour les polarisations circulaire et linéaire et CDF de capacité (distance de 5 m) pour les scénarios CP et 90R et une puissance de transmission constante.

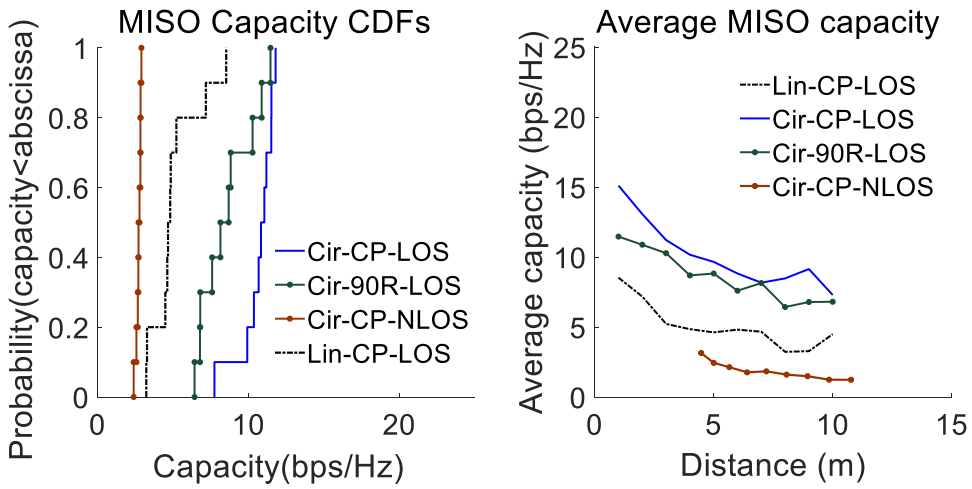

Fig. 10. Capacités moyennes des canaux MISO pour les polarisations circulaires et linéaires et CDF de capacité (pour une distance de 5 m) dans les scénarios CP et 90R et une puissance de transmission constant.

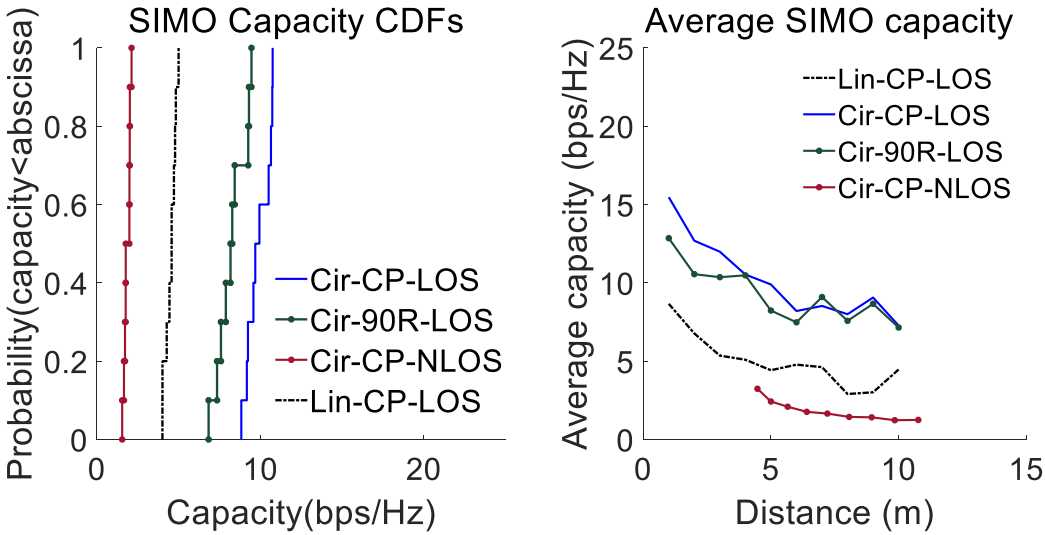

Fig. 11. Capacités moyennes des canaux SIMO pour les polarisations circulaires et linéaires et CDF de capacité (pour une distance de 5 m) dans les scénarios CP et 90R et une puissance de transmission constant.

Les capacités des canaux SIMO, MISO et MIMO dépendent fortement de PL ainsi que de la richesse des composants multi-trajets (à un degré inférieur). Par conséquent, à mesure que la richesse des trajets multiples devient considérable aux distances plus élevées, les capacités des canaux subissent une augmentation occasionnelle malgré l'effet PL ; ce dernier (l'effet de PL) cause une réduction de capacité avec la distance (contrariée par

l’effet de multi trajets). Les puissances des signaux multi trajets sont plus significatives dans le cas des systèmes à polarisation linéaire que dans la configuration à polarisation.

g. Modélisation du canal

La procédure de modélisation consiste à développer la réponse impulsionnelle pour décrire le canal WBAN dans un environnement minier. Ce dernier, qui caractérise complètement le canal B2B, est représenté comme suit [4]:

$$h(t) = \sum_{i=0}^{N-1} a_i \delta(t - t_i) e^{j\theta_i} \quad (11)$$

où N est le nombre de MPC, a_i, t_i et θ_i sont respectivement, l'amplitude aléatoire, le temps d'arrivée et la phase du ième MPC. δ est la fonction delta.

La procédure de modélisation consiste en deux étapes, à savoir, la modélisation des amplitudes des rayons multitrajet (a_i) et des temps de leur arrivée (t_i). Cela se fait en exprimant les amplitudes sous forme de variables gaussiennes aléatoires avec des puissances moyennes décroissant de façon exponentielle, comme représentées par le modèle de canal IEEE 802.11 [4]. Les temps d'arrivée sont modélisés en les comparant aux différentes distributions utilisées dans la littérature. Les phases sont supposées être des variables aléatoires statistiquement indépendantes, uniformément réparties de 0 à 2π [4]. La réponse impulsionnelle modélisée devrait présenter une bonne approximation de la réponse impulsionnelle basée sur des mesures pour le canal B2B étudié.

En ce qui concerne la modélisation de l'amplitude d’une composante multitrajet, le modèle exponentiel (où la puissance diminue de façon exponentielle avec le retard du canal) est utilisé [4]. Les composantes à trajets multiples sont modélisées par des variables

aléatoires gaussiennes complexes et indépendantes avec des puissances moyennes qui suivent le PDP exponentiel [4].

La puissance de chaque composante est donnée par [4]:

$$A_i^2 = A_0^2 * e^{-i*T_s/\sigma_\tau} \tag{12}$$

où i est l'indice de la composante ou rayon (entre 0 et N), T_s est le temps d'échantillonnage, σ_τ est l'étalement efficace du délai de propagation et A_0^2 est la puissance du premier rayon reçue normalisée, donnée par :

$$A_0^2 = \frac{1-e^{-T_s/\sigma_\tau}}{1-e^{-(N+1)T_s/\sigma_\tau}} \tag{13}$$

La modélisation des amplitudes décrites par (12) et (13), nécessite la connaissance de l'étalement efficace du délai de propagation. Cette dernière pourrait être déterminée empiriquement à partir de mesures ou estimée à partir de résultats publiés dans des environnements similaires.

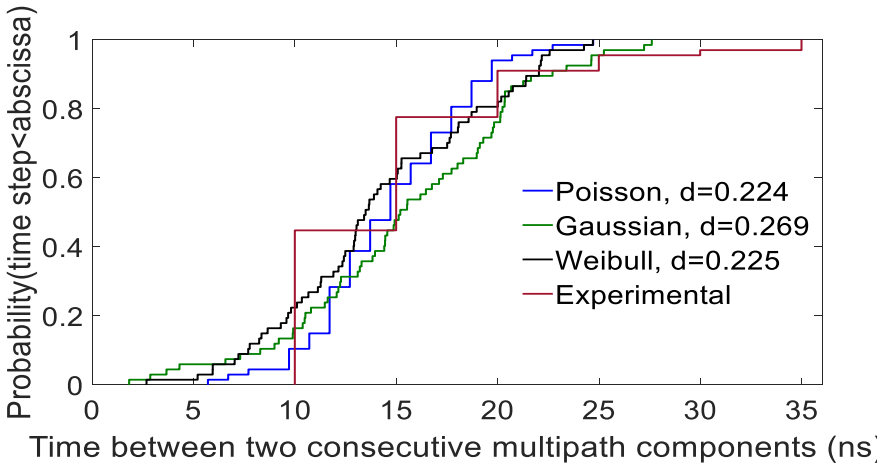

Fig. 12. Comparaison de trois CDF optimales pour représenter les différences de temps entre les MPC.

Les temps d'arrivée sont modélisés de façon stochastique en utilisant la méthode suivante. Les temps d'arrivée des différents MPC sont dérivés des mesures expérimentales

en appliquant un algorithme de détection de pic sur le PDP. La différence de temps entre les pics successifs est considérée afin de générer un ensemble aléatoire pour notre processus. On souligne que le temps d'arrivée n'est pas complètement aléatoire car il croit tout le temps. La distribution des temps d'arrivée est comparée aux différentes distributions aléatoires de la littérature, à savoir, Poisson, Gauss et Weibull. Le test de Kolmogorov – Smirnov (KS) est utilisé pour déterminer la distribution qui décrit le plus fidèlement l'ensemble aléatoire des temps d'arrivée.

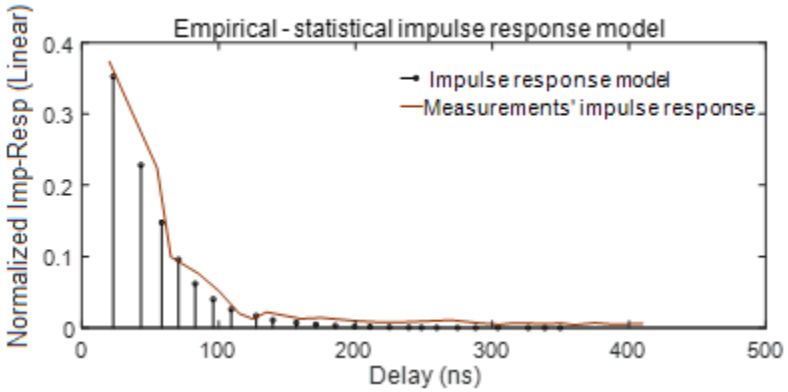

Fig. 13. Réponses impulsionnelles modélisées et mesurées normalisées par leurs puissances totales respectives.

h. Discussion des résultats

Dans cette thèse, le canal MIMO-B2B a été caractérisé à 2.4 GHz dans une galerie minière à l'aide d'antennes polarisées circulairement et linéairement. Différents scénarios ont été considérés, à savoir, LOS et NLOS. Il ressort clairement des résultats du PL, de la capacité et de la dispersion temporelle que les antennes à polarisation circulaire fonctionnent mieux pour les canaux B2B dans un environnement minier en raison de leur pouvoir à supporter le désalignement des antennes. La capacité du canal dépend fortement du PL et un peu moins de l'environnement multitrajet. En effet, à mesure que la richesse en multitrajet

devient significative aux distances plus élevées, la capacité peut connaître une augmentation malgré l'effet du PL. Les résultats du facteur K révèlent que les puissances des MPC par rapport à la puissance dominante sont plus importantes dans le cas de la configuration Lin-MIMO que dans la configuration Cir-MIMO. L'étalement efficace du délai de propagation confirme ce résultat avec des valeurs plus élevées pour Lin-CP, en particulier aux distances plus élevées. La corrélation suit la même tendance que le facteur K et l'effet d'obstruction d'un signal LOS est significatif, comme le montrent les résultats de PL, de capacité et de dispersion temporelle. En fait, les capacités Cir-CP-NLOS sont inférieures à la moitié des capacités Cir-CP-LOS sur des distances Tx-Rx similaires. Cela est attendu, car le rayon LOS est le principal contributeur à la puissance totale, ajouté au fait que la deuxième contribution (la première réflexion) n'est pas effectivement reçue au niveau du récepteur en raison du changement du sens de polarisation. Le gain en capacité MIMO est le plus important pour la configuration NLOS ainsi que la configuration linéaire, puisque la corrélation entre les antennes est faible. En général, la configuration à polarisation circulaire semble très bien adaptée à la propagation B2B à l'intérieur d'une mine, même à des situations NLOS.

Un modèle de réponse impulsionnelle a été développé afin de décrire complètement le canal B2B. La distribution de Poisson décrit le mieux les temps d'arrivée des rayons multi-trajets. Pour les amplitudes des rayons, leurs puissances moyennes sont modélisées par une PDP en décroissance exponentielle, tout en supposant des MPC respectant une distribution gaussienne. La réponse impulsionnelle modélisée est proche de celle mesurée avec une estimation de l'erreur quadratique moyenne minimale (MMSE) de 1.8437×10^{-4}.

Caractérisation des canaux corporels « on-body »

i. Caractérisation du canal corporel « on-body »

Les mesures de propagation MIMO-On-body dans une galerie souterraine et leur analyse statistique sont publiées dans [2]. Dans cette étude, trois scenarios de canal sur le corps, à savoir, ceinture-poitrine, ceinture-tête et ceinture- poignet, sont considérés. L'objectif est de comparer la performance du MIMO 2×2 à celle d'un système SISO. À cet égard, la capacité du canal MIMO à puissance d'émission constante a été manifestement améliorée par rapport à celle de SISO (d'un facteur pouvant atteindre 1.85). Les résultats du facteur K sont corrélés aux valeurs de capacité à une puissance transmise constante. Ces valeurs sont proches pour les trois canaux, reflétant la richesse des trajets multiples et la présence d'une forte composante LOS pour tous ces scénarios. De plus, l'étalement efficace du délai de propagation a été augmenté en raison de la diversité. En effet, MIMO est capable de capturer plus de rayons à trajets multiples que SISO, ce qui explique les résultats d'étalement efficace du délai de propagation. Les résultats pour la capacité du canal (à une puissance transmise constante), le facteur K et les paramètres de dispersion sont présentés dans le Tableau 5. La capacité du canal a également été calculée en supposant un SNR fixe afin d'étudier l'effet des trajets multiples sur la capacité du canal tout en neutralisant l'effet du PL. Pour un SNR de 20 dB, le canal ceinture-poitrine présente une capacité de canal (10.9 bps / Hz) plus élevée que les canaux ceinture-tête (9.48 bps / Hz) et ceinture-poignet (7.95 bps / Hz) comme indiqué sur la Fig. 14. Les canaux ceinture-poitrine et ceinture-tête présentent des phénomènes de trajets multiples similaires, probablement parce que Tx et Rx se font face directement, dans les deux canaux. La capacité ceinture-poitrine est

légèrement supérieure à la capacité ceinture-tête due au fait que les multi-trajets reçue par ce canal sont plus riche en terme de signaux réfléchis par le corps.

Tableau 5. Résumé des résultats pour chaque canal de propagation

Paramètres évalués	Type de canal corporel					
	Ceinture-poitrine		Ceinture-tête		Ceinture-poignet	
	SISO	MIMO	SISO	MIMO	SISO	MIMO
Capacité moyenne du canal (bps/Hz)	9.02	16.6	5.62	7.56	4.65	7.78
Bande de cohérence à 50% de corrélation (MHz)	13.4	10.7	7.20	2.20	3.40	2.70
Bande de cohérence à 90% de corrélation (MHz)	1.34	1.07	0.72	0.22	0.34	0.27
Étalement efficace du délai de propagation (ns)	15.75	18.7	27.8	89.4	59.0	73.7
Facteur de Rice-K (dB)	32.3	32.4	31.5	29.7	30.7	30.9
L'écart-type de K (dB)	1.21	0.14	1.47	0.64	1.70	0.39

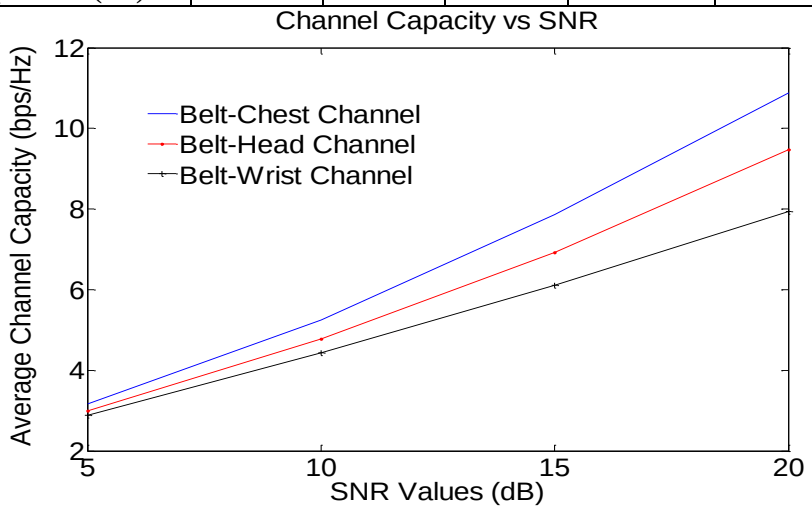

Fig. 14. Capacité moyenne MIMO en fonction du SNR pour les trois canaux corporels

ii. Modélisation stochastique-empirique pour le canal corporel « on-body »

De manière similaire à la modélisation B2B, un modèle statistique-empirique pour le canal corporel est présenté. Ce nouveau modèle permet de générer la réponse impulsionnelle capable d'imiter celle obtenue expérimentalement à 2.4 GHz.

Les temps d'arrivée des rayons et leurs amplitudes respectives sont modélisés de la même façon que celle établie pour le canal B2B. La distribution de Weibull (avec les paramètres de forme et d'échelle égalant successivement 16.5 et 2.6) s'est avérée décrire le mieux les temps d'arrivée. L'estimation MMSE du modèle de réponse impulsionnelle optimale (Fig. 16) est de 0.0019, ce qui montre que le modèle se rapproche bien des mesures.

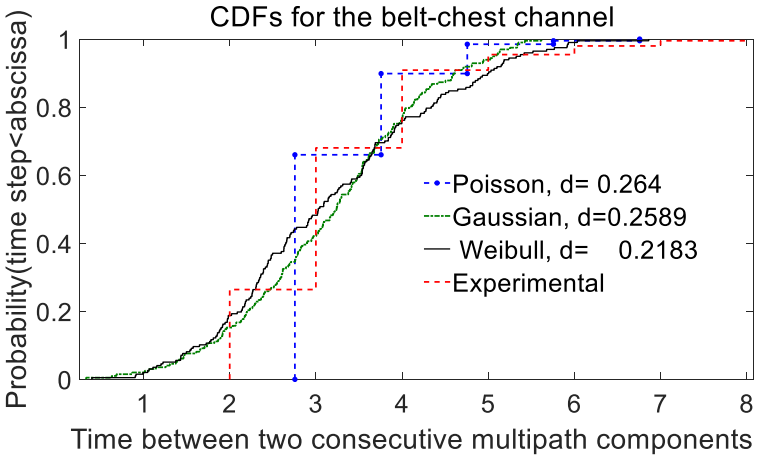

Fig. 15. CDF des temps d'arrivée

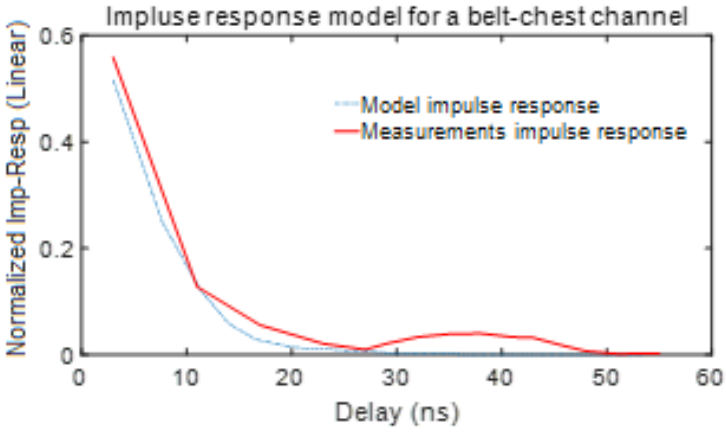

Fig. 16. Réponse impulsionnelle mesurée comparée au modèle

Caractérisation des canaux corporels « off-body »

Dans le cadre de ce travail, plusieurs articles ont été publiés pour caractériser le canal « off-body » à l'intérieur d'une mine. Dans [3], les performances du canal MIMO ont été comparées à celles d'un canal SISO. De plus, étant donné que le lien « off-body » dans un environnement minier est sujet à obstruction, les scénarios NLOS ont été étudiés et comparés aux scénarios LOS. Enfin, l'effet de la directivité sur la liaison MIMO a été exploré à la fois pour LOS [11-12] et pour NLOS [9-10].

Il a été confirmé que le trajet multiple augmente à la fois la capacité du canal et l'étalement efficace du délai de propagation pour les deux scénarios LOS et NLOS. Le facteur K est fortement corrélé à la capacité du canal à un SNR constant (pour LOS et NLOS). Les valeurs NLOS de la capacité et de l'étalement efficace du délai de propagation, lorsqu'on utilise des antennes directives, sont généralement moins favorables que celles d'une configuration monopôle comparable [3]. Cela est dû au fait que les antennes monopôles sont plus capables de capter les signaux à trajets multiples que les antennes patch directives. Pour un SNR variable et une puissance transmise constante, la richesse en multitrajet pour des distances éloignées n'est pas reflétée sur le PL. Aussi, on a constaté que la directivité n'améliorait pas la capacité en raison du PL élevé.

Références

[1] M.E. El Azhari, L. Talbi, L. Arabi, M. Nedil, M. L. Seddiki, and N. Kandil, " Channel Characterization of Circularly Polarized Antenna MIMO System in an Underground Mine," Progress In Electromagnetics Research M, Vol. 67, 9-19, 2018.

[2] M.E. El Azhari, M. Nedil, I. B. Mabrouk, L. Talbi, K. Ghanem, and Y. S. Alj, "Performance evaluation of a MIMO-on-body system in a mine environment," Progress In Electromagnetics Research C, Vol. 61, 55-63, 2016.

[3] M.E. El Azhari, M. Nedil, I. Benmabrouk, K. Ghanem, and L. Talbi, "Characterization of an off-body channel at 2.45 GHz in an underground mine environment," Progress In Electromagnetics Research M, Vol. 43, 91-100, 2015.
[4] M.E. El Azhari, L. Talbi, and M. Nedil, " Body- to-Body Channel Characterization and Modeling Inside an Underground Mine," IEEE Trans. Antennas Propag. (À apparaitre), 2020.
[5] M. E. Azhari, L. Talbi and M. Nedil, " K-factor and Correlation Analysis of a 2×2 MIMO Off-body Channel Inside a Mine," 2019 IEEE International Symposium on Antennas and Propagation & USNC/URSI National Radio Science Meeting, Atlanta, Ga, 2019.
[6] M.E. Azhari, L. Talbi and M. Nedil, " Comparative study of Four Path Loss Models for UWB off-body Propagation Channel Inside a Mine," 2019 IEEE International Symposium on Antennas and Propagation & USNC/URSI National Radio Science Meeting, Atlanta, Ga, 2019.
[7] M.E. Azhari, L. Talbi and M. Nedil, "UWB Off-Body Channel Characterization in a Mine Environment," 2018 IEEE International Symposium on Antennas and Propagation & USNC/URSI National Radio Science Meeting, Boston, MA, 2018, pp. 559-560.
[8] V. A. Fono, L. Talbi and M. E. El Azhari, "Comparative study of three Deterministic Radio Propagation Models in a Complex media," 2018 IEEE International Symposium on Antennas and Propagation & USNC/URSI National Radio Science Meeting, Boston, MA, 2018, pp. 1333-1334.
[9] M. E. Azhari, L. Talbi, M. Nedil and I. Ben Mabrouk, "NLOS Capacity and Time dispersion of a Multipath Fading MIMO Channel Using Directive Antennas in an Underground WBAN Application" IEEE/APS 2017.
[10] M. E. Azhari, L. Talbi, M. Nedil and I. Benmabrouk, "Impact of NLOS on the Path Loss and Channel Capacity of a MIMO Off-body System Inside a Mine " IEEE/APS2017.
[11] L. Arabi, M. E. Azhari, L. Talbi, M. Nedil and S. M. Lamine, "2.4 GHz Radio-Channel Characterization of an Underground Mine using Patch antennas" IEEE/APS2017.
[12] L. Arabi, M. E. Azhari, L. Talbi, M. Nedil and S. M. Lamine, “Radio-Channel Characterization of an Underground Mine using Circularly polorized antennas at 2.4 GHz " IEEE/APS2017.
[13] M. E. Azhari, M. Nedil, I. Ben Mabrouk and L. Talbi, "Multipath effect on off-body channel parametters of a MIMO system using patch antennas inside a mine," 2016 IEEE International Symposium on Antennas and Propagation (APSURSI), Fajardo, 2016, pp. 1693-1694.
[14] M. E. Azhari, M. Nedil, I. Ben Mabrouk and L. Talbi, "Path loss effect on off-body channel capacity of a MIMO system using patch antennas inside a mine," 2016 IEEE International Symposium on Antennas and Propagation (APSURSI), Fajardo, 2016, pp. 1697-1698.
[15] A. Habani, M. Nedil, M.E. Elazhari and F. Ghanem, "High gain off-body antenna based on combination AMC-FSS structure for underground mining communications," 2016 IEEE International Symposium on Antennas and Propagation, Fajardo, 2016, pp. 267-268.

[16] M.E. El Azhari, M. Nedil, and I. B. Mabrouk, "Characterization of an on-body quasi-static channel in underground mine environment," 2015 IEEE Antennas and Propagation Society International Symposium (APSURSI), Jul. 18-25, 2015.
[17] M.E. El-Azhari, M. Nedil, I. Benmabrouk, L. Talbi, and K. Ghanem, "Off-body LOS and NLOS channel characterization in a mine environment," International Conference on Electrical and Information Technologies (ICEIT), Marrakesh, Morocco, 2015.
[18] Y. S. Cho, J. Kim, W. Y. Yang, and C. G. Kang, MIMO-OFDM wireless communications with MATLAB: John Wiley & Sons, 2010.

Chapter 1 Introduction

The propagation channel is the medium where electromagnetic waves are emitted or captured through antennas and are subject to different physical phenomena affecting the quality of the transmission. In underground mines' environments, these physical effects include reflection, diffraction and scattering, caused by barriers and surface roughness that disturb the transmission of information. Moreover, in wireless body area networks (WBAN) the wireless channel includes the surface of the human body, which introduces additional effects and propagation mechanisms. For instance, the microwave signals attach to the human body- as creeping waves- providing secondary paths that could add either constructively or destructively to other multipath signals [1]. To mitigate the effects of these potentially damaging phenomena, the properties of the propagation channel must be known with precision. The channel characterization allows quantifying these properties through the determination of the channel parameters, namely, the impulse response, the RMS delay spread, the Rican K-factor, and the path loss (PL) exponent.

In past decade, the research community has multiplied efforts in studying wireless communication in underground mines. These studies were motivated by an increasing pressure to improve mining conditions by applying reliable underground communication systems [2]. They aim to replace the wired communication link, which requires expensive maintenance and has limited scalability [3], by a reliable and safe wireless link. Wireless links are essential for monitoring underground mines and launching a rescue operation in the case of an accident, which improves in-mine security and reduces cost [2]. The effect

of this particular environment (underground mine) on the WBAN and RF link performance was evaluated. Hence, characterization studies have reported the channel properties for different frequency bands, diversity configurations and antenna selections under different environmental conditions [4-8]. For example, the effect of non-line of sight (NLOS) on the signal propagation is investigated, for ultra-wideband (UWB) radio links [4], using Vivaldi antennas with two different multiple-input multiple-output (MIMO) configurations (parallel and 30 degrees antenna set up). A general improvement of the channel parameters was observed for the 30 degrees MIMO antennas compared to the parallel setup (in terms of correlation and path loss exponent). Regarding the beamforming techniques, the Butler matrix, was investigated in [9] for underground mining uses at 2.4 GHz. Using beamforming, the average channel capacity of a MIMO multipath channel was improved (compared to a conventional uniform linear array). Moreover, since the antenna properties affect the signal, some researchers studied different scenarios where a certain property of the antenna is changed. For example, the effect of directivity on the underground RF channel is studied in [5]. The paper considered the medium-range wireless MIMO communication technologies at 2.4 GHz. It was found that the MIMO channel capacity, using monopole antennas, is better than that of the MIMO setup using patch antennas, in a mine environment. This was explained by the fact that the multipath richness of the environment is best exploited with omnidirectional MIMO systems. In another study [8], it was found that directional antennas setups exhibit a reduction in RMS-delay spread due to the lower multipath receptions and are characterized by a lower channel capacity due to an increased correlation at LOS scenarios. A modification of the shape of the antennas, namely the conformal patch antennas, was studied in [10] at both LOS and NLOS. Results

showed that conformal patch setup performs better than the conventional planar patch array in both LOS and NLOS. Other antenna characteristics, which affect the propagation in underground mines, include polarization, placement and radiation pattern [11-13]. Regarding polarization, different studies have reported measurements results on the horizontal, vertical and cross-polarized planes [14-15]. Some circularly polarized antennas measurements have been reported in railway tunnels [16-17]. They have reported PL and fading characteristics of signal propagation within a tunnel, over long distances reaching up to few thousand meters. They, however, omitted the channel capacity as well as important channel characterization parameters, such as the time dispersion parameters.

The theme of this PhD thesis concerns wireless body area networks (WBAN). WBAN is a conceptual wireless network technology where a set of communicating devices are located on or around the human body [18]. Vital body parameters' data is collected and communicated using short-range wireless communication techniques to a close-by command station. WBAN communication technology encompasses the propagation at the on-body, off-body, and in-body channels. The on-body channel involves a transmitter and a receiver installed on the human body surface, whereas the in-body channel consists of a transmitter within the body. Wireless off-body technology deals with the communication links between devices mounted on the body, and other devices, or access points, away from the body. WBAN technology found applications in the industrial, entertainment, sport, and medical fields. Among the examples of this technology are wearable RF tags (for geo-localization) and medically oriented body-worn sensors (for vital signs monitoring). In WBAN links, much precision and attention should be taken in antenna design, placement, and orientation. For example, in off-body systems, the antennas radiation patterns should

be directed away from the body, while in on-body systems the radiation should be parallel to the body plane for optimum performance (establishing a LOS link) [18].

Recently, the rising accidents rates in the mining field pushed toward exploring new communication schemes destined to the safety of the miners. Indeed, the WBAN technology has emerged as a promising communication scheme dedicated to the miners' safety [1]. Toxic gases levels could be displayed to the miners and vital information could be delivered to the command station, in a timely manner. This allows improving the miners safety and health through the fast detection of potential problems which eases the decision making. However, in a mine environment, the reliability of the WBAN wireless link is affected by short-term and long-term fading mainly caused by multipath communication, and shadowing [18]. Moreover, the WBAN communication link performance depends on the allocated frequency band and the directivity of the transmitter (Tx) and the receiver (Rx) antennas. Hence, characterizing and modeling studies of the WBAN channel in a mine environment are of outmost importance. In fact, modeling the propagation of electromagnetic waves is essential in studying the performance of wireless channels. It allows predicting the behavior of a transmitted and received signal for a given frequency and a given environment, which saves precious time and human resources otherwise allocated to experimental measurements.

The WBAN channels propagation study consists in determining the parameters of the propagation channel in order to understand the propagation mechanism. It consists in the channel characterization, where the different parameters (such as the coherence bandwidth, RMS delay spread and path loss) are determined. The channel capacity is of interest since it describes the maximum achievable bit rate. MIMO technology is recommended in

WBAN systems in order to improve the channel performance [1]. Furthermore, deterministic, empirical and statistical modeling allow predicting the propagation characteristics. Deterministic modeling necessitates the study of the physical phenomena affecting the electromagnetic wave propagation, namely, reflection and diffraction. The uniform theory of diffraction (UTD) is a good tool to predict the diffracted field from surrounding walls and body parts irregularities. There are three types of deterministic modeling, namely, the closed-form approach (such as the two-path signal model), empirical (based on measurement) approach and ray tracing approach. All three types of deterministic modeling are tedious and mathematically involving [19]. In fact, in deterministic modeling, there is a compromise between simplicity and accuracy. One need to give up much of the accuracy of the model in order to achieve a reasonable simplicity. This is not the case for statistical modeling which offers a good tradeoff between simplicity and accuracy [19]. In fact, statistical modeling can reliably generate simulated impulse responses for a given environment at particular frequency, based on models with good accuracy (derived from experimental measurements). In short, the different measurement data are evaluated to determine which distributions best describe the environment. Then this information is used in statistical simulations to simulate the impulse response of such an environment at a given frequency and derive the important parameters. The accuracy of such method is satisfactory and the complexity is reasonable. This PhD Thesis studies the WBAN channel inside a real mine for different scenarios and configurations. It is a necessary work aimed to characterize the WBAN channels at different frequency bands, taking into consideration the effect of directivity, polarization and spatial diversity. The studies compare different link conditions (such as LOS vs NLOS). In addition, statistical-

empirical models are derived for the impulse responses. This allows a complete characterization of the underground channel. While the off-body propagation channel is majorly affected by the mine gallery reflection and diffraction signals, the on-body channel is effectively affected by the LOS signal, the creeping wave signal and the body parts reflections. The reflections from the mine gallery are greatly reduced in strength compared to the body parts reflections (for the on-body channel), and hence their effect is minimal. Consequently, the on-body model shall apply to a wide range of mining environments, while the off-body one applies to mines with similar dimensions and electrical properties. In fact, it was empirically observed, that the RMS delay spread (which is used in the model to include the effect of multipath) is somewhat similar for both the CANMET and Vale de L'Or gold mines [1, 20].

1.1 Motivation

For many years, the mining companies and government agencies have been concerned with preventing the mining accidents. In fact, workers are priceless resources in the mining industry, which makes it of paramount importance to ensure their health and safety. The decreasing frequency of accidents demonstrates the seriousness with which mining companies approach this issue. Moreover, in order to better co-ordinate mine rescuing efforts, when an accident occurs, the rescue team needs to depend on a reliable communication and localization system. To help meet this need, several companies (such as Meglab Inc. and Becker Inc.) have invested in developing communication systems dedicated to the safety of the mining personnel. This includes fancy localization, tracking and collision awareness systems. Along with the industry effort to improve the existing

communication systems inside the mines, some universities are researching to characterize and model the mining environment for wireless propagation. These researches are very appealing to the industry who searches to minimize their communication systems cost. It is much more cost effective to implement wireless communication systems inside the mine than to run leaky feeder wires and repeaters all over the galleries. The R&D time involved with such systems is greatly decreased when an accurate model for the channel is available.

1.2 Research problems and objectives

In an underground environment, WBAN wireless communication systems need to provide reliable high-speed services. These systems are destined to the safety and security of the miners. Examples of such systems include the localization of the miners for prompt intervention in the case of accidents and the collision avoidance systems protecting the miners from passing-by mining machines. Moreover, the capacity of conventional communication systems, using a Single-Input Single-Output (SISO) transmit and receive antenna, is directly limited by the transmitted power and the available bandwidth [22]. To overcome these limitations, using multiple antennas at both ends of the transmission (MIMO) chain is a widely approved approach for WBAN system designers. In fact, it has been proven that the maximum capacity of the MIMO channels increases proportionally with the minimum number of transmit and receive antennas [23]. However, the implementation of WBAN MIMO systems inside the mine is not an easy task. Several physical phenomena affect the signal propagation, namely reflection, diffraction and scattering [1]. These phenomena result from the structure of the mine and the complexity of the effect of each phenomenon is directly related to the randomness of the mine

geometry. The mine itself is a very humid environment which include many water bodies and dust particles, affecting the signal propagation.

The implementation of WBAN MIMO services inside the mine requires a detailed channel characterization study. Moreover, the establishment of a model for the channel allows reducing the R&D cost to build WBAN MIMO systems inside the mine. However, the randomness of the mine geometry makes it quasi-impossible to implement a deterministic model for the channel. Hence, a stochastic-empirical approach is chosen for underground WBAN channel modeling.

1.3 Thesis Contribution

The focus of this PhD Thesis is to study WBAN channels propagation inside an underground mine. The first contribution consists in determining the parameters of the propagation channel in order to understand the WBAN propagation mechanism. In this channel characterization, different parameters (such as the coherence bandwidth, RMS delay spread, Rican K-factor and path loss) are determined. The channel capacity is studied for different WBAN configurations. MIMO technology proved advantageous for WBAN systems in order to improve the propagation performance in a mine gallery [1]. The second contribution of this thesis consists in statistical-empirical modeling, which allows predicting the WBAN channel impulse response in a certain mine gallery. This approach offers a good tradeoff between simplicity and accuracy [21]. In fact, statistical-empirical modeling can reliably generate simulated impulse responses for a given environment at particular frequency, based on experimental measurements. This novel modeling method is based in modeling the multipath amplitudes as an exponentially decaying PDP, while

the time of arrival is stochastically modeled by comparing the measurements results to different random distributions from the literature (such as Poisson, Gaussian, and Weibull) [22]. Hence, the impulse response of the WBAN channel was determined by joining the MPCs' amplitude model vector to its corresponding arrival times vector. The proposed model is functional and approaches the measurements.

The novelty of this PhD work is five folds: First, propagation study using circular polarization inside a mine has never been reported; very few propagation studies dealt with circular polarization in regular tunnels but only focused in PL results [16-17]. Second, cross-polarization and co-polarization results in the context of WBAN MIMO system inside a mine are specific to this study. Third, the study of the effect of directivity on WBAN-MIMO channel inside a mine has solely been reported in this work. Forth, the project studies the body-to-body (B2B), the off-body and on-body channels over two frequency bands (namely 2.4 GHz and UWB) and using different diversity schemes (SISO, SIMO, MISO and MIMO). Fifth, novel statistical-empirical models are generated for the WBAN channel, whose accuracy is proven through comparison with measurements results.

1.4 Thesis Structure

This thesis covers nine chapters. The first chapter introduces the thesis. The motivation of the work, the problem and the engineering contribution of this thesis are summarized. The themes of following chapters are detailed as follows:

Chapter 2 explains the channel characterization theory.

Chapter 3 presents an overview of MIMO systems.

Chapter 4 explains the WBAN systems and its different applications then focuses on underground studies and presents their measurement procedures.

Chapter 5 presents the main publication of this project, entitled "body-to-body channel characterization and modeling inside an underground mine" [J1]. The performance of a circular setup is compared to that a regular patch system (for different diversity schemes). The channel parameters are presented for different scenarios (LOS *vs.* NLOS and circular polarization *vs.* linear polarization) and a statistical-empirical model is also presented.

Chapter 6 summarizes the published results for an underground point-to-point channel characterization using circularly and linearly polarized antennas.

Chapter 7 combines the published on-body channel characterization and modeling results (from journal and conference articles) and presents them in a comprehensive manner.

Chapter 8 presents and discusses the off-body channel characterization results, based on different publications. The performance of the monopole setup is compared to that of the patch setup under LOS and NLOS scenarios for both MIMO and SISO configurations.

Chapter 9 discusses the presented results and the open research problems.

1.5 Publications

1.5.1 Papers published or accepted in peer-reviewed journals

[J1] M.E. El Azhari, L. Talbi, and M. Nedil, "Body- to-Body Channel Characterization and Modeling Inside an Underground Mine," in *IEEE Transactions on Antennas and Propagation*, 2020.

[J2] M.E. El Azhari, L. Talbi, L. Arabi, M. Nedil, M. L. Seddiki, and N. Kandil, “Channel Characterization of Circularly Polarized Antenna MIMO System in an Underground Mine,” Progress In Electromagnetics Research M, Vol. 67, 9-19, 2018.

[J3] M.E. El Azhari, M. Nedil, I. B. Mabrouk, L. Talbi, K. Ghanem, and Y. S. Alj, “Performance evaluation of a MIMO-on-body system in a mine environment,” Progress In Electromagnetics Research C, Vol. 61, 55-63, 2016.

[J4] M.E. El Azhari, M. Nedil, I. Benmabrouk, K. Ghanem, and L. Talbi, “Characterization of an off-body channel at 2.45 GHz in an underground mine environment,” Progress In Electromagnetics Research M, Vol. 43, 91-100, 2015.

1.5.2 Conference Papers

[C5] M. E. Azhari, L. TaIbi and M. Nedil, " Stochastical-Emperical Modeling for an on-Body Channel Inside a Mine," 2020 IEEE International Symposium on Antennas and Propagation & USNC/URSI National Radio Science Meeting, Montreal, Qc, 2020.

[C6] M. E. El Azhari, L. TaIbi and M. Nedil, " K-factor and Correlation Analysis of a 2×2 MIMO Off-body Channel Inside a Mine," 2019 IEEE International Symposium on Antennas and Propagation & USNC/URSI National Radio Science Meeting, Atlanta, Ga, 2019.

[C7] M. E. El Azhari, L. TaIbi and M. Nedil, " Comparative study of Four Path Loss Models for UWB off-body Propagation Channel Inside a Mine," 2019 IEEE International Symposium on Antennas and Propagation & USNC/URSI National Radio Science Meeting, Atlanta, Ga, 2019.

[C8] M. E. El Azhari, L. TaIbi and M. Nedil, "UWB Off-Body Channel Characterization in a Mine Environment," 2018 IEEE International Symposium on Antennas and

Propagation & USNC/URSI National Radio Science Meeting, Boston, MA, 2018, pp. 559-560.

[C9] V. A. Fono, L. Talbi and M.E. El Azhari, "Comparative study of three Deterministic Radio Propagation Models in a Complex media," 2018 IEEE International Symposium on Antennas and Propagation & USNC/URSI National Radio Science Meeting, Boston, MA, 2018, pp. 1333-1334.

[C10] M.E. El Azhari, L. Talbi, M. Nedil and I. BenMabrouk, "NLOS Capacity and Time dispersion of a Multipath Fading MIMO Channel Using Directive Antennas in an Underground WBAN Application" IEEE/APS 2017.

[C11] M. E. El Azhari, L. Talbi, M. Nedil and I. BenMabrouk, "Impact of NLOS on the Path Loss and Channel Capacity of a MIMO Off-body System Inside a Mine " IEEE/APS2017.

[C12] L. Arabi, M.E. El Azhari, L. Talbi, M. Nedil and S. M. Lamine, "2.4 GHz Radio-Channel Characterization of an Underground Mine using Patch antennas," IEEE/APS2017.

[C13] L. Arabi, M.E. El Azhari, L. Talbi, M. Nedil and S. M. Lamine, “Radio-Channel Characterization of an Underground Mine using Circularly polorized antennas at 2.4 GHz " IEEE/APS2017.

[C14] M.E. El Azhari, M. Nedil, I. BenMabrouk and L. Talbi, "Multipath effect on off-body channel parametters of a MIMO system using patch antennas inside a mine," 2016 IEEE International Symposium on Antennas and Propagation (APSURSI), Fajardo, 2016, pp. 1693-1694.

[C15] M.E. El Azhari, M. Nedil, I. BenMabrouk and L. Talbi, "Path loss effect on off-body channel capacity of a MIMO system using patch antennas inside a mine," 2016 IEEE International Symposium on Antennas and Propagation (APSURSI), Fajardo, 2016, pp. 1697-1698.

[C16] A. Habani, M. Nedil, M.E. El Azhari and F. Ghanem, "High gain off-body antenna based on combination AMC-FSS structure for underground mining communications," 2016 IEEE International Symposium on Antennas and Propagation, Fajardo, 2016, pp. 267-268.

[C17] M.E. El Azhari, M. Nedil, and I. BenMabrouk, "Characterization of an on-body quasi-static channel in underground mine environment," 2015 IEEE Antennas and Propagation Society International Symposium (APSURSI), Jul. 18-25, 2015.

[C18] M.E. El Azhari, M. Nedil, I. BenMabrouk, L. Talbi, and K. Ghanem, “Off-body LOS and NLOS channel characterization in a mine environment,” International Conference on Electrical and Information Technologies (ICEIT), Marrakesh, Morocco, 2015.

1.6 References

[1] M.E. El Azhari, M. Nedil, I. BenMabrouk, K. Ghanem, and L. Talbi, "Characterization of an off-body channel at 2.45 GHz in an underground mine environment," Progress In Electromagnetics Research M, Vol. 43, 91-100, 2015.

[2] A.E. Forooshani, S. Bashir, D.G. Michelson and S. Noghanian, "A Survey of Wireless Communications and Propagation Modeling in Underground Mines," Communications Surveys & Tutorials, IEEE , vol.15, no.4, pp.1524,1545, Fourth Quarter 2013.

[3] L. Mo and Y. Liu, “Underground Coal Mine Monitoring with Wireless Sensor Networks” ACM Transactions on Sensor Networks, March 2009, Vol. 5.

[4] I. BenMabrouk, L. Talbi, M. Nedil, and K.Hettak, “MIMO-UWB Channel Characterization Within an Underground Mine Gallery”, IEEE Transactions on Antennas and Propagation, vol. 60, pp. 4866- 4874, Oct. 2012.

[5] I. BenMabrouk, L. Talbi, M. Nedil, "Performance evaluation of a MIMO system in underground mine gallery", IEEE Antennas Wireless Propag. Lett., vol. 11, pp. 830-833, 2012

[6] A. Arvanitis, G. Anagnostou, N. Moraitis, P. Constantinou, "Capacity study of a multiple element antenna configuration in an indoor wireless channel at 60 GHz", Proc. IEEE 65th Vehicular Tech. Conf., pp. 609-613, 2007-Apr.

[7] B. Mnasri, M. Nedil, N. Kandil, L. Talbi, and I. BenMabrouk, "Experimental characterization of wireless MIMO channel at 5.8 GHz in underground gold mine," Progress In Electromagnetics Research C, Vol. 36, 169-180, 2013

[8] I. BenMabrouk, L. Talbi, M. Nedil, Y. Coulibaly and T. A. Denidni, "Effect of antenna directivity on performance of multiple input multiple output systems in an underground gold mine," in IET Microwaves, Antennas & Propagation, vol. 6, no. 5, pp. 555-561, April 12 2012

[9] B. Mnasri, " Caractérisation d'un canal de propagation souterrain en utilisant la technologie MIMO et le traitement dans le domaine angulaire", Master thesis, Université du Québec en Abitibi-Témiscamingue, 2013. [Online]. Available : http://depositum.uqat.ca/626/1/Elazhari,%20Moulay%20Elhassan.pdf

[10] M. Ghaddar, M. Nedil, I. BenMabrouk and L. Talbi, "Multiple-input multiple-output beam-space for high-speed wireless communication in underground mine," in Microwaves, Antennas & Propagation, IET , vol.10, no.1, pp.8-15, 1 9 2015.

[11] Z. Sun and I. F. Akyildiz, “Channel Modeling and Analysis for Wireless Networks in Underground Mines and Road Tunnels,” IEEE Transactions On Communications, Vol. 58, No. 6, June 2010.

[12] S. Wang, “Radio wave attenuation character in the confined environments of rectangular mine tunnel,” Modern Applied Science,vol. 4, no. 2, pp. 65–70, 2010.

[13] Y. Huo, Z. Xu, H. D. Zheng, and X. Zhou, “Effect of antenna on propagation characteristics of electromagnetic waves in tunnel environments,” in Microelectronics Electronics, 2009. PrimeAsia 2009. Asia Pacific Conference on Postgraduate Research in, 2009, pp. 268-271.

[14] Chenming Zhou, Timothy Plass, Ronald Jacksha, and Joseph A. Waynert, “RF Propagation in Mines and Tunnels: Extensive measurements for vertically, horizontally, and cross-polarized signals in mines and tunnels,” IEEE Antennas & Propagation Magazine, August 2015.

[15] A.E. Forooshani, S. Bashir, D.G. Michelson, S. Noghanian, "A Survey of Wireless Communications and Propagation Modeling in Underground Mines," Communications Surveys & Tutorials, IEEE , vol.15, no.4, pp.1524,1545, Fourth Quarter 2013.

[16] C. Briso-Rodriguez, J. M. Cruz and J. I. Alonso, "Measurements and Modeling of Distributed Antenna Systems in Railway Tunnels," in IEEE Transactions on Vehicular Technology, vol. 56, no. 5, pp. 2870-2879, Sept. 2007.

[17] K. Guan, Z. Zhong, J. I. Alonso and C. Briso-Rodriguez, "Measurement of Distributed Antenna Systems at 2.4 GHz in a Realistic Subway Tunnel Environment," in IEEE Transactions on Vehicular Technology, vol. 61, no. 2, pp. 834-837, Feb. 2012.

[18] I. Khan, “Diversity and MIMO for body-centric wireless communication channels”, PhD thesis report, University of Birmingham, September 2009.

[19] S. R. Saunders, Antennas and Propagation for Wireless Communication Systems. Editor John Wiley, & Sons, 1999.

[20] M.E. El Azhari, L. Talbi, L. Arabi, M. Nedil, M. L. Seddiki, and N. Kandil, “Channel Characterization of Circularly Polarized Antenna MIMO System in an Underground Mine,” Progress In Electromagnetics Research M, Vol. 67, 9-19, 2018.

[21] Y. S. Cho, J. Kim, W. Y. Yang, and C. G. Kang, MIMO-OFDM wireless communications with MATLAB. Ed. John Wiley & Sons, 2010.

[22] M.E. El Azhari, L. Talbi, and M. Nedil, “Body- to-Body Channel Characterization and Modeling Inside an Underground Mine,” To appear in *IEEE Transactions on Antennas and Propagation*, 2020.

Chapter 2 Overview of channel characterization

A system (that could be linear or non-linear) is described by a block having at least one input and at least one output. Communication systems which have the objective of transmitting the information between a transmitter and a receiver could be described in the same way. The information sent through a communication system is modified due to the effect of the medium, which we describe by the word channel. This channel is generally presented by its functional diagram as seen in Fig. 2.1. In fact, prior to reaching the receiving antenna, a transmitted signal undergoes a filtering effect caused by the propagation channel. The filtering nature of the channel is caused by the summation of the multiple arriving waves amplitudes and phases at any instant of time [1]. When a static channel exhibits little or no changes over time, it can be considered as a linear time invariant filter having an impulse response h(t). The equivalent filter will be varying over time, when the channel varies over time, due to the mobility of the transmitters and receivers.

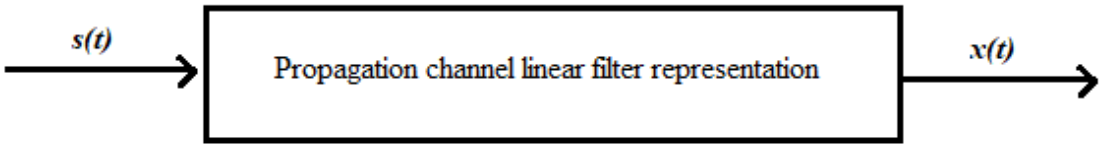

Fig. 2.1. Propagation channel linear filter representation [1]

The transmitted and the received baseband signals are related by the well-known simple convolution:

$$x(t)=h(t)\otimes s(t) \tag{2.1}$$

where h(t) and s(t) are respectively the impulse response of the propagation channel and the input signal.

The time invariant channel input response is denoted by the following formula [1]:

$$h(t) = \sum_{i=0}^{N} a_i e^{-j\theta_i}\, \delta(t - t_i) \tag{2.2}$$

Where a_i and θ_i are the amplitude and phase of the i^{th} arriving multipath component; δ is the Kronecker delta function. Practically, a short duration probing pulse is used instead of the theoretical delta function. The propagation channel is described by its impulse response h (t) where t denotes the time of the various paths of the transmitted signal.

When frequency measurements methods are adopted, the channel impulse response h(t) is acquired using the Inverse Fourier Transform (IFT) of the measured channel frequency responses. Fig. 2 shows an example of the impulse responses and the frequency responses for off-body channels at UWB, which reveal the multipath richness and the fading affecting the received signal [2].

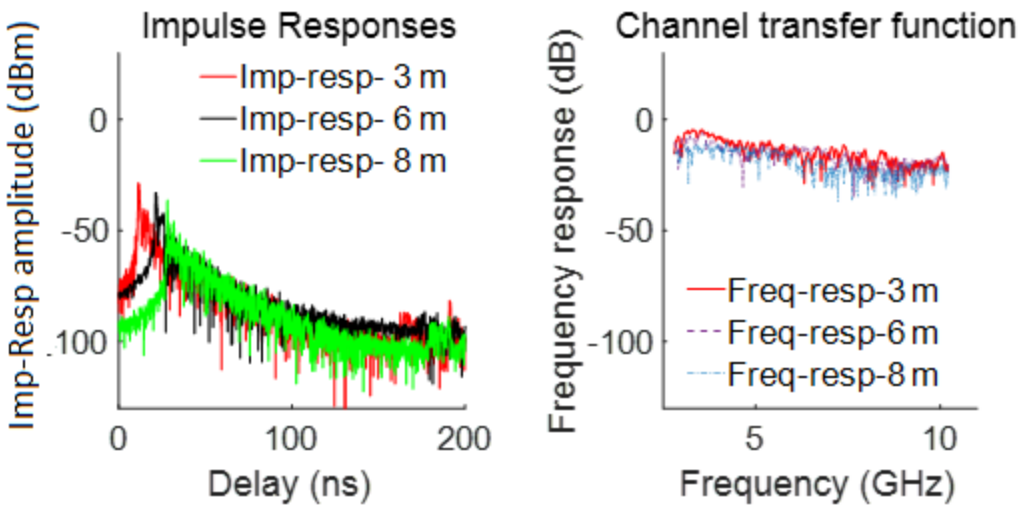

Fig. 2.2. Impulse and frequency responses for three off-body measurements distances: (3 m, 6 m and 8 m) at UWB [2]

There exist two important channel properties that can be characterized: large-scale and small-scale channel characterizations, as detailed in subsequent sections.

2.1 Large-scale channel characterization

Large-scale channel characterization consists of path loss (PL) and shadowing effects. In addition to free-space loss, depending on the frequency of operation, the channel may endure additional losses due to oxygen absorption and rain attenuation [3]. This poses a severe challenge in delivering a gigabit wireless transmission with reliable link margin.

Shadowing signifies the average signal power received over a large area (a few tens of wavelengths) due to the dynamic evolution of propagation paths, whereby new paths arise and old paths disappear [3].

2.1.1 Path loss

The path loss (*PL*) is defined as the difference (in dB) between the effective transmitted power and the received power [1]. It is obtained from the path gains, by averaging over the frequencies, snapshots and the number of antennas, and is mathematically represented as follows [4]:

$$PL_{dB} = 20\text{Log}10\ (\xi\ \{H_{x,y,f}\}) \tag{2.3}$$

where *PL* or PL_{dB} is the path loss at a certain position, $H_{x,y,f}$ is the spatial sub-channel path strength at a given frequency and ξ is the averaging operator over all receiving antennas, transmitting antennas, frequencies, and snapshots [4].

When expressed in terms of the Tx-Rx distance, the path loss is modeled as follows [6]:

$$PL(d) = PL_{dB}(d_0) + 10.\alpha.log_{10}\left(\frac{d}{d_0}\right) + X \tag{2.4}$$

where $PL_{dB}(d_0)$ is the mean *PL* at the reference distance d_0, d is the distance where the *PL* is calculated, α is the path loss exponent (obtained using least square linear regression), and X is a zero mean Gaussian random variable (in dB) representing shadowing [4].

2.2 Small-scale channel characterization

Small-scale channel characterization consists of small scale fading which is caused by the multipath signals that arrive at the receiver with random phases that add either constructively or destructively. Small-scale fading causes rapid changes in signal amplitude over a small distance (less than 10 wavelengths). Over this small local area, the

small-scale fading is approximately superimposed on the constant large-scale fading, as seen in Fig. 2.3.

The small-scale fading caused by the multipath components manifests in the following ways [1]:

- Steep fluctuations in the received signal through small distance intervals.
- Random frequency shifts due to the Doppler Effect on the different multipath signals.
- Time dispersion caused by the different multipath delays.

Small scale fading is especially of importance in urban area, tunnels, and galleries, where the direct LOS is not always present, and the environment is rich in reflectors and scattering objects. Even in the presence of a LOS, the reflections from ground and other objects will cause multipath propagation. There are several physical factors which may affect the small-scale fading [1].

- Multipath propagation caused by the presence of reflecting or scattering objects and in the channel. As a result, multiple replicas of the signal arrive at the receiver with different delays. The different multipath signals have random phases and amplitudes. When combining at the receiver, they result in random fluctuations in the received signal strength.
- The relative motion between the transmitter and the receiver will result in random frequency shifts of the multipath components due to the Doppler Effect.

- The movement of the surrounding objects will induce a time varying Doppler shifts in the multipath signals contributing to the small-scale fading.
- The limited channel coherence bandwidth will cause a distortion in the received signal (if the coherence bandwidth is lower than transmitted signal bandwidth).

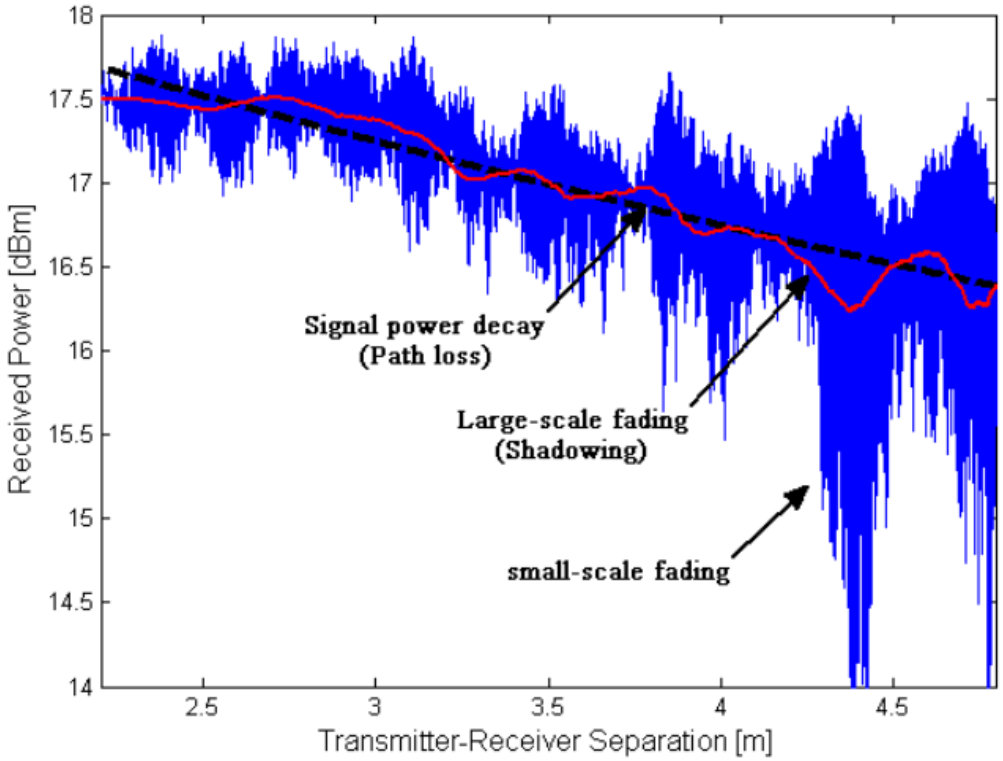

Fig. 2.3. Example of signal propagation in an indoor environment highlighting the types of fading [5].

2.2.1 Rican K-Factor

The Rician K-factor is an indication of link quality [4], measured as the relative strength of the direct and scattered components of the received signal, as expressed in the following equation [5]:

$$\boldsymbol{K = \frac{P_D}{2P_R}} \tag{2.5}$$

where P_D corresponds to the power of the LOS component and $2P_R$ is the power of the reflected, diffracted, or diffusely scattered components.

2.2.2 Time dispersion parameters

The time dispersion parameters are determined from the power delay profile (PDP), which represents the power received in the time domain.

The RMS delay spread and the coherence bandwidth are determined using equations (2.6) and (2.7) respectively, as follow [1]:

$$\tau_{RMS} = \sqrt{\overline{\tau^2} - \bar{\tau}^2} \tag{2.6}$$

where $\bar{\tau}$ denotes the mean excess delay and $\overline{\tau^2}$ is the second moment of the PDP. The coherence bandwidth is represented as follows:

$$B_c \simeq \frac{1}{5\tau_{RMS}} \tag{2.7}$$

2.3 References

[1] T. S. Rappaport, “Mobile Radiop Propagation: Small scale Fading and Multipath,” in Wireless communications: principle and practice, 2nd ed, Prentice Hall, 2001.

[2] M. E. Azhari, L. TaIbi and M. Nedil, " Comparative study of Four Path Loss Models for UWB off-body Propagation Channel Inside a Mine," 2019 IEEE International Symposium on Antennas and Propagation & USNC/URSI National Radio Science Meeting, Atlanta, Ga, 2019.

[3] Su-Khiong Yong, Pengfei Xia, Alberto Valdes-Garcia, "60 GHz technology for Gbps \VLAN and WPAN, from theory to practice," John Wiley & Sons Ltd, 2011, pp.3-61.

[4] I. BenMabrouk, L. Talbi, M. Nedil and K. Hettak, “MIMO-UWB Channel Characterization Within an Underground Mine Gallery,” IEEE Transactions on Antennas and Propagation, Vol. 60, No. 10, pp. 4866-4874, Oct. 2012.

[5] Mohamad Ghaddar, “Experimental Characterization and Modeling of Short-Range Wireless Propagation Channels in the Unlicensed 60 GHz Band”, PhD thesis, Université du Québec en Outaouais, 2012.

Chapter 3 Overview of MIMO systems and diversity schemes

Diversity is a method aiming to improve the reliability of a communication system by using multiple communication channels to send or receive information [1]. It is a well-known technique known to combat fading and co-channel interference and improves the bit error rate [1, 2]. Diversity techniques improve the gain and capacity of the system benefitting from the fact that different channels undergo different levels of fading and interference. The multipath richness is exploited to improve the diversity gain. The general idea is to use multiple uncorrelated branches with statistically independent fading characteristics. The fading on the individual channels will be independent due to the different channel conditions, when the different channels are sufficiently separated in time, frequency, space, radiation pattern, and / or polarization. Hence, the SNR can be improved due to the deep fades reduction, with proper combining of the branches [1]. Fig. 3.1 denotes an example of diversity at the reception.

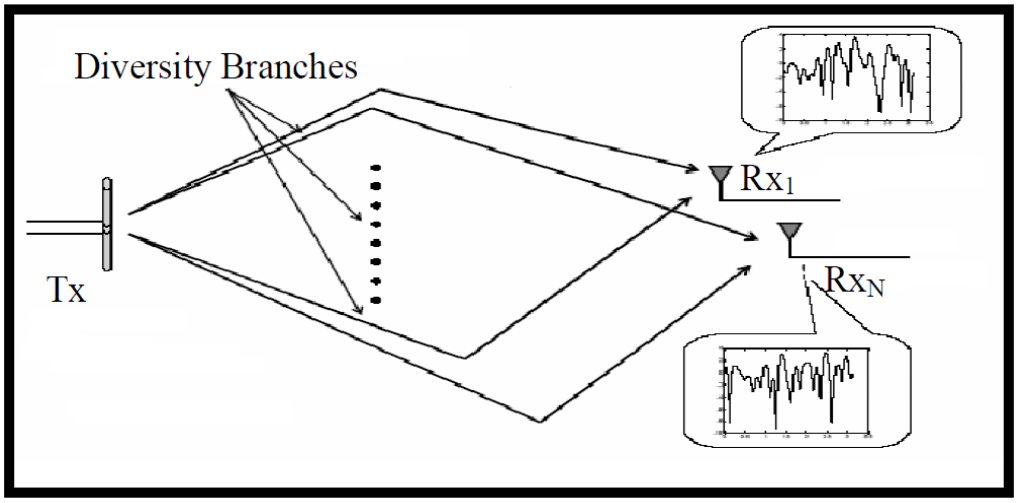

Fig. 3.1. Diversity at the reception [1].

3.1 Diversity techniques

Diversity techniques are used to mitigate fading based on the following principle: the probability that several independent sub-channels simultaneously suffer from strong fading is very low. These techniques are, therefore, intended to improve the quality of the communication link and could take various forms such as the following [3]:

- Spatial diversity: Antennas separated by a sufficiently large distance, allow the creation of independent sub-channels. The same information can thus be sent on the different propagation channels. Antennas spacing of half wavelength is usually considered suitable for most of the applications [1].
- Time diversity: The same information is transmitted over different time slots, separated by a time interval greater than the coherence time of the channel (which statistically quantifies the time duration where the channel impulse response is considered unchanged).

- Frequency diversity: The same information is transmitted (in redundancy) on different frequency bands separated by a frequency range greater than the coherence bandwidth.
- Angle Diversity: Several receiving antennas with different directivities allow receiving different versions of the same signal at different angles.

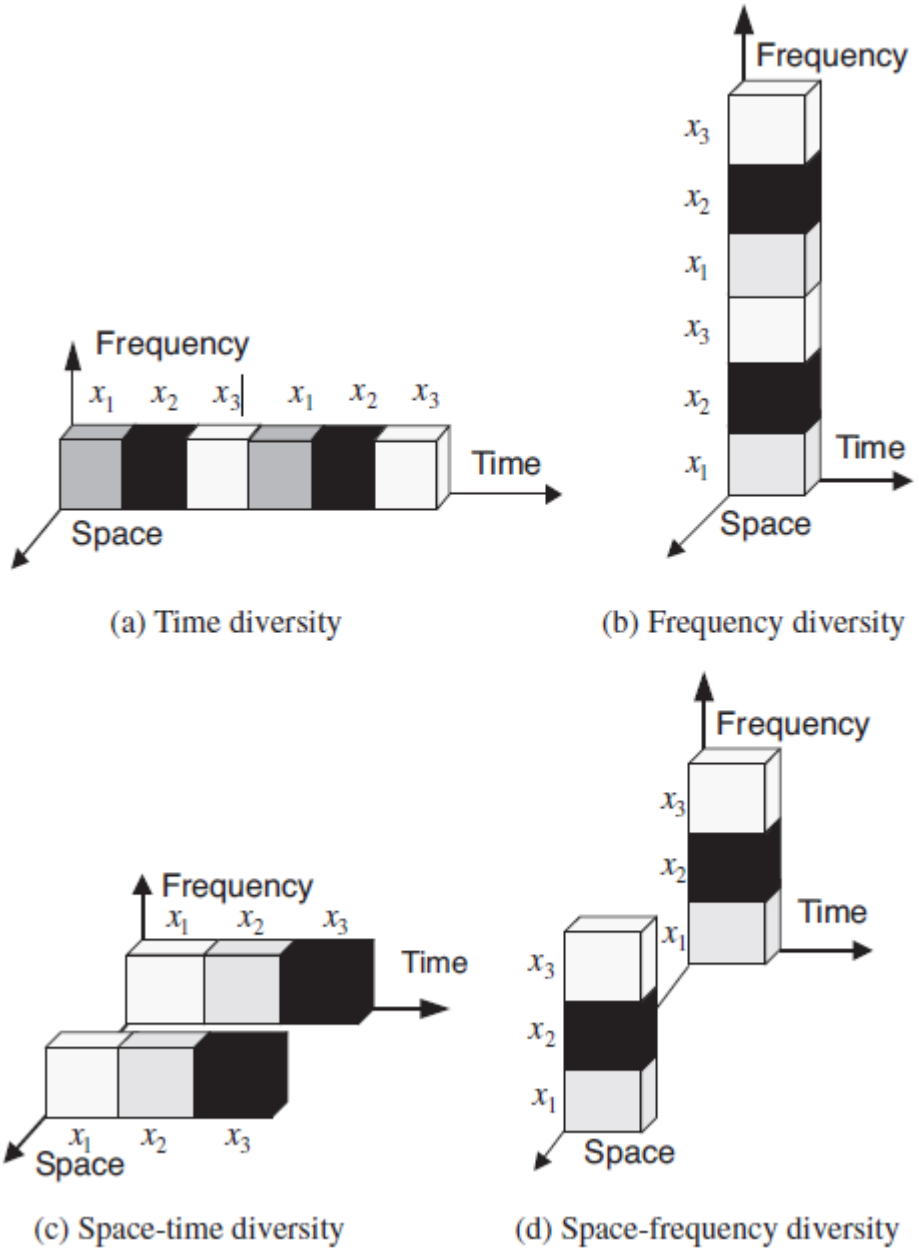

Fig. 3.2. Graphical representation of time, frequency, and spatial diversity methods. [3]

3.2 Antenna diversity

As described above, antenna diversity (also known as spatial diversity) uses two or more antennas at the transmission or/and at the reception to improve the wireless link quality and reliability, by exploiting the multipath richness of the environment. It is mainly effective in urban and indoor environments where there is rarely a clear line-of-sight (LOS) [1]. The multipath components usually exhibit phase shifts, time delays, attenuations, and distortions and can destructively interfere with one another at a receiver. Spatial diversity, because of its inherent multi-view of the received signal, is effective at mitigating these multipath issues. In fact, the signal will fade differently at each antenna. Thus, if one antenna experiences a deep fade, it is unlikely that the other antennas will behave in the same manner. Hence, the overall performance of the link is improved [1]. In order to understand antenna diversity, the systems in Fig. 3.3 are presented. A system with single antenna at the receiver and at the transmitter is referred to as Single-Input Single-Output (SISO) system. Single-Input Multiple-Output (SIMO) systems, also referred to as receive-diversity systems, use multiple antennas for reception. Multiple-Input Single-Output (MISO) systems, also called transmit-diversity, use multiple antennas at the transmission. The Multiple Input-Multiple Output (MIMO) systems use multiple antennas for both the transmission and the reception. These systems differ upon complexity and capacity performance. SIMO systems are characterized by an additional cost and complexity at the receiver compared to a SISO system. In the MISO systems, this complexity (and cost) is isolated at the transmitter side, while the receiver has a single antenna, which is usually cheaper than implementing diversity at the receiver. In terms of channel capacity, SIMO

systems outperform MISO [9]. Fig. 3.4 represents the classification of the communications systems according to the number of antennas at the transmission and the reception.

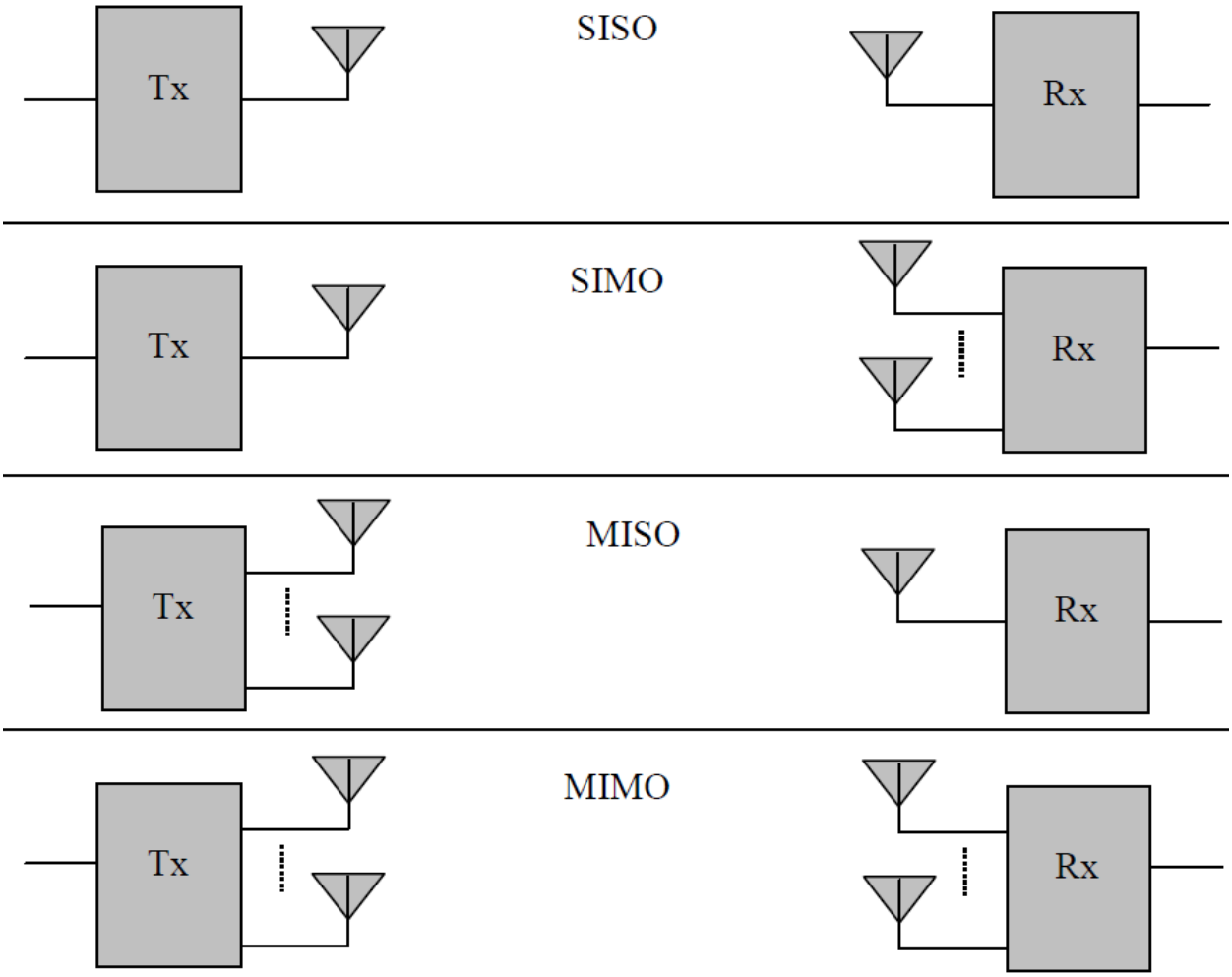

Fig. 3.3. Communication system classification based on number of antennas [1]

MIMO techniques are known to significantly improve the reliability of wireless systems by lowering the bit error rate (BER), improving the signal to noise ratio, and enhancing the capacity of the system. This could be achieved through diversity which proved to be powerful in lowering fading. Diversity provides the best results when the fading at the different branches is uncorrelated and the branch signals have the same average power [1].

In general, it is demonstrated that MIMO systems have the ability to turn multipath propagation, traditionally a disadvantage of wireless transmissions in a benefit to the user. They benefit from the random fading and the multipath to expand transfer rates [1-2].

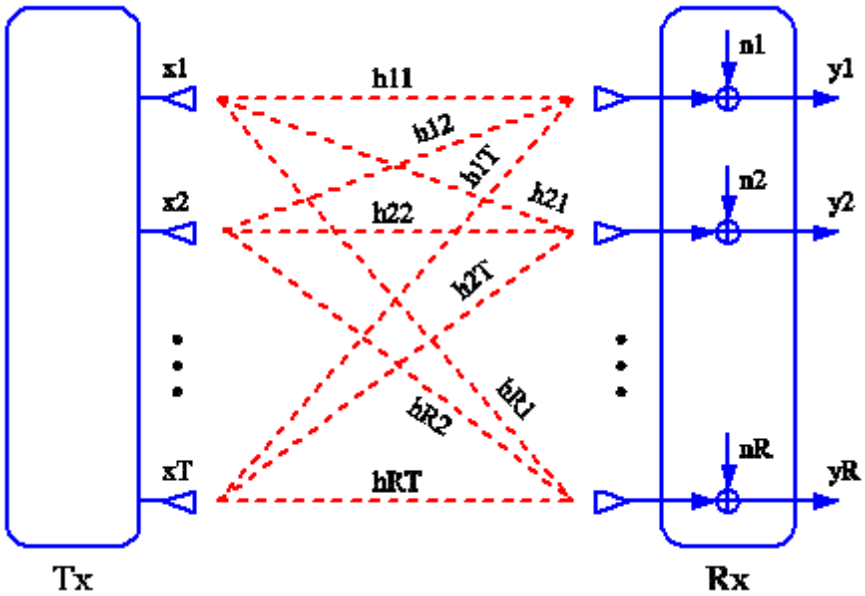

Figure 3.4. Block diagram of a MIMO system [5]

3.3 Diversity Gain

The improvement due to the use of diversity could manifest in terms of SNR, signal strength, or bit error rate (BER), over a single antenna with no diversity at a certain level of outage probability [1]. It is expressed by what is called diversity gain (DG), which is commonly calculated as the difference between the diversity combined signal power (in dB) and a reference signal (the strongest branch signal at some outage probability), as denoted by (3.1) [1].

$$DG = P_{div} - P_{ref} \quad \text{(dB)} \tag{3.1}$$

where P_{div} is the power level of the diversity combined signal and P_{ref} is the power level of the reference signal.

3.4 Multiplexing gain

While spatial diversity aims to improve the link quality, the purpose of using the multiplexing techniques is to increase throughput [6]. In this case, each spatial channel carries independent information, thereby increasing the data rate of the system. In spatial multiplexing, if the scattering by the environment is rich enough, multiple parallel channels are created in the same allocated bandwidth. Hence, the multiplexing gain is achieved without increasing the bandwidth nor the transmission power. It was demonstrated that for a system with m transmitting antennas and n receiving antennas, the number of parallel channels is the minimum of n and m, hence providing spatial multiplexing gain of *min(n,m)* over a SISO system [1]. This, however, comes with a significant complexity in the signal processing for adequate data stream recovery at the receiver.

3.5 MIMO matrix

The MIMO input-output relationship between m transmit and n receive antennas is described by the following equation [7]:

$$Y = H \times X + N \tag{3.2}$$

where X is the [m × 1] transmitted vector, Y is the [n × 1] received vector, N is the receive additive white Gaussian noise (AWGN) vector, and H is the n × m channel matrix which for the case of the 2×2 MIMO considered channel is reduced to

$$H = \begin{bmatrix} h_{11} & h_{12} \\ h_{21} & h_{22} \end{bmatrix} \tag{3.3}$$

where h_{ij} is the complex random variable that represents the complex sub-channel gain from the ith transmitting antenna to the jth receiving antenna. In RF measurements, the values of the parameters S_{21} correspond to the different h_{ij} values.

3.6 Correlation of the branch signals

The branch signals correlation greatly affects the performance of a MIMO receiver. When this correlation is low, the different branch signals fade differently, allowing an increase in the ergodic capacity at the receiver [7]. For most of the mobile communication scenarios, correlation coefficient of 0.7 is considered suitable [1]. One useful measure of the branch correlation is the complex signal correlation coefficient ρs, which contains both the phase and amplitude correlation.

$$\rho_S = \frac{\sum_{i=1}^{N} V_1(i)\, V_2{}^*(i)}{\sqrt{\sum_{i=1}^{N} V_1(i)\, V_1{}^*(i)}\sqrt{\sum_{i=1}^{N} V_2(i)\, V_2{}^*(i)}} \tag{3.4}$$

where V1 and V2 represent the zero-mean complex voltage signals of port 1 and 2, respectively and N is the total number of samples [7].

3.7 MIMO channel capacity

The channel capacity is a measure of the theoretical maximum data rate per unit of bandwidth that can be reliably transmitted through a certain channel [8].

In general, the MIMO channel capacity is used to measure the performance of the MIMO link taking in consideration the effect of the SNR and the multipath richness.

Channel ergodic capacity for a regular SISO configuration is calculated using the well-known Shannon formula [8]:

$$C_{SISO}[bps/Hz] = log_2(1 + \rho|H|^2). \quad (3.5)$$

where H is the normalized channel response and ρ is the average SNR. Similarly, the channel capacity with MIMO configuration is computed using the following formula [8]:

$$C_{MIMO}\left[\frac{bps}{Hz}\right] = log_2\left(\det\left[\boldsymbol{I}_n + \frac{SNR_{av}}{m}\boldsymbol{H}\boldsymbol{H}^*\right]\right) \quad (3.6)$$

Where H is the normalized m × n channel response (m ≥ n), SNR_{av} is the average signal to noise ratio, $\boldsymbol{I}_n$is the n × n identity matrix, and * represents the complex conjugate transpose. In general, H matrix is normalized such that at each realization, the square of its Frobenius norm is equal to the product of its dimensions ($\|H\|_F^2 = nm$) [8].

The Frobenius normalization method allows investigating the multipath richness of the environment [8]. While the fading envelope of the WBAN channels ideally follows a Rayleigh distribution (when subchannels of the MIMO system are independent and identically distributed (iid)), it has been reported that for practical systems, the fading envelope is Rician distributed (especially in the presence of a strong LOS component) [1]. The capacity increase in Rician fading channels depends in the offered degree of decorrelation as well as the SNR [1], as clearly demonstrated by the achieved results in subsequent chapters.

3.8 References

[1] Imdad Khan, "Diversity and MIMO for body-centric wireless communication channels", PhD thesis report, University of Birmingham, September 2009.

[2] T. S. Rappaport, "Mobile Radiop Propagation: Small scale Fading and Multipath," in Wireless communications: principle and practice, 2nd ed, Prentice Hall, 2001.

[3] Y. S. Cho, J. Kim, W. Y. Yang, and C. G. Kang, MIMO-OFDM wireless communications with MATLAB: John Wiley & Sons, 2010.

[4] J.Gong, J.F.Hayes and M.R.Soleymani, “Comparison of Capacities of the Transmit Antenna Diversity with the Receive Antenna Diversity in the MIMO Scheme”, in Proc. IEEE CCECE, May 4–7, 2003, vol. 1, pp. 179–182.

[5] Bilel Mnasri, “Caractérisation d'un canal de propagation souterrain en utilisant la technologie MIMO et le traitement dans le domaine angulaire”, Master thesis, Université du Québec en Abitibi-Témiscamingue, 2013.

[6] Y. Hongwei, "A road to future broadband wireless access: MIMO-OFDM-Based air interface," IEEE Communications Magazine, vol. 43, pp. 53-60, 2005.

[7] I. Khan, P.S. Hall, "Experimental Evaluation of MIMO Capacity and Correlation for Narrowband Body-Centric Wireless Channels," Antennas and Propagation, IEEE Transactions on , vol.58, no.1, pp.195-202, Jan. 2010.

[8] M.E. El Azhari, M. Nedil, I. Benmabrouk, K. Ghanem, and L. Talbi, "Characterization of an off-body channel at 2.45 GHz in an underground mine environment," Progress In Electromagnetics Research M, Vol. 43, 91-100, 2015.

Chapter 4 WBAN systems

In Body-Centric communications, the human body is used as a supporting medium for communication between two or more devices on or around the body [1]. The Wireless Body Area Network (WBAN) signal is deteriorated by the presence of the human body, with skin, tissues, muscle, and bones each having its own electrical properties affecting the propagating signal. In WBAN, the signal, might be reflected or diffracted by the surface of the body. At microwave frequencies or higher, the signal can attach to the body as a creeping wave. The propagating creeping wave signal may be severely deteriorated by the body movement. Moreover, there generally exists multipath propagation due to multiple propagation paths around the body and due to reflections from the surrounding environment and the body parts. Additionally, at microwave and millimeter frequencies, the propagation through the body is either null or negligible, because the skin depth is greatly reduced as the frequency increases. Consequently, in WBAN systems, there exist two main forms of EM waves propagation, namely, creeping wave communication and multipath propagation (due to reflection and diffraction).

4.1 Application areas of WBAN

WBAN found applications in the industrial, entertainment, sport, and medical fields. Among the examples of this technology are wearable RFID tags and medically oriented body-worn sensors. Application areas for the WBAN technology also include: security,

police, fire fighters, personal identification, fashion, and personalized communications. In the last few years, the mining field got increasingly interested in WBAN as a technology dedicated for the miners safety. Several companies are already developing underground WBAN security systems such as the collision awareness and the miner localization systems (offered by Meglab Inc. and Beckers Inc.).

4.2 WBAN studies in underground mines

Although there is a serious tendency in implementing wireless communication systems in underground mines, the studies of WBAN propagation inside a mine are still at their early stages. Previous studies concerned the channel characterization of on-body and off-body systems at the 2.4 GHz band [1, 2]. The focus was to characterize the MIMO-WBAN channel as compared to the SISO counterpart. The effect of directivity was also emphasized through the comparison between the monopole and patch antenna setups [1, 3, 4]. In addition, the multipath richness effect on the MIMO capacity was discussed through the study of the Rican K-factor and RMS delay spread at both LOS and NLOS [3, 5]. The effect of the path loss on the channel capacity was also quantified for LOS and NLOS [4, 6]. The UWB channel was explored for underground applications in [1]. Finally, different models, for PL [7] and impulse response [8], were developed for underground WBAN applications.

4.3 Measurement techniques

Radio channel characterization requires the analysis of a large number of propagation measurements. In order to carry out a measurement campaign, two measurement techniques are available, frequency and time techniques. In this section, we will present a description of these technologies, their advantages and disadvantages, as well as the system of measurements, the scenarios and the used equipment.

4.3.1 Time domain measurement methods-impulse response

Time domain measurements techniques consist in determining the impulse response of the system, which is represented for a slowly varying system as:

$$h(\tau) = \sum_{n=1}^{N} a_n \, e^{-j\theta_n} \gamma \, (\tau - \tau_n) \qquad (4.1)$$

where τ_n is the time delay, a_n is the magnitude and θ_n is the phase characterizing the individual paths between the transmitter (Tx) and the receiver (Rx) [10].

In time domain measurements, the impulse response is determined through the transmission of a short RF pulse and observing the receiver for the different received paths. In practice, a stream of pulses with a low duty cycle and a high peak to average power ratio are transmitted. Time resolution is inversely proportional to the bandwidth of the measurements system. A Digital Sampling Oscilloscope (DSO) is usually used at the reception. The main advantage of this technique lies in its low acquisition time, the impulse response being recovered in real time. However, this method also has several disadvantages. The generation of Short-term pulses require high power generation from the power amplifiers for a short time, followed by periods of inactivity. The low average power of this activity results in a low signal - to - noise ratio (SNR).

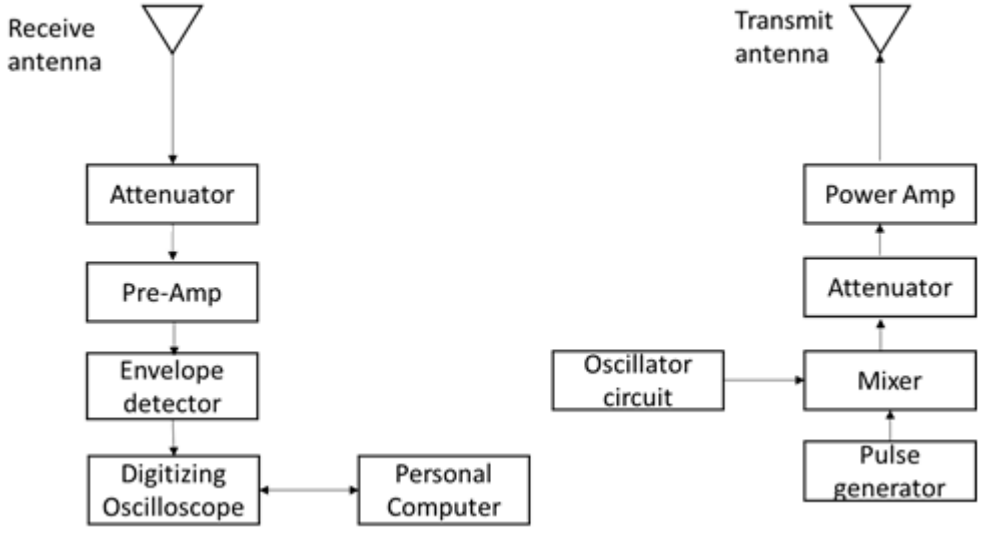

Figure 4.1. Simple pulse transmission measurement system used for wideband time-domain measurements of indoor radio propagation. [10]

4.3.2 Frequency-domain measurement methods

In this method, the measurement is carried out in the frequency domain by scanning the entire range of frequencies via a vector network analyzer (VNA). The purpose of the measurements is to extract the S parameters from the VNA; The S_{21} parameter represents the transmission coefficient between the transmitting and the receiving antenna. This technique makes it possible to measure the variations in amplitude and phase of the transmitted signal over the desired frequency range [11-12]. Fig. 9 represents the frequency-domain test set up [13]. At different frequency steps, the S-parameter test set transmits a known signal at port one and monitors the signal level at port 2. The frequency sweeper scans, in a discrete sense, a particular frequency band centered on the design frequency. The complex frequency response (S_{21} (f)) is determined and an inverse discrete Fourier transform (IDFT) is performed to get a band limited version of the impulse response [13].

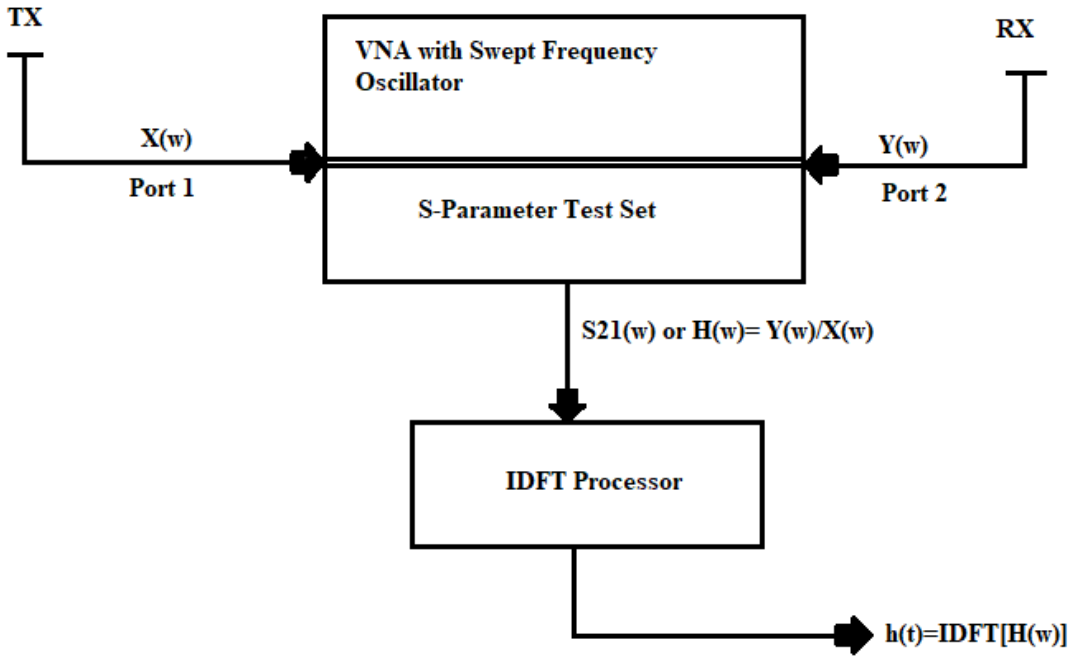

Figure 4.2. Frequency domain channel measurement system [13]

Among the properties of the frequency-domain measurement technique we have:

- It is easy to implement since VNA acts as a transmitter and a receiver at the same time.
- The calibration phase cancels the effects of all measurement components such as cables.
- It directly obtains the module and phase of the frequency response.
- Since the VNA is used as transceiver, this limits the Tx-Rx distance restricting the use of this technique in outdoor measurement scenarios.

4.4 References

[1] M.E. El Azhari, M. Nedil, I. BenMabrouk, K. Ghanem, and L. Talbi, "Characterization of an off-body channel at 2.45 GHz in an underground mine environment," Progress In Electromagnetics Research M, Vol. 43, 91-100, 2015

[2] M. El Azhari, M. Nedil, I. BenMabrouk, L. Talbi, K. Ghanem, and Y. S. Alj, "Performance evaluation of a MIMO-on-body system in a mine environment," Progress In Electromagnetics Research C, Vol. 61, 55-63, 2016.

[3] M. E. Azhari, M. Nedil, I. BenMabrouk and L. Talbi, "Multipath effect on off-body channel parametters of a MIMO system using patch antennas inside a mine," 2016 IEEE International Symposium on Antennas and Propagation (APSURSI), Fajardo, 2016, pp. 1693-1694

[4] M. E. Azhari, M. Nedil, I. BenMabrouk and L. Talbi, "Path loss effect on off-body channel capacity of a MIMO system using patch antennas inside a mine," 2016 IEEE International Symposium on Antennas and Propagation (APSURSI), Fajardo, 2016, pp. 1697-1698.

[5] M. E. Azhari, L. Talbi, M. Nedil and I. BenMabrouk, "NLOS Capacity and Time dispersion of a Multipath Fading MIMO Channel Using Directive Antennas in an Underground WBAN Application" IEEE/APS2017

[6] M. E. Azhari, L. Talbi, M. Nedil and I. BenMabrouk, "Impact of NLOS on the Path Loss and Channel Capacity of a MIMO Off-body System Inside a Mine " IEEE/APS2017

[7] M. E. Azhari, L. TaIbi and M. Nedil, "UWB Off-Body Channel Characterization in a Mine Environment," 2018 IEEE International Symposium on Antennas and Propagation & USNC/URSI National Radio Science Meeting, Boston, MA, 2018, pp. 559-560.

[8] M. E. Azhari, L. TaIbi and M. Nedil, " Comparative study of Four Path Loss Models for UWB off-body Propagation Channel Inside a Mine," 2019 IEEE International Symposium on Antennas and Propagation & USNC/URSI National Radio Science Meeting, Atlanta, Ga, 2019.

[9] M. El Azhari, L. Talbi, and M. Nedil, " Body- to-Body Channel Characterization and Modeling Inside an Underground Mine," IEEE Trans. Antennas Propag., 2020

[10] Kaveh Pahlavan, Allen H. Levesque "Wireless Information Networks" John Wiley & Sons, Nov 7, 2005 - Technology & Engineering

[11] K. Sarabandi, N. Behdad, A. Nashashibi, M. Casciato, L. Pierce, F. Wang, "A measurement system for ultra wide-band communication channel characterization," IEEE Transactions on Antennas and Propagation, vol. 53, Jul 2005, pp. 2146-2155.

[12] M. Moutairou, G. Y. Delisle, "Underground mines propagation channel characterization at UHF frequencies", International Conference on Wireless Communications in Unusual and Confined Areas (ICWCUCA), Clermont Ferrand, 28-30 Aug. 2012, pp. 1-5.

[13] M. E. Azhari, M. Nedil, I. BenMabrouk and L. Talbi, "Multipath effect on off-body channel parameters of a MIMO system using patch antennas inside a mine," 2016 IEEE International Symposium on Antennas and Propagation (APSURSI), Fajardo, 2016, pp. 1693-1694

Chapter 5 Body-to-Body Channel Characterization and Modeling

5.1 Abstract

In this paper, the use of circularly polarized multiple-input-multiple-output (MIMO) antenna systems is proposed as a new solution for future body-to-body (B2B) systems. Novel experimental characterization studies of four B2B channels- using linearly and circularly polarized 2×2 MIMO antennas- have been performed in an underground gold mine. The statistical parameters of the B2B channels using co-positioned (CP) and 90 degrees rotated (90R) antennas have been determined. Path loss (PL) exponent values varied between 2.33 and 1.26. The time dispersion parameters and channel capacities are computed and discussed for both CP and 90R scenarios. Moreover, channel correlation matrices and the Rician K-factor have been determined and discussed in terms of their effect on capacity and Root mean Square (RMS) delay spread. Overall, the circularly polarized setup exhibits the best performance in terms of PL, RMS delay spread and channel capacity. The NLOS situation caused a significant drop in channel capacity due to the significant increase in PL, and an increase in the RMS delay spread due to the multipath richness. When comparing to single-input sing-output (SISO) configurations, it is found that the MIMO-NLOS scenario exhibits the highest throughput gain of 1.752 (at an SNR of 20 dB), due to its low branch correlation. A model of the B2B impulse response has

been created based on a statistical-empirical approach, to determine the optimal path amplitudes and time of arrival.

5.2 Introduction

The human body is considered as a challenging environment for the wireless communication systems. In fact, the wireless body area networks (WBAN) channel is affected by the complex antenna-body electromagnetic interaction, body movement and the propagation characteristics of the local environment [1]. The characterization of the WBAN channel is of interest to an increasing number of research areas such as medical, military, sports and recreational applications [1]. For instance, a WBAN deployed to the medical field may use sensors to monitor life vitals, such as heart rate and body temperature. Similarly, in the mining field, vital signs, acceleration and proximity sensors (attached to the miners) could be used to improve the miners' safety and help coordinate mine rescue efforts when an accident occurs.

Motivated by an increasing pressure to improve in-mine communication systems, numerous studies have focused on underground channel characterizations and modeling. Hence, characterization studies have reported the channel properties for different frequency bands, diversity configurations and antenna selections under different environmental conditions [2-6]. BenMabrouk [7] studied the effect of NLOS on the signal propagation at UWB using Vivaldi antennas for two different MIMO configurations (parallel and 30 degrees antenna set up, where the antenna planes form 30 degrees angle). The 30 degrees MIMO antennas exhibited better branch correlation, PL exponent and channel capacity compared to the parallel setup. With regards to beamforming techniques, the Butler matrix,

was investigated in [8] for underground mining uses at 2.4 GHz. The beamforming module was found to improve the average channel capacity of a MIMO multipath channel (compared to a conventional uniform linear array). Moreover, the effect of directivity on the 2.4 GHz underground RF channel is studied in [9] for a point-to-point system and in [10-11] for an off-body system. It was found that the monopole-MIMO channel capacity is better than that of the patch-MIMO setup, in a mine environment for both point-to-point (without the effect of the body) and Off-body scenarios. The On-body channel in an underground mine for both static and dynamic topologies have been also studied [12]. The effectiveness of spatial diversity was confirmed for On-body channels at both static and dynamic scenarios.

With regards to WBAN channel models, Reusens et al. [13] presented a path loss (PL) model based on measurements of the static On-body channel for Tx-Rx separations of 5 to 40cm. It is often easier to use statistical approaches to analyze RF channels in a non-uniform environment such as the WBAN channel [14]. In fact, the geometry of the human body allows a multitude of signal path trajectories of similar lengths but different propagation mechanisms. This include the Line-Of-Sight (LOS), Non-Line-Of-Sight (NLOS) and creeping wave scenarios, which greatly affects the signal propagation. Hence, it is difficult to fit a general distance related path loss (PL) model to the data obtained for WBAN systems. Moreover, the peculiarity of the underground environment adds to the complexity of the WBAN channel and makes the received signal even more difficult to predict with reasonable accuracy [15]. Several approaches have been proposed to model PL for underground propagation channels. A Friis based statistical model has been investigated in [9-12] to derive the PL exponent through the linear regression analysis of

the PL results as a function of the logarithm of the distance. The dual-slope PL model is proposed in [16]. Other PL models use multiples breakpoints (three or more) to separate the areas characterized by different PL exponents, due to a major change in the geometry of the mine gallery [17]. The linear regression model seems suitable for WBAN studies because of its simplicity and accuracy, especially that propagation distances are generally small, compared to the point-to-point RF studies. Moreover, this model conveniently reveals crucial shadowing information [14].

As for the short-term fading channel models, which consist in developing a model for the impulse response, different models are presented in the literatures, such as the 2-ray model, the exponential model and the Saleh-Valenzuela (S-V) Channel Model [14]-[18]. They were adopted for indoor environments with different levels of accuracy, which usually compromises simplicity. The S-V Channel model is used when measurements indicate the presence of multiple clusters, while the 2-ray model is rarely accurate [14]-[18]. The exponential model is known to be appropriate for indoor channels [18]. In underground mines, stochastic and empirical approached have been experimented to model the path amplitudes and time of arrival [19]. These techniques avoid the complexity of deterministic models, which seems to be inaccurate in the presence of rough structures such as a mine [19]. They present the stochastic distributions that best describe the path amplitude and time of arrival. However, they failed to present an impulse-response channel model.

The design of an in-mine communication system requires carefully choosing the antenna characteristics. It is experimentally observed that the underground wireless communications suffer from some degree of depolarization due to the miners movement

and rough surfaces reflections [15]. Hence, communication quality could be significantly improved through the use of circularly polarized antennas, which radiate energy in both the horizontal and vertical planes and exhibit low polarization miss-match losses [15].

This work experimentally characterizes the body-to-body (B2B) channel using circularly polarized antennas and compares the results to those of a linear patch antenna. This part aims to study the effect of circular polarization on the MIMO-B2B channel in a mine environment. Moreover, the effect of antennas misalignment and that of NLOS are also studied. The different considered scenarios are summarized in Table 5.1.

In order to study the small-scale fading, the time dispersion parameters have been used and compared for both polarization scenarios. The channel capacity is then determined with two methods, namely at a constant SNR and at a fixed transmitting power, to study the effect of multipath components (MPCs) and that of the PL, as explained in [20]. The multipath richness is quantified using the Rican K-factor. Moreover, the branch correlations are determined and used to explain the MIMO throughput gain. The noise floor was deduced empirically by visually inspecting a set of impulse responses; a chosen value of -80 dBm is higher than the VNA sensitivity (-110 dBm) and the calculated thermal noise (about -114 dBm), which gives conservative SNR values. The large-scale fading is analyzed in terms of PL, which has been modeled with a simple PL exponent model using linear regression analysis. An impulse response channel model has been developed through empirical and statistical approaches in order to characterize the B2B channel.

To the best of the authors knowledge, no B2B channel characterization and modeling study was performed for in-mine applications. The novelty of this paper consists of four main contributions: First, the B2B channel characterization in a mine gallery is presented,

for the first time. Second, the circular polarization is compared to the linear one for B2B applications. Third, the co-positioned (CP) antennas scenario is compared to the 90 degrees rotated (90R) antennas one and LOS is compared to NLOS for the B2B channels. Fourth, a novel impulse response model based on statistical and empirical approaches was developed, which closely approximated a measurement-based channel impulse response.

The paper is organized as follows: Section II describes measurement procedure. Section III explains the experimental results. Finally, in Section IV, the paper is concluded.

Table 5.1. Studied scenarios

Polarization	Circular (Cir)			Linear (Lin)
Scenario	CP-LOS	90R-LOS	CP-NLOS	CP-LOS

5.3 Measurement procedure

5.3.1 Description of the Underground Mine

In a currently non-operating gold mine, located in Val d'Or city (in northern Quebec), a gallery at a depth of 90 m was used for the 2.4 GH measurements. This gallery is characterized by very rough surfaces, humidity nearing 100 %, temperature around 8 ° C and lots of dust particles. It stretches over a length of 20 m with a height of about 2.45 m and width of approximately 5 m. Water puddles, mining machines and ceiling implanted metal rods and nets are present along the gallery. This usual mine environment favors the multipath phenomenon due to reflection and diffraction from the rough surfaces.

Fig. 5.1. Photo of the mine gallery setup

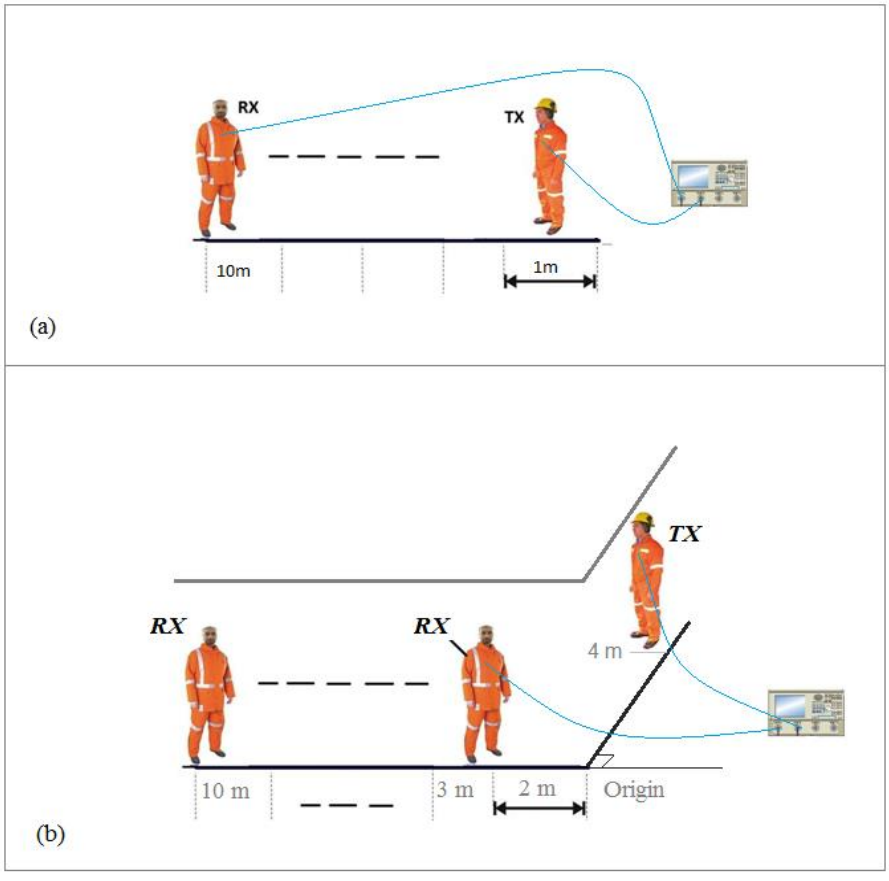

Fig. 5.2. Underground experiment setups for LOS (a) and NLOS (b) scenarios

5.3.2 Measurement setup

Two MIMO antenna systems, namely, a 2 × 2 MIMO circularly polarized (Cir) patch antenna system and a 2 × 2 MIMO linearly polarized (Lin) patch antenna system, are used in the measurements. The polarization plane for the linear setup is vertical. The two antennas have a gain of 6.6 dBi and an axial ratio (AR) less than 3 dB at 2.4 GHz. The spatial diversity antenna separation is equal to half of the wave length (λ/2). A Vector Network Analyzer (VNA) is used to measure the S parameters at the 2.3 GHz - 2.5 GHz band. During the measurements, the transmitting (Tx) and receiving (Rx) antennas were fixed on the chest of two students wearing a miner outfit, as illustrated in Fig. 5.1-5.2. The receiving human subject was displacing at 1 m steps from a starting position of 1 m to a final distance of 10 m for the LOS measurements. In the NLOS scenario, the receiving and transmitting human subjects were standing at two different mine tunnels as denoted in Fig. 5.1-5.2. The transmitter is positioned at 4 m distance from the origin and the receiver is positioned at different distances from the origin, starting from 2 m to a final distance of 10 m. In the post processing results, the NLOS distances are represented by notation: 4m/xm, where xm is the distance (in meters) of Rx from the origin. 10 snap shots (each with 2049 frequency points) were taken at each measurement position. The measurement parameters are described in Table 5.2.

Table 5.2. Measurement system parameters

Parameter	Value
Frequency	2.3–2.5 GHz
Bandwidth	200 MHz
Transmitting power	-10 dBm
Sweep points	2049
Noise floor	-80 dBm
Tx gain	6.6 dBi
Rx gain	6.6 dBi
Cable loss	0.6 dB/m
Antenna types	Linearly and circularly polarized patch
Antenna height	1.5 m
Human subjects height	1.80 m

5.4 Measurement results

5.4.1 Channel impulse response

The S parameters were measured for the B2B-MIMO channel using a VNA; 2049 frequency points were considered at the 2.3 GHz - 2.5 GHz band. In order to determine the impulse response (which characterizes this B2B MIMO transmission channel), an Inverse Fast Fourier Transform (IFFT) was applied to the MIMO transfer function (corresponding to the average of the measured S21 values over the number of snap shots and MIMO sub-channels), using a hamming window. The hamming window, is meant to correct for the IFFT induced ripple in the delay domain (since the frequency response has limited band).

Moreover, the power delay profile (PDP) (which gives the relative received power as a function of the excess delay) was determined from the impulse response as follows [7]:

$$\text{PDP (t)} = \|h(n)\|^2 \tag{5.1}$$

where $\|.\|$ is the modulus operation and $h(n)$ is the impulse response.

The effect of circular polarization and that of NLOS were considered. Specifically, the circular co-positioned (Cir-CP) MIMO setup was compared to the circular-90 degrees rotated (Cir-90R) MIMO setup. The Cir-CP was also compared to the linear-co-positioned (Lin-CP) setup. Finally, the Cir-CP at LOS was compared to the Cir-CP at NLOS.

The normalized B2B MIMO impulse responses for both circularly and linearly polarized patch antennas at CP and 90R scenarios, with LOS and NLOS topologies are represented in Fig. 5.3-5.4.

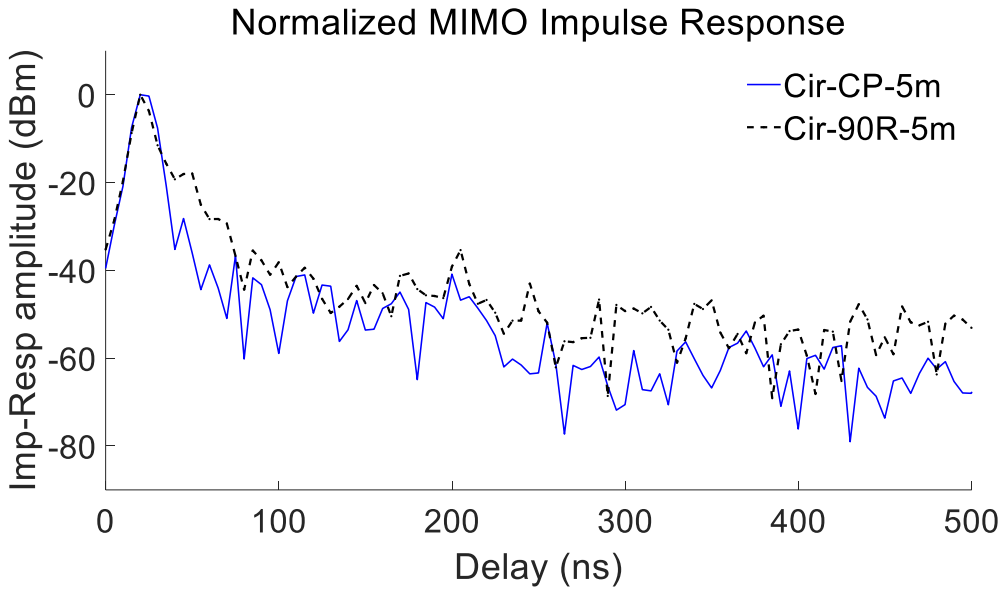

Fig. 5.3. MIMO-B2B normalized impulse responses amplitudes for the Cir-CP and Cir-90R setups, at the LOS 5 m distance.

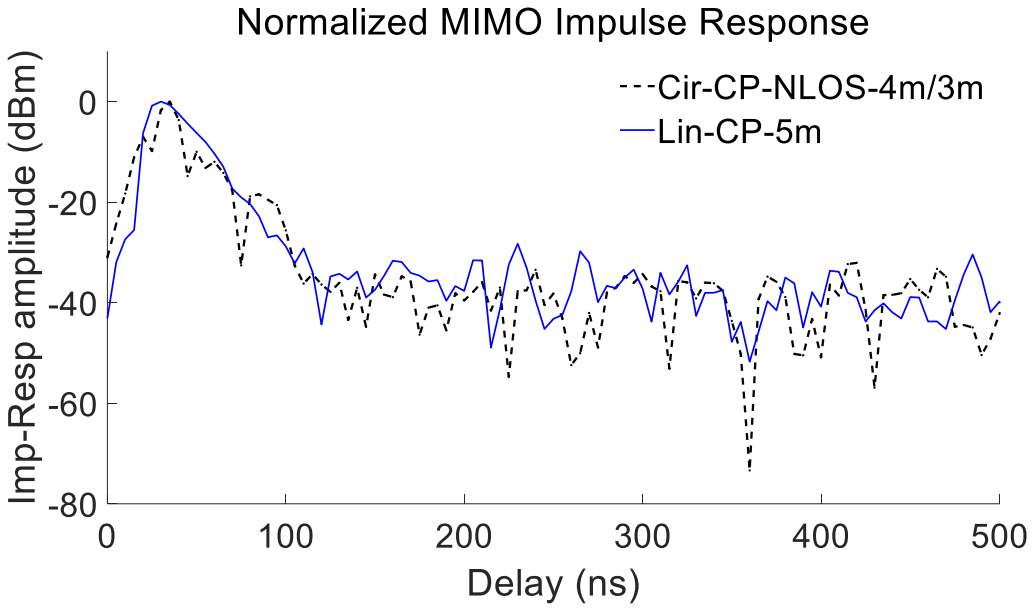

Fig. 5.4. MIMO-B2B normalized impulse responses' amplitudes for the Cir-CP setup at NLOS and Lin-CP setup at LOS for a distance of 5 m.

From the above impulse responses, it is noticed that the Cir-MIMO-CP MPCs power content is similar to that of the Cir-MIMO-90R one. In fact, at LOS, both the Cir-MIMO-CP and the Cir-MIMO-90R exhibit low multipath component powers and a significant deterministic power content. This is expected since the circularly polarized antenna is able to effectively receive signals at both horizontal and vertical directions; at the same time, some of the multipath components are filtered due to a change in the handedness nature of the reflected signal [21]. Regarding the NLOS situation, it is clear that the Cir-CP-NLOS impulse response exhibits a dominant MPC and other smaller less significant MPCs; in addition, this configuration is the most abundant in deep fades. Comparing the Cir-CP to the Lin-CP, it is noticed that the linear setup receives somewhat higher multipath powers. This is due to the fact that the linear setup is able to effectively receive reflected signals from the mine walls and body surfaces. These multipath signals reach the receiver at

different phase shifts and often add in a destructive manner, as it shall be seen from the PL results.

5.4.2 Path loss

The path loss is defined as the ratio of the transmitted power and a local average of the received power, and is usually computed using following formula [7]:

$$PL_{dB} = 20Log_{10}(\xi\{H_{x,y,f}\}) \quad (5.2)$$

Where PL_{dB} is the PL at a certain position, $H_{x,y,f}$ is the spatial sub-channel path strength at a given frequency and ξ is the averaging operator over all receiving antennas, transmitting antennas, frequencies, and snapshots [7].

Usually, the PL is modeled as a function of the Tx-Rx distance d as follows [20]:

$$PL(d) = PL_{dB}(d_0) + 10.\alpha.log_{10}\left(\frac{d}{d_0}\right) + X \quad (5.3)$$

Where $PL_{dB}(d_0)$ represents the mean path loss at the reference distance d_0, $10.\alpha.log_{10}\left(\frac{d}{d_0}\right)$ is the mean path loss referenced to d_0, d is the distance between the Tx and Rx, α is the PL exponent, and X is a zero mean Gaussian variable (in dB) representing shadowing [20].

PL as a function of distance, for the different MIMO-B2B scenarios, is shown in Fig. 5.5. The mean PL and the PL exponent α were determined through least square regression analysis. The shadowing (X) standard deviation is designated by the Greek letter σ.

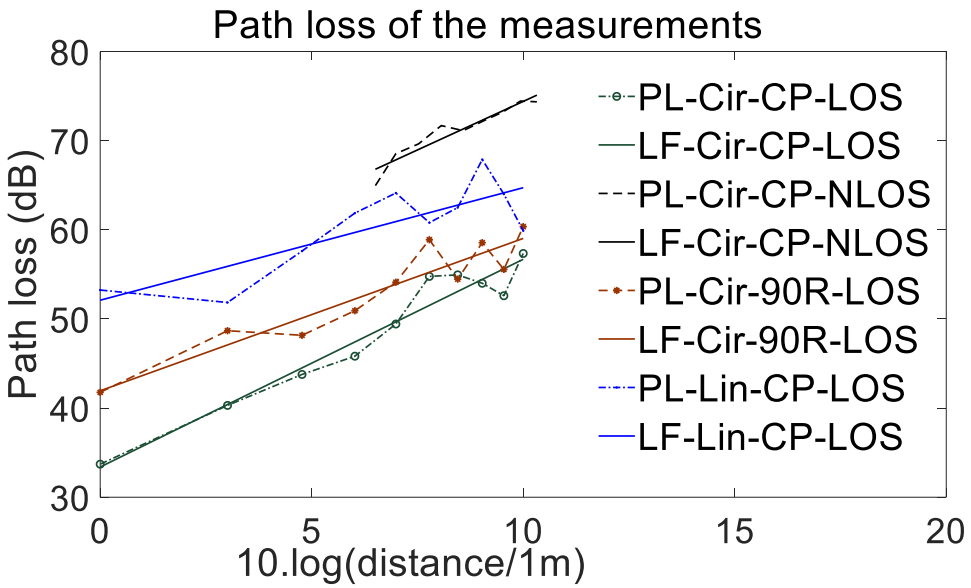

Fig. 5.5. Cir and Lin polarizations PL and linear fitting (LF) at the MIMO-CP and MIMO-90R scenario for LOS and NLOS configurations.

From the PL results, it is noticed that the Cir-CP-LOS B2B channel performs best with regards to the PL values (the lowest of all configurations), followed closely by the Cir-90R-LOS. The cross-polarization does not affect much the PL results since the circularly polarized antennas are able to receive the signal in both the horizontal and vertical planes. Comparing the linear and the circular polarizations, it is noticed that the circular polarization (Cir-CP) performs better than the linear polarization (Lin-CP) in terms of PL values but not in terms of PL exponents. It seems that the wave reflections from the body surfaces and surrounding objects (shifted in phase compared to the original wave) often add destructively to the received signal. This is clearly explained by the two-ray model in [14] where the reflected wave is demonstrated to be 180 degrees out of phase compared to the incident wave for small values of the incident angle (i.e. grazing incidence) and a perfect reflection (conductive surface). Regarding the circular polarization, which effectively suppress the first reflection [21], the destructive combining of the reflected

signal (especially the 1rst and 3rd reflections) with the LOS signal is not possible. In fact, these reflected waves have an opposite handedness making it undetectable in the reception. It was observed that the PL exponent is smaller than the free-space PL exponent (which is equal to 2) for the Cir-XP-LOS and the Lin-CP-LOS configurations due to the wave guide effect of the mine tunnel. The effect of an obstructed line of sight is characterized by a significant increase in PL for the Cir-CP-NLOS compared to the Cir-CP-LOS (about 30 dB increase at the 5 m distance). Moreover, mining machinery presence in the vicinity of a short-range B2B link often leads to shadowing and scattering that affect the PL results. Expectedly, while the mean shadowing is close to zero for all situations, the STD of the shadowing ($\boldsymbol{\sigma}$) shows a wider variability of the received signal with respect to the theoretical linear approximation, at the LOS situations. This is due to the time variation of signal power at the receiver caused by the changes in the transmission path, which is referred to as fading. The different MPCs add sometimes constructively and in other times destructively leading to the variations of PL around the mean as seen in Fig. 5.5. It should be noticed that at NLOS, the presence of a mining machine causes a strong reflection which dominates the other multipath arriving by diffraction and rough-walls reflections. In LOS, there are two strong signals arriving to the receiver, namely, the LOS signal and the reflection from a close by mining machine. The creeping wave arriving to the receiver from the body surface is not a significant contributor, since the patch antenna does not effectively receive a signal parallel to the plane of the antenna. From the root mean square error (RMSE) results in Table 5.3, it is observed that the straight-line PL model is a good approximation of the PL results.

Table 5.3. PL exponent values for the different channel configurations.

Polarization	Circular			Linear
Parameters	CP-LOS	90R-LOS	CP-NLOS	CP
PL-exponent	2.33	1.71	2.18	1.26
RMSE (dB)	1.84	2.10	1.01	3.10
Shadowing- STD $\boldsymbol{\sigma}$ (dB)	1.73	1.98	0.946	2.92
Shadowing- Mean (dB)	-0.0038	-0.0036	-0.0035	-0.0018

5.4.3 Spatial Correlation Matrices

The spatial correlation matrix consists of the correlation coefficients among the subchannels of the MIMO system. It is reported that the presence of a strong ray increases correlation among the subchannels [7] [22]. The correlation coefficient between subchannels h_{AB} and h_{CD} is represented by [7] [22]:

$$\rho_{AB}^{CD} = \frac{cov(h_{AB},h_{CD})}{\sigma_{AB} \times \sigma_{CD}} \tag{5.4}$$

where $cov(.)$ is the covariance operator and σ_{AB} and σ_{CD} represent the standard deviations of the complex signals for h_{AB} and h_{CD} respectively.

The spatial correlation matrix of the 2×2 MIMO-B2B channel, which we name R, can be written as [23]:

$$\mathbf{R} = \begin{bmatrix} 1 & \rho_{11}^{12} & \rho_{11}^{21} & \rho_{11}^{22} \\ \rho_{12}^{11} & 1 & \rho_{12}^{21} & \rho_{12}^{22} \\ \rho_{21}^{11} & \rho_{21}^{12} & 1 & \rho_{21}^{22} \\ \rho_{22}^{11} & \rho_{22}^{12} & \rho_{22}^{21} & 1 \end{bmatrix} \tag{5.5}$$

Where ρ_{AB}^{CD} is the correlation coefficient between subchannels h_{AB} and h_{CD} as represented in (4).

The spatial correlation matrices of the 2×2 B2B MIMO channels are derived using (5.5) and represented in Table 5.4.

Table 5.4. Correlation matrices for different setups at the 5 m distance.

Cir-CP-LOS

$$\begin{bmatrix} 1 & 0.46-0.51i & 0.39-0.37i & 0.35-0.44i \\ 0.46+0.51i & 1 & 0.8674 & 0.83-0.07i \\ 0.39+0.37i & 0.8674 & 1 & 0.92+0.04i \\ 0.35+0.44i & 0.83+0.07i & 0.92-0.04i & 1 \end{bmatrix}$$

Cir-90R-LOS

$$\begin{bmatrix} 1 & 0.84-0.06i & 0.44-0.51i & 0.53-0.66i \\ 0.84+0.06i & 1 & 0.59-0.36i & 0.64-0.64i \\ 0.44+0.51i & 0.59+0.36i & 1 & 0.73 \\ 0.53+0.66i & 0.64+0.64i & 0.73 & 1 \end{bmatrix}$$

Cir-CP-NLOS

$$\begin{bmatrix} 1 & 0.11-0.18i & 0.31-0.21i & 0.02-0.16i \\ 0.11-0.18i & 1 & 0.26-0.22i & 0.271-0.13i \\ 0.31-0.21i & 0.26-0.22i & 1 & 0.34-0.13i \\ 0.02-0.16i & 0.271-0.13i & 0.34-0.13i & 1 \end{bmatrix}$$

Lin-CP-LOS

$$\begin{bmatrix} 1 & 0.06-0.46i & 0.59-0.41i & 0.72-0.13i \\ 0.06-0.46i & 1 & -0.25-0.45i & 0.04-0.49i \\ 0.59-0.41i & -0.25-0.45i & 1 & 0.69-0.30i \\ 0.72-0.13i & 0.04-0.49i & 0.69-0.30i & 1 \end{bmatrix}$$

A well-established method for the evaluation of MIMO-B2B performance is to compare the transmit and the receive correlation [7]. From the spatial correlation matrices, the

transmit correlation (between the two transmitting signals) is determined. It is equal to ρ_{11}^{12} at receiving antenna 1, and ρ_{21}^{22} at receiving antenna 2. Similarly, the receive correlation (between two received signal) is determined assuming the signal transmitted from transmitting antenna 1 as ρ_{11}^{21}, and assuming the signal transmitted from transmitting antenna 2 as ρ_{22}^{12}. The modulus operator ($|.|$) is used to get easily comparable values as in [22].

Table 5.5. Correlation between two transmitted signals at a certain Rx antenna and correlation between two received signals for a certain Tx antenna at the 5 m distance.

	Correlation between transmitted signals		Correlation between received signals	
	$\lvert\rho_{11}^{12}\rvert$	$\lvert\rho_{21}^{22}\rvert$	$\lvert\rho_{11}^{21}\rvert$	$\lvert\rho_{22}^{12}\rvert$
Cir-CP-LOS	0.68	0.92	0.54	0.84
Cir-90R-LOS	0.69	0.73	0.68	0.85
Cir-CP-NLOS	0.21	0.37	0.37	0.30
Lin-CP-LOS	0.46	0.75	0.72	0.49

From the results in Table 5.5, it is clear that at LOS situations, both the transmit and the receive correlations are significant, especially for the circularly polarized setup. The linearly polarized MIMO-B2B channel reflects somewhat lower correlation than the circularly polarized setup, in most situations. This is due to the fact that the fading for the two signals received by the Cir setup (which rejects much of the first reflection power) are somewhat less independent than those received by the Lin setup, due to the presence of a stronger LOS component in the case of the Cir setup. It is important to note that both the Tx and Rx surrounding environments are rich in scattering objects and reflection mediums. Hence, both the receive and transmit correlations are close in values. Moreover, it is observed that the transmit correlation at receiving antenna 1 and the receive correlation for

transmitting antenna 1 are lower than those corresponding to the receiving antenna 2 and transmitting antenna 2, respectively. This is due to the fact that the position 1 for both the transmitter and the receiver is closer to the scattering objects than the position 2. We conclude that at LOS situations, the half wave length separations between Tx and Rx does not grantee a low level of correlation as seen in [24]. With regards to the NLOS situation, expectedly, the transmit and receive correlations are considerably lower than the corresponding LOS ones, due to the significantly lower dominant MPC and to the rich scattering phenomenon.

5.4.4 RMS delay spread and coherence bandwidth

The Root mean Square (RMS) delay spread is equal to the square root of the second central moment of the power delay profile (PDP) [14], and is derived using the following formulas [14]:

$$\tau_{RMS} = \sqrt{\overline{\tau^2} - \bar{\tau}^2} \tag{5.6}$$

Where $\overline{\tau^2}$ represents the second moment of the PDP and $\bar{\tau}$ denotes the mean excess delay, which is expressed as follows [14]:

$$\bar{\tau} = \frac{\sum_k p(t_k) t_k}{\sum_k p(t_k)} \tag{5.7}$$

where $p(t_k)$ denotes the power of the kth path and t_k its corresponding delay.

The coherence bandwidth (Bc) is derived from the RMS delay spread (for a frequency correlation function above 0.5) as follows [14]:

$$B_c \simeq \frac{1}{5\tau_{RMS}} \tag{5.8}$$

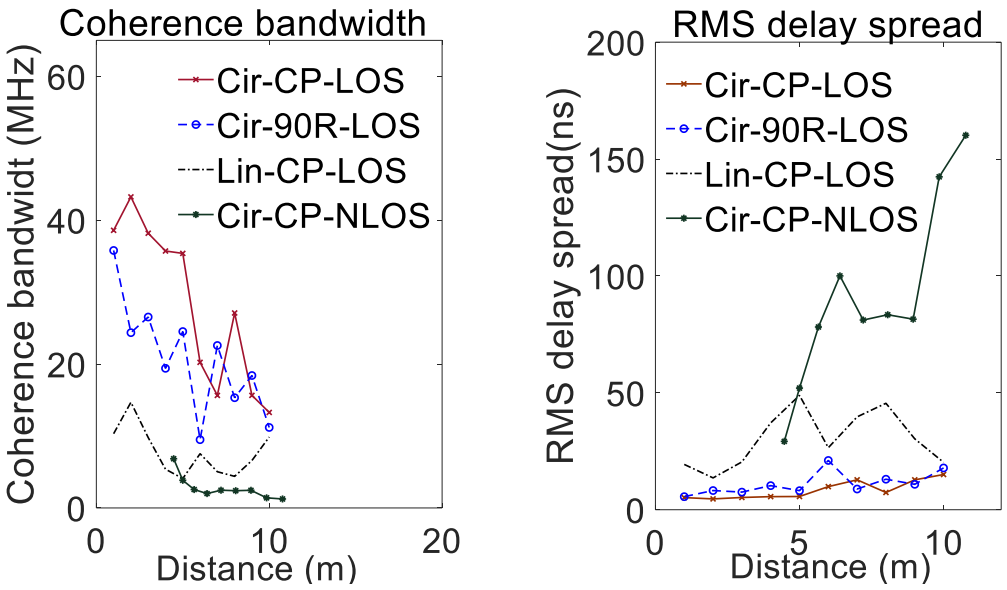

Fig. 5.6. RMS delay spread and coherence bandwidth, compared for Cir vs. Lin polarizations, MIMO-CP vs. MIMO 90R scenarios and LOS vs. NLOS.

The RMS delay spread and coherence bandwidth have been computed for each measured PDP of the MIMO B2B channels under the different scenarios of Table 5.1. From Fig. 5.6, it is observed that for the LOS topologies, the RMS delay spreads and coherence bandwidth do not have a monotonic trend with distance. This is due to the fact that the multipath richness is not necessarily increasing with distance, as clearly demonstrated by the K-factor results in the next section. The linear setup, exhibits higher RMS delay spread than the circular setup, and the NLOS setup exhibit higher RMS delay spread than its LOS counterpart. This is due to the fact that the circular setup suppresses the first reflection, because of a change in the handedness nature of the reflected signal compared to the original signal. These secondary reflections are not totally suppressed due to the surface roughness depolarization [25], but they are greatly reduced in strength. With regards to the coherence bandwidth, it has the opposite behavior of the RMS delay spread, due to the inverse proportionality of the two parameters. In general, the Cir-CP-LOS setup exhibits

the best time dispersion results (with RMS delay spreads ranging from 8.1 ns to 19.8 ns) followed closely by the Cir-XP-LOS.

5.4.5 Rican K-factor

The Rician K-factor is defined as [26]:

$$K = \frac{P_D}{2P_R} \tag{5.9}$$

where P_D corresponds to the power of the dominant component and $2P_R$ is the power of the reflected, diffracted, or diffusely scattered components.

It is directly determined from the impulse response as [26]:

$$K = \frac{|V_D|^2}{\sum_{m=1}^{M}|a_m|^2} \tag{5.10}$$

where M is the number of MPCs, a_m is the random amplitude of the MPC and V_D is the amplitude of the dominant component (usually equaling the deterministic LOS component).

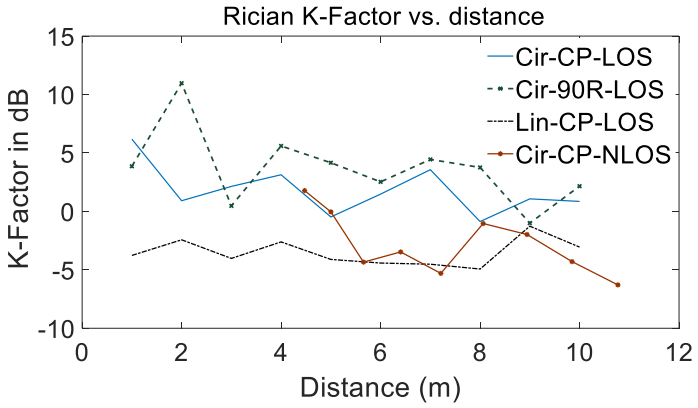

Fig. 5.7. Rican K-factor for the B2B channels

Since the measurements involved LOS and NLOS situations for different path lengths, the K-factor (denoted in Fig. 5.7) varied depending on the studied situation and the Tx-Rx distance. The K-factors for the LOS links are clearly higher than that of a NLOS link due to the strong dominant components at LOS. With regards to the effect of polarization, it is

shown that the K-factor for the Lin-MIMO setup is generally lower than that of the circularly polarized setup due to the effective rejection of some significant MPCs by the circular antennas. In fact, it is emphasized by the impulse responses results (Figs.5.3-5.4) that the MPCs powers (relative to the dominant power) are more significant in the case of the Lin-MIMO setup. These MPCs experience different phase shifts, which often lead to destructive power combination at the receiver, as previously demonstrated by the PL results. It is noticed that the Rician K-factor generally reflects the opposite behavior of the RMS delay spread. This could be explained by the fact that the RMS delay spread generally increase with the increase of MPCs richness. A more precise relationship between the K-factor and the RMS delay spread was proposed by Witrisal et al. [27]. Moreover, it is observed that a higher Rician K-factor corresponds to a higher correlation. This is due to direct effect of scattering (which enriches multipath) in lowering both the correlation as well as the K-factor.

5.4.6 Channel Capacity

The aim of the capacity study is to show the effect of the PL - on the one hand- and that of the multipath- on the other hand- on the different MIMO-B2B channels. This is achieved by assuming a constant transmitted power and variable SNR in the first case and by assuming a fixed SNR in the second case [20].

The MIMO channel capacity is derived using the following formula [20]:

$$C_{MIMO}[bps/Hz] = log_2(\det[\boldsymbol{I}_n + \frac{SNR_{av}}{m}\boldsymbol{H}\boldsymbol{H}^*]) \quad (5.11)$$

Where $\boldsymbol{I}_n$ is the identity matrix, SNR_{av} is the average SNR, H is the normalized m × n channel response and * signifies the complex conjugate transpose operator.

5.4.6.1 Capacity at a constant SNR

When fixing the SNR value, the PL is isolated from the capacity calculations [20]. Hence, this study allows to analyze the effect of the multipath on the MIMO-B2B capacity.

Fig. 5.8 represents the channel capacity results at an SNR of 20 dB, for the different MIMO-B2B configurations. From the average capacities and the capacity Cumulative distribution functions (CDFs), it is clear that the circular setup exhibits higher fluctuations in the channel capacity when changing the distance and also at different snap shots for the same distance. This is due to roughness of the walls which affect the first reflection depolarization [25] and hence its contribution to channel capacity. Expectedly, in the lower distances, the circular setup was not able to receive effectively enough multipath power and exhibited lower capacity values. This is due to the fact that, at the lower distances, the main multipath power is generated by the body parts reflections, rather than the reflection and diffraction from the relatively distant mine walls. The body, being a smooth surface, causes the signal handedness to change and the reflection is effectively suppressed at the reception. Moreover, it is observed that the channel capacity, at a constant SNR, is somewhat stable for the linear setup and the Cir-NLOS setup. This is due to the fact that a linear setup is receiving multipath contributions from both the body and mine walls reflections. Moreover, the mine walls reflections are the main contributors to the Cir-NLOS multipath richness. The availability of these reflections is somewhat stable for the measurement distances.

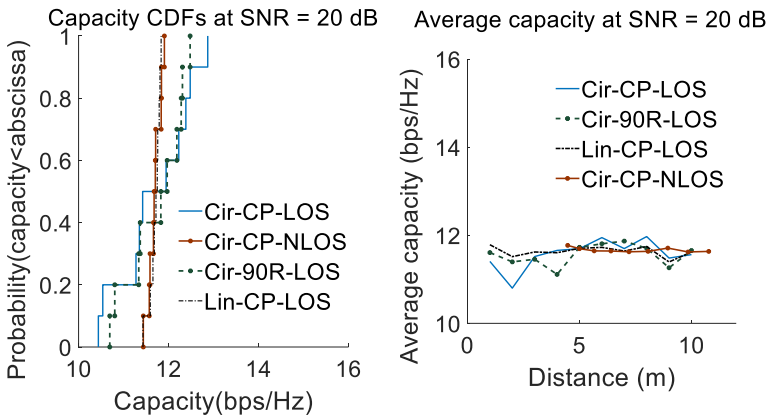

Fig. 5.8. Cir and Lin polarizations MIMO channel average capacities and capacity CDFs (for a 5 m distance) at the CP and 90R scenarios, assuming a fixed SNR of 20 dB

Table 5.6. Throughput gain for the B2B channels when SNR=20 dB

Channel	**Throughput gain**
Cir-CP-LOS	1.738
Cir-90R-LOS	1.736
Cir-CP-NLOS	1.752
Lin-CP-LOS	1.748

Additionally, the improvement in channel capacity offered by MIMO over the corresponding SISO link is studied. The throughput gain values, which quantify this improvement, are close for all studied configurations (slightly higher for the Cap-Cir-CP-NLOS and the Cap-Lin-CP-LOS channels, due to their smaller correlation values). Moreover, these throughput gains (summarized in Table 5.6.) are expectedly less than 2 due to correlation.

5.4.6.2 Capacity at a constant transmit power

At a constant transmit power of -10 dBm, the channel capacity was computed for the different MIMO B2B configurations. In this study, both the multipath richness and the PL have an effect on the channel capacity. Fig. 5.9 denotes the derived results for the MIMO configuration.

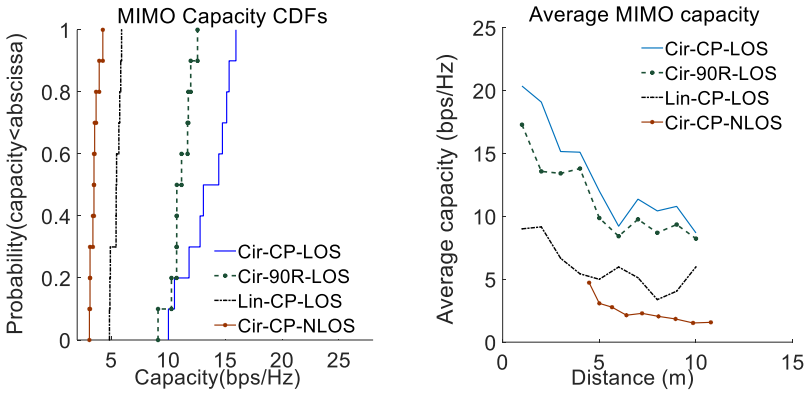

Fig. 5.9. Circular and linear polarizations MIMO average channel capacities and capacity CDFs (for a 5 m distance) at the CP and 90R scenarios and a constant transmit power.

Expectedly, the channel capacity results- when a constant transmitted power is considered- show that the average channel capacity decreases with distance. In fact, the smaller distances correspond to higher received average powers and hence higher average SNRs which has a direct impact on the capacity as denoted in (11). Comparing the MIMO-Cir-CP-LOS to the MIMO-Lin-CP-LOS B2B channels, it is clear that the circular setup outperforms the linear one, beside the fact that the multipath richness is actually higher when using the linear setup. This is due to the destructive combination of the MPCs, resulting in a lower total received power for the Lin setup. In fact, some reflected signals are out of phase compared to the incident wave as explained in the PL section. In some distances, however, a constructive combining of the MPCs occurs, which explains the relative increase in the channel capacity for the linear setup at these distances (2 m, 6 m, 9 m and 10 m). This result is also observed in the PL graph, where the PL values for the Lin-CP-LOS are below the linear approximation due to the constructive MPCs combining at these distances. Concerning the circular setup, both the CP and 90R configurations exhibit close results. Comparing the Cir-CP-LOS to the Cir-CP-NLOS, it is clear that the LOS topology exhibits a considerably higher capacity, due to the lower PL at the LOS scenario.

It is noticed that the capacity CDFs (for a 5 m distance) confirm the same results observed from the average capacity graphs. Moreover, these CDFs show a greater variation (between 10 and 15 bps/Hz) for the measured capacities of the Cir-CP-LOS at the different snapshot, compared to the other scenarios. It seems that the reflected signals from the walls are depolarized in different ways, each time a snap shot is taken due to the random roughness of the walls which receive the signals at considerably different angles at each snapshot. Hence, sometimes, the first reflection is suppressed mostly and in other times some power of this reflection is available due to depolarization from the rough surface and adds as a power contribution at the receiver.

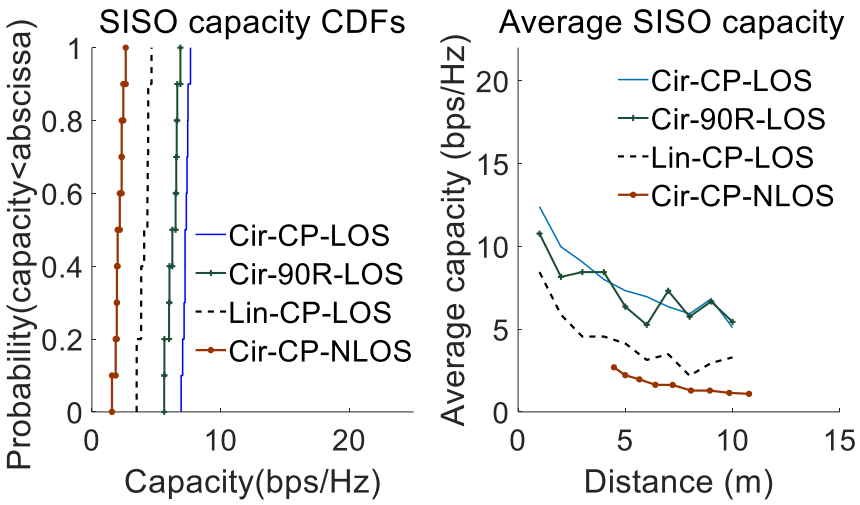

Fig. 5.10. Circular and linear polarizations SISO average channel capacities and capacity CDFs (for a 5 m distance) at the CP and 90R scenarios and a constant transmit power.

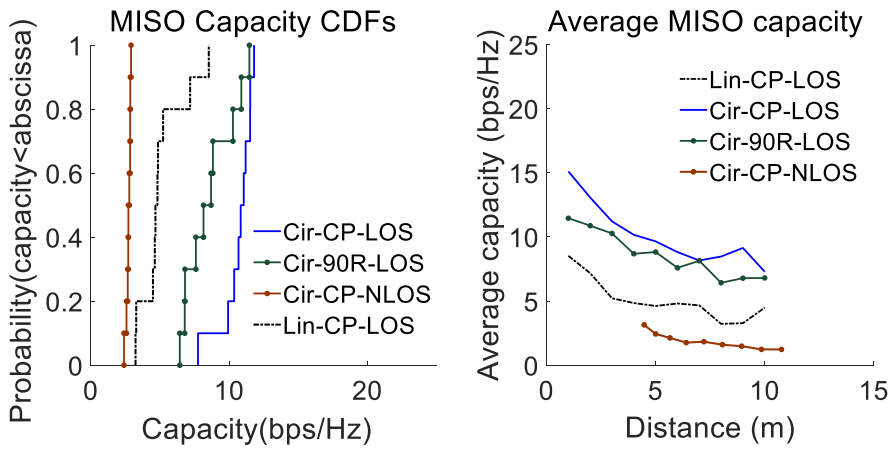

Figure 5.11. Circular and linear polarizations MISO average channel capacities and capacity CDFs at the CP and 90R scenarios and a constant transmit power.

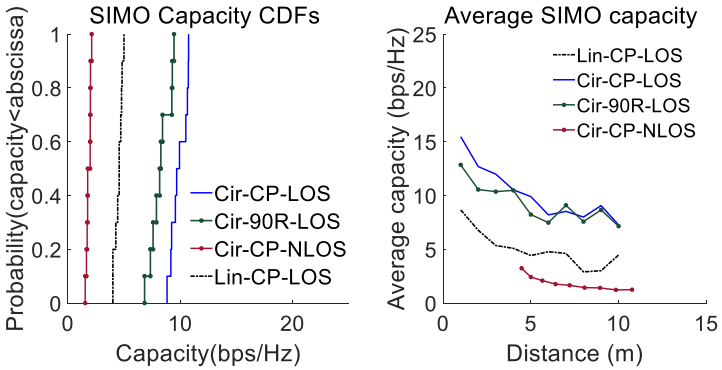

Figure 5.12. Circular and linear polarizations SIMO average channel capacities and capacity CDFs at the CP and 90R scenarios and a constant transmit power.

Comparison of the MIMO capacity results to their corresponding MISO, SIMO and SISO results shows a considerable improvement of the channel capacity, despite the relatively strong correlation among the sub-channels, especially at LOS. Moreover, it is observed that MISO systems perform worse than the SIMO in terms of throughput gain (improvement relative to SISO). For instance, it is calculated for the Cir-CP scenarios- at the 5m distance and a constant transmitted power- to be 1.66 for MIMO, 1.37 for the SIMO and 1.32 for MISO. It is lower than 2 for the MIMO scenario because of the considerable correlation at both the transmission and the reception. In addition, since the receive

correlation is somewhat lower than the transmit correlation, the SIMO throughput gain is slightly higher in the case of SIMO as was also noticed in several WBAN publication [23].

Hence, the circular polarization combined with MIMO proved to be a viable solution for the B2B communication inside a mine.

5.4.7 Channel modeling

The modeling procedure consists in developing the impulse response to describe the B2B system in a mining environment. The impulse response is represented as follows [16]:

$$h(t) = \sum_{i=0}^{N-1} a_i \delta(t - t_i) e^{j\theta_i} \quad (5.11)$$

where N is the number of MPCs, a_i, t_i and θ_i are respectively, the random amplitude, arrival time and phase of the ith MPC. δ is the Kronecker delta function.

The modeling procedure consists in two steps, namely the path amplitudes (a_i) and arrival times (t_i) modeling. This is done by expressing the path amplitudes as random Gaussian variable with average powers decaying exponentially, as represented by the IEEE 802.11 Channel Model [15]. The arrival times are modeled by comparing them to different distributions used in the literature. The phases are assumed to be statistically independent random variables, uniformly distributed from 0 to 2π [16]. The modeled impulse response shall approximate the measurements-based impulse response for the studied B2B channel.

5.4.7.1 Path amplitude modeling

One of the most popular indoor channel models is the exponential model where power decreases exponentially with the channel delay [15]. Based on the exponential model, the IEEE 802.11b Task Group has created a model, where the channel impulse response is represented by the output of finite impulse response (FIR) filter. The different channel taps

(representing the multipath components) are modeled by independent complex Gaussian random variables with average powers that follow the exponential PDP [15].

The power of each channel tap is given by [15]:

$$A_i^2 = A_0^2 * e^{-i*T_s/\sigma_\tau} \tag{5.12}$$

Where i is the tap index (between 0 and N), T_s is the sampling time, σ_τ is the RMS delay spread and A_0^2 is the power of the first tap determined in such a way to make the average received power equal to one, as follows:

$$A_0^2 = \frac{1-e^{-T_s/\sigma_\tau}}{1-e^{-(N+1)T_s/\sigma_\tau}} \tag{5.13}$$

The modeling of the path amplitudes described by (5.12) and (5.13), requires the knowledge of the RMS delay spread. This latest could either be determined empirically from measurements or estimated from published results in similar environments. In our case, we have used the RMS delay spread that was calculated from our SISO-B2B measurements at the chosen 6 m distance as 12 ns.

5.4.7.2 Time of arrival modeling

The time of arrivals of the different MPCs are derived from the measurements by applying a peak detection algorithm on the measured PDP. The time difference between successive peaks is considered, in order to generate a random set for our process; in fact, the mere time of arrival is not completely random since it is always increasing. The distribution of the arrival times steps is compared to the different random distributions from the literature, namely, Poisson, Gaussian, and Weibull. Kolmogorov–Smirnov (KS) test is used to determine the distribution that most closely describes the random set of time steps. Results in Fig. 5.13 show that the Poisson distribution offers the best fit for these time

steps, followed closely by the Weibull distribution. The supremum of the set of distances (differences between the measurements and model CDFs) for the Poisson, Weibull and Gaussian are 0.224, 0.225 and 0.269 respectively. The time differences between peaks of the MPCs can now be generated using as a random vector following the optimal distribution. The first time of arrival is nothing more than that of the LOS signal denoted by the well-known formula:

$$T=D/V \tag{5.13}$$

where V is the wave velocity (empirically estimated from a set of measured PDPs to be 0.9*C, where C is the speed of light) and D is the measurements distance. Finally, the time of arrivals are determined by adding the individual time steps from the random vector to their corresponding arrival times. For instance, the first arrival time added to the first time step will give the second time of arrival.

The impulse response is readily determined by matching the arrival times to the path amplitudes as denoted in Fig. 5.14. In order to compare the modeled and measured impulse responses, the measured impulse response was also determined so as to make the average received power equal to one. This is done by dividing the received power over the sum of all the MPCs powers. The modeled impulse response is found to be close to the measured one with a calculated MMSE of 1.8437e-04.

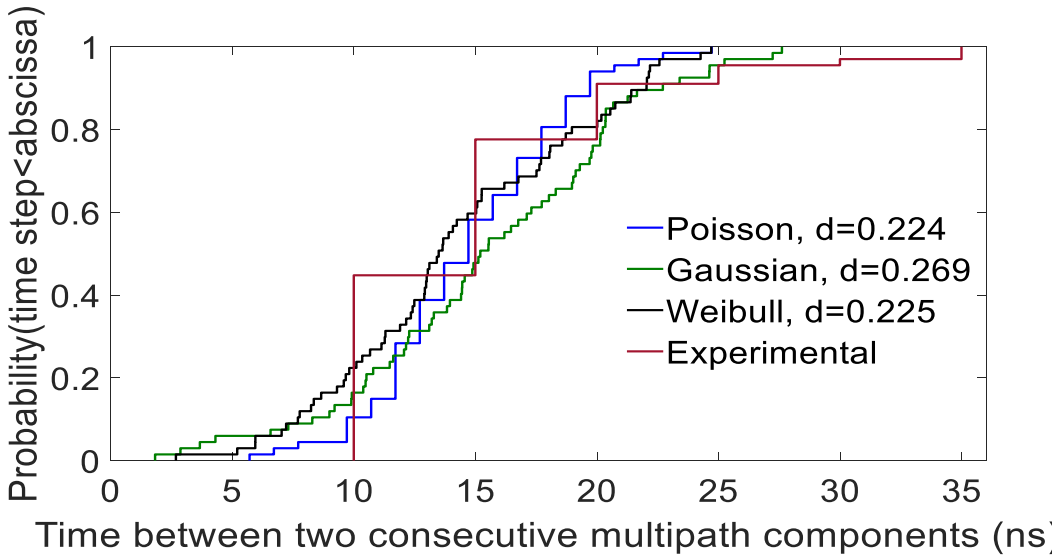

Figure 5.13. Comparison of three optimal CDFs to represent the time differences between MPCs.

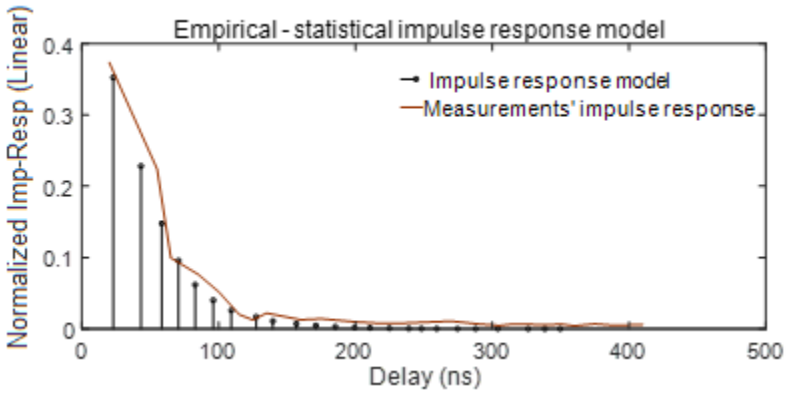

Figure 5.14.modeled vs. measured impulse responses normalized by their respective total powers.

5.5 Conclusion

In this study, the MIMO B2B channel was characterized at 2.4 GHz in a mine gallery using circularly and linearly polarized antennas. Different scenarios were considered, namely CP and 90R at LOS and NLOS. It is clear from the PL, capacity and time dispersion results that the circularly polarized antennas perform best for B2B channels in a mine environment, due to their resilience to antennas misalignments. The channel capacities are

strongly dependent upon PL as well as the multipath richness at a lower degree. Hence, as the multipath richness becomes significant at the higher distances, the channel capacities experience an occasional increase despite PL effect. K-factor results reveal that the MPCs powers relative to the dominant power is more significant in the case of the Lin-MIMO setup than the Cir-MIMO setup. The RMS delay spread shows this result with higher values for Lin-CP especially at the higher distances. Correlation follows the same trend as the K-factor due to the effect of scattering in lowering both the correlation as well as the K-factor. The effect of an obstructed LOS signal is significant as seen from the PL, capacity and time dispersion results. In fact, the Cir-CP-NLOS capacities are lower than half of the Cir-CP-LOS capacities at similar Tx-Rx separations. This is expected, since the LOS is the main contributor to the total power, added to the fact that the second contribution (the 1rst reflection) is not effectively received at the receiver, due to the relative change of handedness of the reflected circularly polarized signal. The MIMO throughput gain is most significant for the NLOS setup as well as the linear setup, because of their low branch correlation. In general, the circularly polarized setup seems to be very well suited for the B2B propagation inside a mine, even at NLOS.

An impulse response model has been developed in order to completely describe the B2B channel. The Poisson distribution best describes the path arrivals time steps. The path amplitudes are modeled using the exponential model that assumes that the MPCs amplitudes follow a Gaussian distribution while their average powers follow an exponentially decaying PDP.

5.6 References

[1] M. El Hassan El Azhari, M. Nedil, I. B. Mabrouk, L. Talbi, K. Ghanem, and Y. S. Alj, "Performance Evaluation of a MIMO-on-Body System in a Mine Environment," Progress In Electromagnetics Research C, Vol. 61, 55-63, 2016.

[2] Y. Rissafi, L. Talbi, and M. Ghaddar, "Experimental characterization of an UWB propagation channel in underground mines," IEEE Trans. Antennas Propagat., vol. 60, no. 1, pp. 240–246, 2012.

[3] A. Benzakour, S. Affes, C. Despins and P. M. Tardif., "Wideband measurements of channel characteristics at 2.4 and 5.8 GHz in underground mining environments," in Vehicular Technology Conference, 2004.

[4] C. Briso-Rodriguez, J. M. Cruz and J. I. Alonso, "Measurements and Modeling of Distributed Antenna Systems in Railway Tunnels," in IEEE Transactions on Vehicular Technology, vol. 56, no. 5, pp. 2870-2879, Sept. 2007.

[5] K. Guan, Z. Zhong, J. I. Alonso and C. Briso-Rodriguez, "Measurement of Distributed Antenna Systems at 2.4 GHz in a Realistic Subway Tunnel Environment," in IEEE Transactions on Vehicular Technology, vol. 61, no. 2, pp. 834-837, Feb. 2012.

[6] G. R. Valenzuela, Depolarization of E-M waves by slightly rough surfaces, 3rd ed. IEEE Trans. Antennas Propagat., vol. AP- 15, pp. 552-557, 1967.

[7] I.B. Mabrouk, L. Talbi, M. Nedil, and K. Hettak, "MIMO-UWB channel characterization within an underground mine gallery," IEEE Transactions on Antennas and Propagation, Vol. 60, 4866– 4874, Oct. 2012.

[8] B. Mnasri, M. Nedil, N. Kandil, M. Ghaddar and L. Talbi "Experimental Investigation of 2.4 GHz MIMO Channel Capacity using 4x4 Butler Matrix in Underground Mine Gallery" IEEE Trans. Antennas Propagat., 2013

[9] I. B. Mabrouk, L. Talbi, M. Nedil, Y. Coulibaly and T. A. Denidni, "Effect of antenna directivity on performance of multiple input multiple output systems in an underground gold mine," in IET Microwaves, Antennas & Propagation, vol. 6, no. 5, pp. 555-561, April 12 2012.

[10] M. E. Azhari, M. Nedil, I. Ben Mabrouk and L. Talbi, "Multipath effect on off-body channel parametters of a MIMO system using patch antennas inside a mine," 2016 IEEE International Symposium on Antennas and Propagation (APSURSI), Fajardo, 2016, pp. 1693-1694

[11] M. E. Azhari, M. Nedil, I. Ben Mabrouk and L. Talbi, "Path loss effect on off-body channel capacity of a MIMO system using patch antennas inside a mine," 2016 IEEE International Symposium on Antennas and Propagation (APSURSI), Fajardo, 2016, pp. 1697-1698.

[12] M. El Azhari, M. Nedil, I. B. Mabrouk, L. Talbi, K. Ghanem, and Y. S. Alj, "Performance evaluation of a MIMO-on-body system in a mine environment," Progress In Electromagnetics Research C, Vol. 61, 55-63, 2016.

[13] E. Reusens, W. Joseph, B. Latre, et al, " IEEE Characterization of On-Body Communication Channel and Energy Efficient Topology Design for Wireless Body Area Networks", Information Technology in Biomedicine, IEEE Transactions on , vol.13, no.6, pp.933-945, Nov. 2009

[14] T. S. Rappaport, Wireless Communications: Principles & Practice, 2nd Ed., Prentice-Hall: Upper Saddle River, NJ, 2002, ISBN 0-13042232-0.

[15] M. El Hassan El Azhari, L. Talbi, L. Arabi, M. Nedil, M. L. Seddiki, and N. Kandil, " Channel Characterization of Circularly Polarized Antenna MIMO System in an Underground Mine," Progress In Electromagnetics Research M, Vol. 67, 9-19, 2018.

[16] J. Ryckaert, P. De Doncker, R. Meys, A. de Le Hoye and S. Donnay, "Channel model for wireless communication around human body," in Electronics Letters, vol. 40, no. 9, pp. 543-544, 29 April 2004.

[17] A. E. Forooshani, S. Bashir, D. G. Michelson and S. Noghanian, "A Survey of Wireless Communications and Propagation Modeling in Underground Mines," Communications Surveys & Tutorials, IEEE , vol.15, no.4, pp.1524,1545, Fourth Quarter 2013.

[18] Y. S. Cho, J. Kim, W. Y. Yang and C. G. Kang, “MIMO-OFDM Wireless Communications with MATLAB,” W. & S. Pte Ltd, 2010, pp. 25–30.

[19] Boutin, M.; Benzakour, A.; Despins, C.L.; Affes, S., "Radio Wave Characterization and Modeling in Underground Mine Tunnels," in Antennas and Propagation, IEEE Transactions on , vol.56, no.2, pp.540-549, Feb. 2008.

[20] M.E. El Azhari, M. Nedil, I. Benmabrouk, K. Ghanem, and L. Talbi, "Characterization of an off-body channel at 2.45 GHz in an underground mine environment," Progress In Electromagnetics Research M, Vol. 43, 91-100, 2015.

[21] Jackson, J. D., Classical Electrodynamics, 3rd Edition, Wiley, New York, 1998.

[22] R. E. Jaramillo, O. Fernandez, and R. P. Torres, “Empirical analysis of 2 2 MIMO channel in outdoor-indoor scenarios for BFWA applications,” IEEE Antennas Propag. Mag., vol. 48, no. 6, pp. 57–69, Dec.2006

[23] I. Khan and P. S. Hall, “Experimental evaluation of MIMO capacity and correlation for narrowband body-centric wireless channels,” IEEE Trans. Antennas Propag., Vol. 58, No. 1, 195–202, Jan. 2010.

[24] J. S. Colburn, Y. Rahmat-Samii, M. A. Jensen, and G. J. Pottie, “Evaluation of personal communications dual-antenna handset diversity performance,” IEEE Trans. Veh. Technol., vol. 47, pp. 737–746, Aug. 19

[25] S-C Kwon, GL Stuber, Geometrical Theory of Channel Depolarization. IEEE Trans. Veh. Technol. 60(8), 3542-3556 (2011)

[26] Tang, Pan & Zhang, Jianhua & F. Molisch, Andreas & Smith, Peter & Shafi, Mansoor & Tian, Lei. (2018). Estimation of the K-factor for Temporal Fading from Single-Snapshot Wideband Measurements. IEEE Transactions on Vehicular Technology. PP. 1-1. 10.1109/TVT.2018.2878352.

[27] K. Witrisal, Y.-H. Kim, and R. Prasad, "A New Method to Measure Parameters of Frequency-Selective Radio Channels Using Power Measurements," accepted for IEEE Transactions on Communications

Chapter 6 Characterization of MIMO point-to-point links

In a study published in [1], the effect of circular polarization on an RF channel at both co-polarized (CP) and cross polarized (XP) scenarios has been investigated. This study provides is a comparative reference for the B2B results presented in the earlier section. Measurements were performed at the cité de l'or mine near Val d'Or. The gallery is situated at a depth of 90 meters, having a length of approximately 18 m, a height of about 2.45 m and width of approximately 5 m, which sketch is represented in Fig. 6.1.

Measurements were conducted using two MIMO antenna systems, namely, a 2 × 2 MIMO circularly polarized (MIMO-cir) patch antenna system and a 2 × 2 MIMO regular patch (MIMO-p) antenna system. The antennas were designed using the High Frequency Structure Simulator (HFSS) antenna design software and fabricated in the LRTCS laboratory. The two antennas have a gain of 6.6 dBi and an axial ratio (AR) less than 3 dB at 2.4 GHz. It was found that the integration of circular polarization and MIMO radio technologies improves the performance of an underground RF channel. In fact, a remarkable improvement is achieved through the use of MIMO combined with circular polarization compared to the regular MIMO-p antenna system, in terms of channel capacity and PL. A summary of the results is presented subsequently.

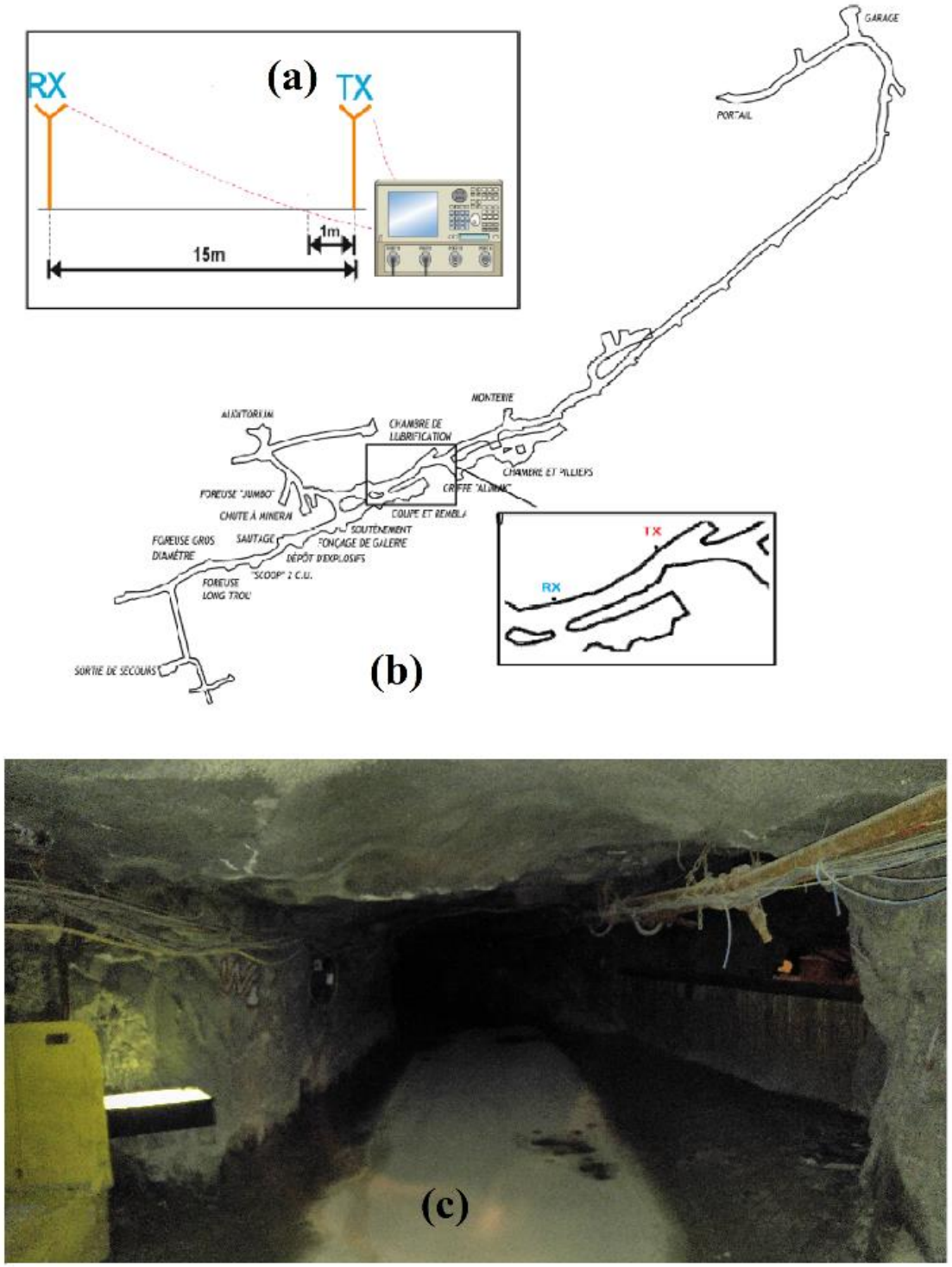

Fig. 6.1. Experiment setup (a), map of the mine (b) and photo of the gallery (c)

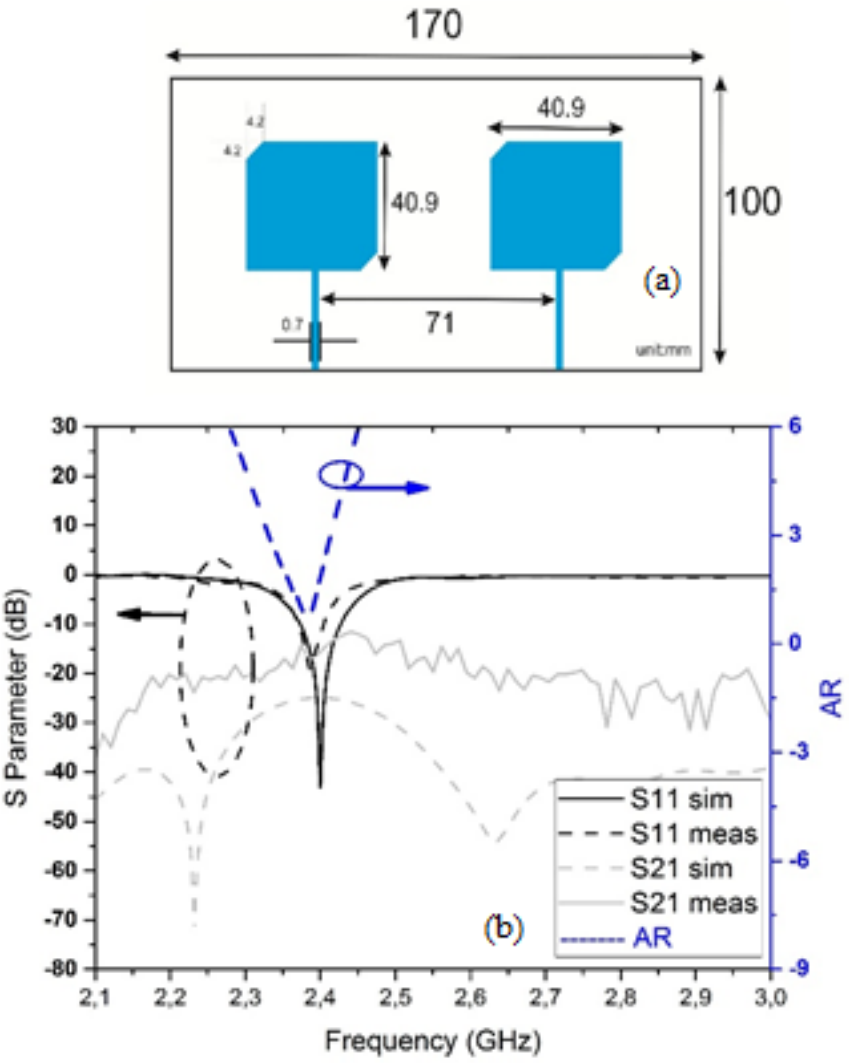

Fig. 6.2. Dimensions of the circularly polarized antenna (a), simulated (HFSS) and measured S parameters (b).

The circularly polarized antennas used the RT 5880 substrate with overall dimension 100 mm (width), 100 mm (length) and 1.6 mm (thickness). Other characteristics consisted of a copper thickness of 0.035mm, substrate dielectric constant (ε_r) of 2.2 and tangent loss (tan δ) equaling 0.019. Two symmetric truncated corners (4.2×4.2 mm) on a metal radiator patch cause the antenna to radiate in circular polarity as demonstrated in [2]. The dimensions and the characteristics of the antenna are represented in Fig. 6.2. Since the performance of the MIMO antenna is quantified through the S-parameters, measurements

and simulation results (Fig. 6.2) show that the antenna resonates at the design frequency (2.4 GHz). Moreover, the measured coupling level is found to be about 15 dB within the 2.4 industrial, scientific and medical (ISM) band. Simulation results exhibit a broad 3-dB Axial Ratio (AR) bandwidth of 8.3 % (between 2.3 and 2.5 GHz), which covers the WLAN 2.4 GHz operating bands.

The MIMO antennas are separated by a distance of about 7 cm, which is equivalent to half of the wave length (λ/2). A 30 dB power amplifier is used at the transmission side and a VNA is used to measure the S parameters at the band surrounding the center frequency (2.3 GHz-2.5 GHz). During the measurements, the propagation channel was considered to be stationary; the transmitting and receiving antennas (Tx and Rx) were fixed on two supporting rods at the same height of 1.50 m. In order to characterize the RF channel, the receiver was moved at 1 m steps from a starting position of 1 m to a final distance of 15 m (from the transmitter), as shown in Fig. 6.1. At each measurement position, 10 snap shots were taken for 2049 frequency points around 2.4 GHz. A description of the measurement parameters is listed in Table 6.1.

Table 6.1. Measurement system configurations

Parameter	**Value**
frequency	2.3–2.5 GHz
bandwidth	200 MHz
transmitting power	-10 dBm
sweep points	2049
noise floor	-90 dBm
Tx gain	6.6 dBi
Rx gain	6.6 dBi
cable loss	0.6 dB/m

antenna types	Linearly and circularly polarized patch
antenna height	1.5 m

6.1 Channel impulse response and path loss

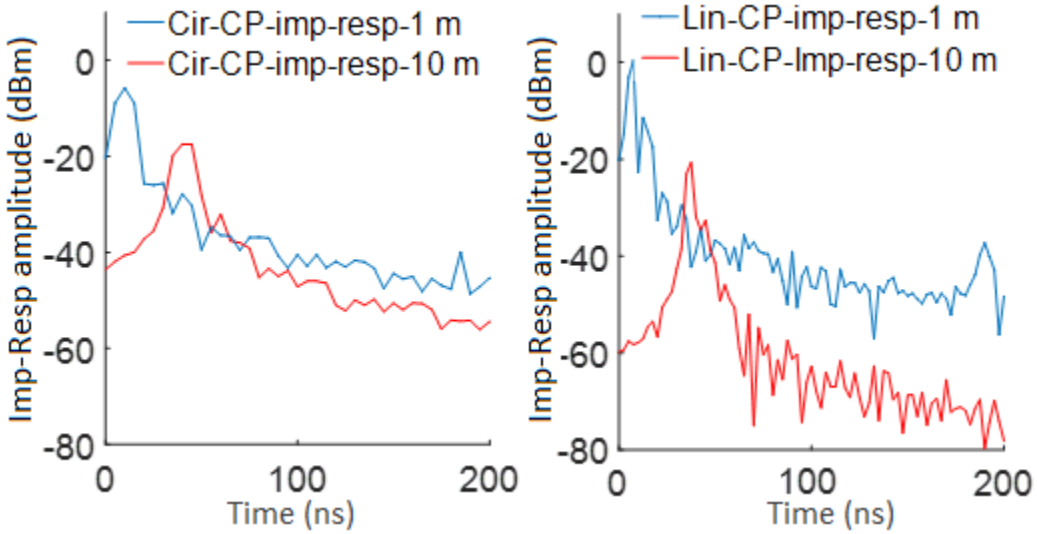

Fig. 6.3. Circular (Cir) and linear (Lin) polarizations impulse responses for four distances at the CP scenario

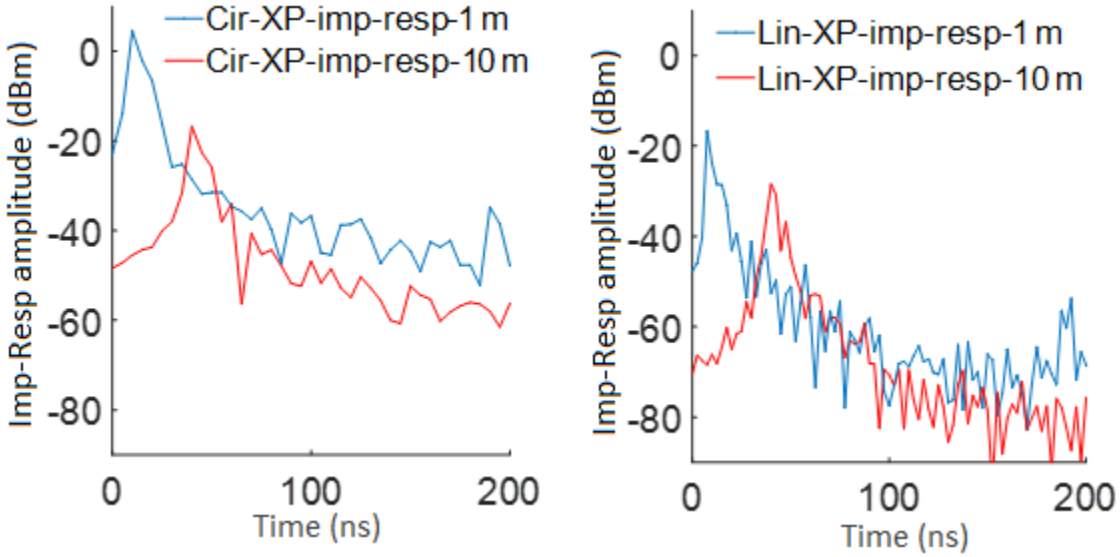

Fig. 6.4. Circular (Cir) and linear (Lin) polarizations impulse responses for four distances at the XP scenario

From the above figures (Fig. 6.3-4), it is clear that cross polarization has a significant impact on the linearly polarized setup results. The power of the greatest multipath component, for the regular patch set up, is significantly decreased at the XP scenario compared to the circularly polarized antenna results. This result is expected since the circularly polarized antenna is able to effectively receive signal at both horizontal and vertical direction.

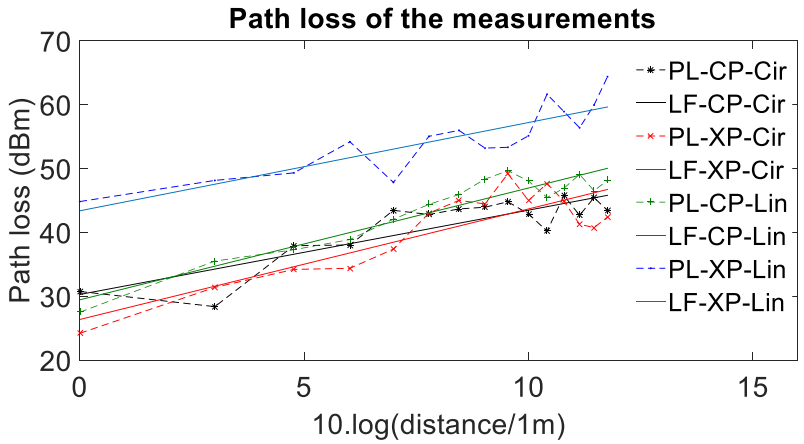

Figure 6.5. Circular (Cir) and linear (Lin) polarizations path loss (PL) and linear fitting (LF) at the CP and XP scenario

Table 6.2. PL exponent values for the different channel configurations

Polarization	**Circular**		**Linear**	
Parameters	CP	XP	CP	XP
PL-exponent	1.320	1.731	1.751	1.382
Average shadowing (dB)	0.0008	-0.0016	-0.0002	0.0005
Shadowing STD	2.6228	3.4229	1.9447	2.7221

For all the configurations, the path loss exponent α is smaller than the free-space path-loss exponent (which is equal to 2), as depicted in Table 6.2. This is due to the wave guiding property of the mine gallery. Additionally, from the linear regression analysis, the circularly polarized signal is found to decay with a slower rate than the linearly polarized one at the CP configuration. Expectedly, the XP signal for the regular MIMO-p setup has the worst PL results among all scenarios because of its inherent LOS signal suppression. The shadowing results show that the PL values are closer to their linear approximation when linear polarization is used than in the circular polarization case. This is due to the lesser variations around the linear fitting in the case of linear polarization, where the LOS signal is the main contribution to the received power. Comparing to previously published SISO results, it is observed that the MIMO PL exponents are better than the SISO counterparts [3-4] due to the MIMO ability to combat fading.

6.2 RMS delay spread, coherence bandwidth and Rican K-Factor

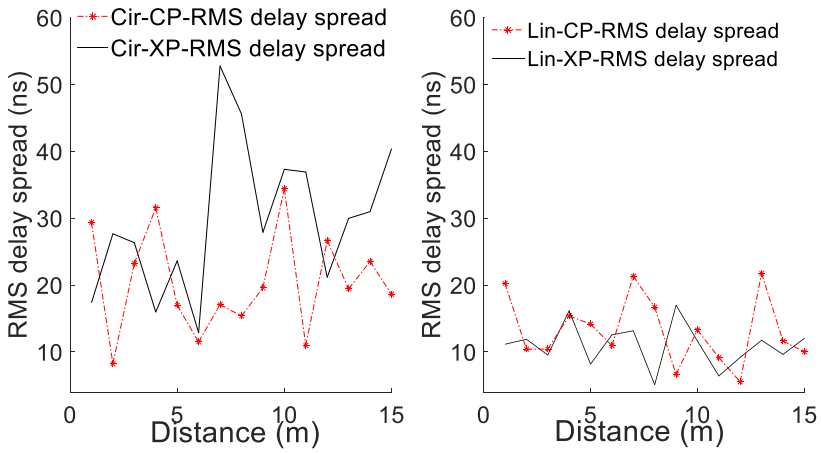

Fig. 6.6. Circular (Cir) and linear (Lin) polarizations RMS delay spread at the CP and XP scenario

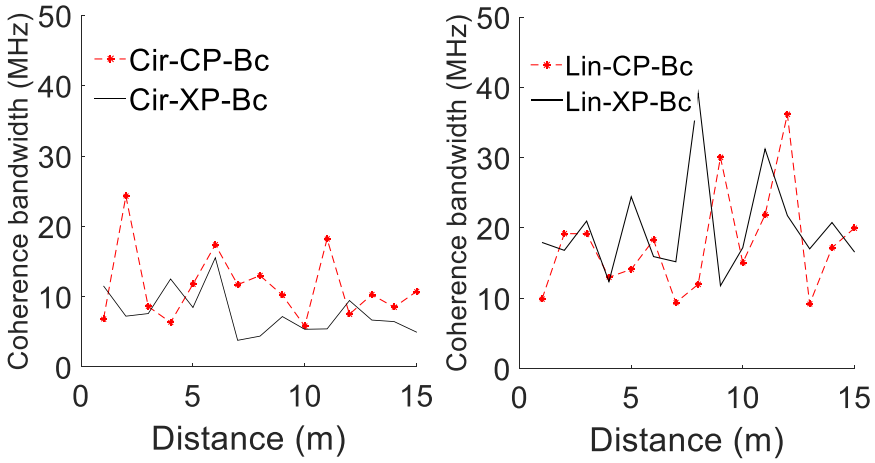

Fig. 6.7. Circular (Cir) and linear (Lin) polarizations coherence bandwidth (Bc) at the CP and XP scenario

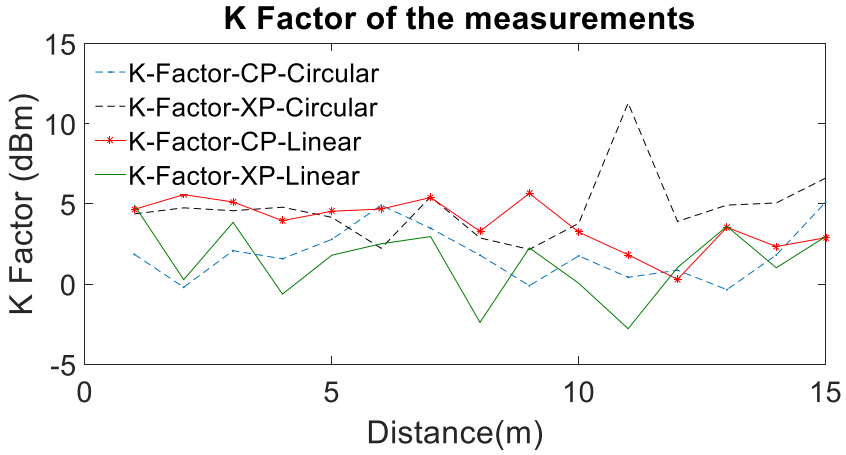

Fig. 6.8. Circular (Cir) and linear (Lin) polarizations K-factor results at the CP and XP scenario

From Fig. 6.6-6.8, it is observed that the RMS delay spread does not necessarily increase with distance. In fact, the reflected signals sometimes add constructively and in other times destructively for this RF channel, resulting in multipath components that do not necessarily increase in number nor in strength as the distance increases. It is observed from the same figure that the circular antenna set up exhibits larger RMS delay spreads and smaller coherence bandwidth compared to the Linear MIMO setup. This is due to the fact that the circular MIMO (MIMO-cir) set up, which radiates in the horizontal and vertical directions, is able to receive more multipath powers than the MIMO-p setup.

In a regular indoor environment, a circularly polarized electromagnetic wave changes its handedness after a reflection from a smooth surface [5]. This first order reflection, which is generally suppressed in a regular tunnel environment, is not suppressed as efficiently in a mine gallery due to the surface roughness [6-8].

With regards to the K-factor results (shown in Fig. 6.8 and Table 6.3), the linear MIMO set up at the XP scenario exhibits the lowest K-factor because of the lack of a dominant component. It is, however, observed that even at this scenario (Linear-XP), a certain amount of multipath power is received due to the surface roughness which causes a signal depolarization. This depolarization makes the cross-polarization less severe; hence, a transmission is possible even using the linear MIMO setup at the XP scenario, but with a decreased quality. Moreover, the K-factor is highest for the XP-circular and the CP-linear set ups due to the fact that the LOS component is strongest for these topologies. From the statistical K-factor results, it is observed that the K-factor at the circular co-polarized (Cir-CP) MIMO setup is less than that of the linear co-polarized (Lin-CP) MIMO setup due to the multipath richness.

Table 6.3. Statistics of the K-factor for the RF channels inside the mine gallery (Minimum, Maximum, average and standard deviation measured values).

Polarization	**Circular**		**Linear**	
Parameters	CP	XP	CP	XP
K-factor-Average (dB)	1.8561	4.7311	3.8015	1.4313
K-factor-STD (dB)	1.6799	2.1634	1.5293	2.2286

6.3 Channel Capacity

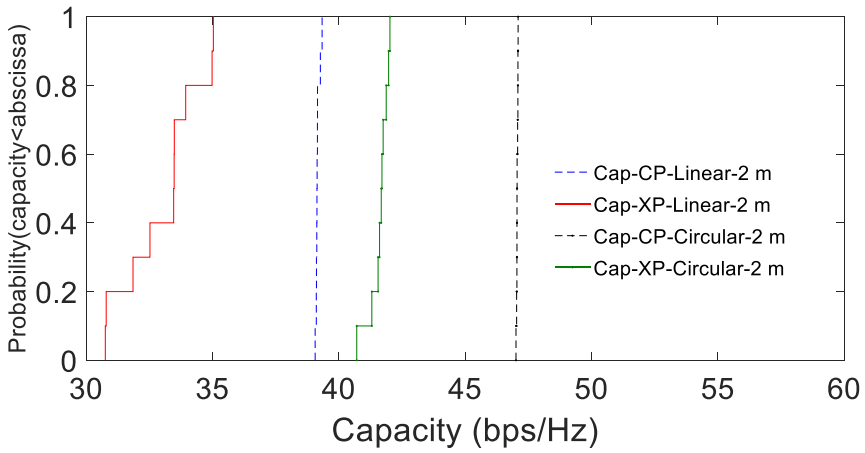

Fig. 6.9. Circular and linear polarizations MIMO channel capacity CDFs at the CP and XP scenario and a constant transmitted power.

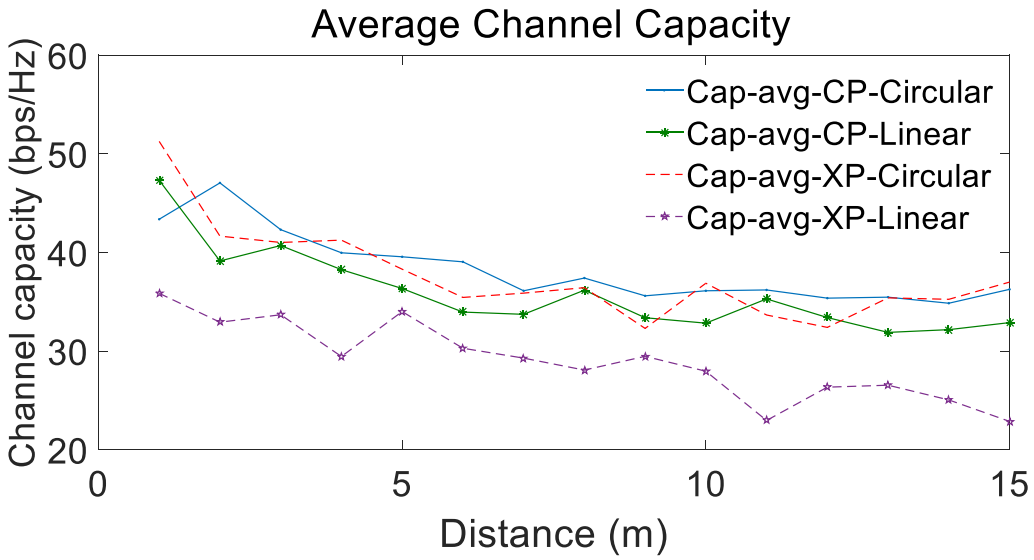

Fig. 6.10. Average MIMO channel capacities at constant transmitted power for Circular and linear polarizations

The MIMO channel capacity is derived with two different methods. The first method assumes a variable SNR and constant transmitting power. This method allows to study the effect of PL on the MIMO channel [2]. The second method uses a fixed SNR and gives the channel capacity when the PL effect is cancelled [2]. The channel capacity results for a constant transmit power (denoted in Fig. 6.10) show that the channel capacity decreases with distance. This is explained by the fact that the smaller distances correspond to higher received average powers and hence higher average SNRs which have a direct impact on the capacity. Moreover, it is observed that the circularly polarized antenna setup capacities are higher than the linear polarization setup channel capacities, for both the CP and the XP configurations. This is due to the suitability of the circular MIMO setup to capture multipath signal at a rough environment. It is to note that the suppression of the reflected wave (for the circular polarization) signals is not done efficiently due to the rough environment [6-8]. The cross-polarized linear MIMO setup exhibits the lowest capacities due to the effective suppression of the LOS signal. The multipath signals still exist,

however, due to the additional depolarization caused by the rough surfaces, making the reflected signal visible at the receiver, although with little strength. Expectedly, compared to the previously published SISO results (CP scenarios) [3-4], the MIMO capacities are considerably higher (more than 1.5 times the SISO capacities).

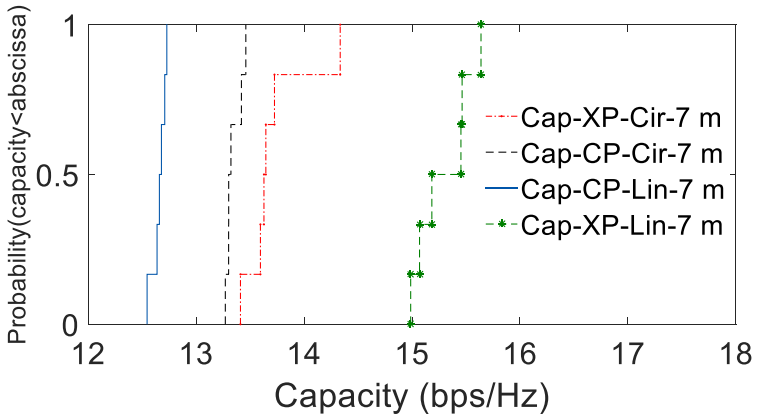

Fig. 6.11. Circular (Cir) and linear (Lin) polarizations MIMO channel capacity CDFs at the CP and XP scenario and a fixed SNR

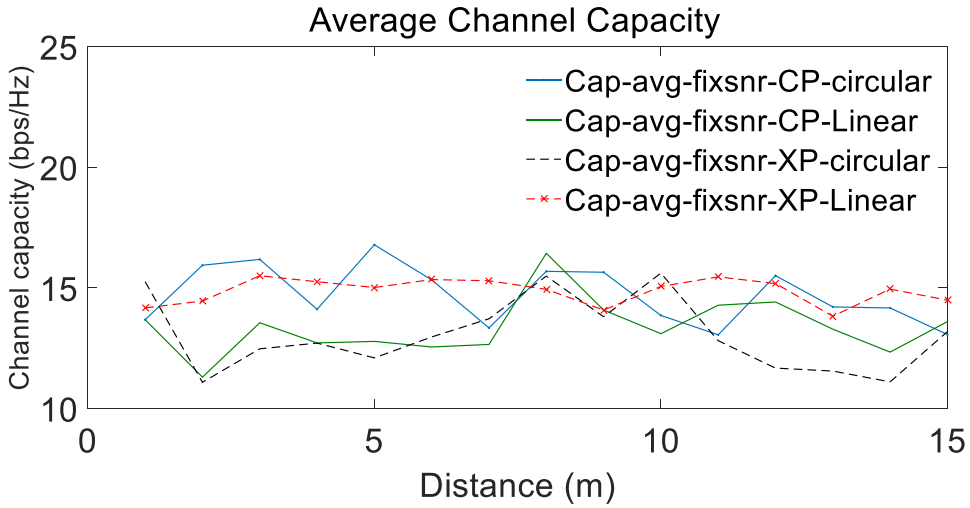

Fig. 6.12. Average MIMO channel capacities at constant SNR for Circular and linear polarizations

The channel capacity results at a fixed SNR (20 dB)- depicted in Fig. 6.12- are very close for all the different configurations (ranging between range between 11.1 bps/Hz and 16.7 bps/Hz). It is observed that the curves do not follow a monotonic trend, suggesting that the multipath richness is random for these channels. The circularly polarized MIMO setup

generally has the highest channel capacities, at the CP scenario, due to its ability to capture multipath signals. The Linear setup at the CP scenario and the circular setup at the XP scenario generally exhibit the lowest capacities at an SNR of 20 dB, meaning that these two topologies are the least capable to capture the multipath signals. These results are correlated to the K-factor results in Table 6.3.

6.4 References

[1] M. El Hassan El Azhari, L. Talbi, L. Arabi, M. Nedil, M. L. Seddiki, and N. Kandil, " Channel Characterization of Circularly Polarized Antenna MIMO System in an Underground Mine," Progress In Electromagnetics Research M, Vol. 67, 9-19, 2018.

[2] M. Yahya and Z. Awang, "Cross polarization ratio analysis of circular polarized patch antenna," 2010 International Conference on Electromagnetics in Advanced Applications, Sydney, NSW, 2010, pp. 442-445.

[3] A. Benzakour, S. Affes, C. Despins and P. M. Tardif., "Wideband measurements of channel characteristics at 2.4 and 5.8 GHz in underground mining environments," in Vehicular Technology Conference, 2004.

[4] C. Briso-Rodriguez, J. M. Cruz and J. I. Alonso, "Measurements and Modeling of Distributed Antenna Systems in Railway Tunnels," in IEEE Transactions on Vehicular Technology, vol. 56, no. 5, pp. 2870-2879, Sept. 2007.

[5] K. Guan, Z. Zhong, J. I. Alonso and C. Briso-Rodriguez, "Measurement of Distributed Antenna Systems at 2.4 GHz in a Realistic Subway Tunnel Environment," in IEEE Transactions on Vehicular Technology, vol. 61, no. 2, pp. 834-837, Feb. 2012.

[6] G. R. Valenzuela, “Depolarization of E-M waves by slightly rough surfaces”, 3rd ed. IEEE Trans. Antennas Propagat., vol. AP- 15, pp. 552-557, 1967.

[7] J. W. Wright, “A new model for sea clutter," IEEE Trans. Antennas Prop., vol. AP-16, pp. 217-223, 1968.

[8] H.R.Raemer, D.D. Preis, “Aspects of Parallel-Polarized and CrossPolarized Radar Returns from a Rough Sea Surface”, IEEE Trans. on Electromagnetic Compatibility, vol EMC-22, Issue 1, pp. 29 - 44, Feb. 1980.

Chapter 7 Performance evaluation of on-body systems

The results of this contribution are published in [1]. The On-body propagation measurements at 40 m underground mine gallery and their statistical analysis are presented. Monopole antennas were installed on the body in order to form three on-body channels, namely belt-chest, belt-wrist and belt-head. The channel parameters of a 2 × 2 Multiple-Input Multiple-Output (MIMO) On-body system are evaluated and compared to the single-input single-output (SISO) system parameters. It was shown that the RMS delay spread and capacity values of the MIMO channels are higher than those of the SISO channels. The average value of the Rican K-factor shows little difference between the MIMO and SISO belt-chest measurements. The calculated capacity values for a constant signal to noise ratio (SNR) and those calculated at a constant transmitted power demonstrate that the propagation performance is significantly improved by using the MIMO compared to the conventional SISO scheme. Hence, MIMO technology is a suitable candidate for On-body underground communications.

7.1 Measurements procedure

In an experimental gold mine of northern Quebec, measurements were performed at the 40 m level gallery of about 4 m in height and width. The measurement environment

consisted of floor, walls and ceiling of irregular geometries. The ceiling and walls contain many metallic nets and rods. The wall roughness (standard deviation) is estimated to be 6 cm with a maximum and average roughness thickness values estimated around 37 and 20 cm, respectively [2]. The temperature is maintained at 6 °C, with a humidity level of nearly 100 % throughout the year. The 40 m underground gallery is illustrated in Fig. 7.1.

In order to characterize the On-body SISO and MIMO channels in a mining environment at 2.45 GHz, three On-body channels were considered for measurements. For each On-body channel, the transmitting antenna set (Tx) was placed at the left side position of the belt. The receiving antenna set (Rx) was placed alternatively at the right side of the chest (Rx 1), the right side of the head (Rx 2), and at the right wrist position (Rx 3), thus forming three On-body channels: belt-chest, belt-wrist, and belt-head as shown in Fig. 7.2. The transmitting antenna set was placed to point upward, and the receiving antenna set pointing downward. The distance between the body and the antenna was kept at about 5-10 mm. The transmitting and receiving antennas were connected to the two ports of the VNA. The system calibration is performed with the cables connected to the VNA in order to remove the losses introduced by the cables from the measured frequency response S_{21}. After the calibration, all the parameters were configured, namely the transmitting power, the frequency range, and the number of points. The noise floor for the measurement was considered at -90 dBm (based on the observation of measured impulse responses). Fig. 7.2 shows the human test subject and antenna connections in the mine environment. The experiments were performed on a 1.80 m, 75 Kg human male subject, in a very rough, dusty, and humid environment. In order to study the significance of using MIMO on the channel parameters, a 2×2 MIMO antenna set was used. These omnidirectional antennas

have gain of about 2.2 dBi, bandwidth of about 10% and beam width of 360 and 65^{o} in the azimuth and elevation planes, respectively. Fig. 7.3 shows the measured return loss S_{11} and mutual coupling S_{21} between the antenna elements. In the operating band, S_{11} is lower than -10 dB.

During measurements, 6 data snapshots were collected, and the S21 parameter values are recorded for 6401 frequency samples around the center frequency of 2.45 GHz. These S21 values are used in the post processing MATLAB codes in order to determine the channel parameters, as detailed in subsequent paragraphs.

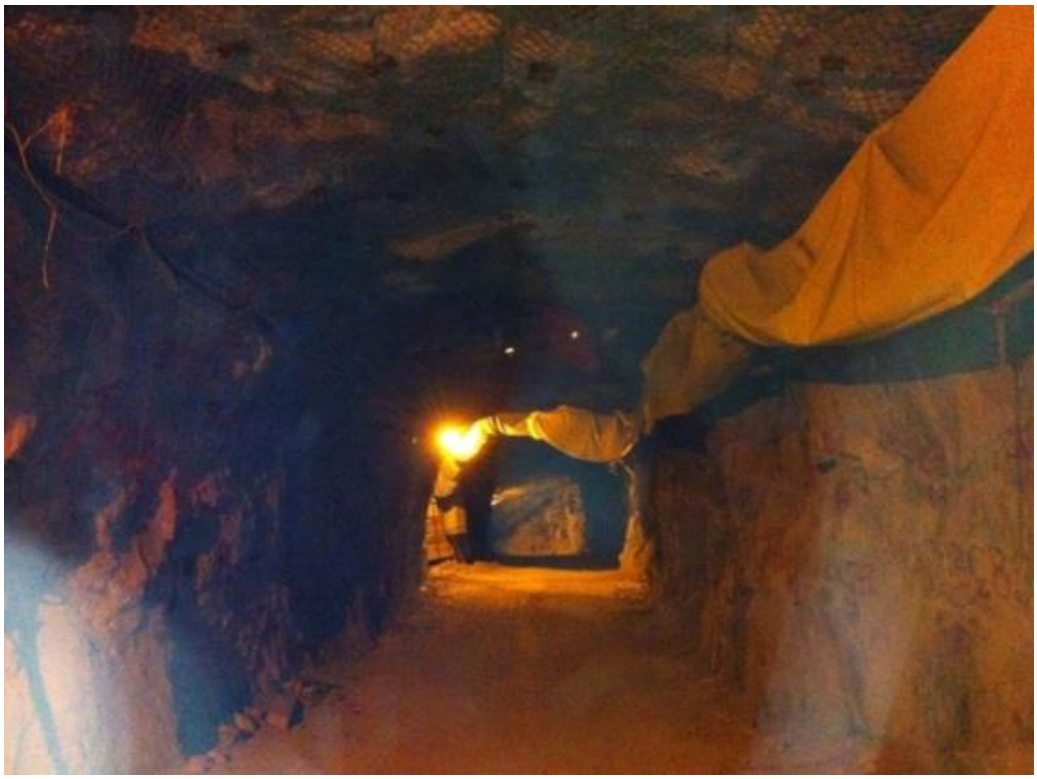

Fig. 7.1. Digital photo of the mine gallery

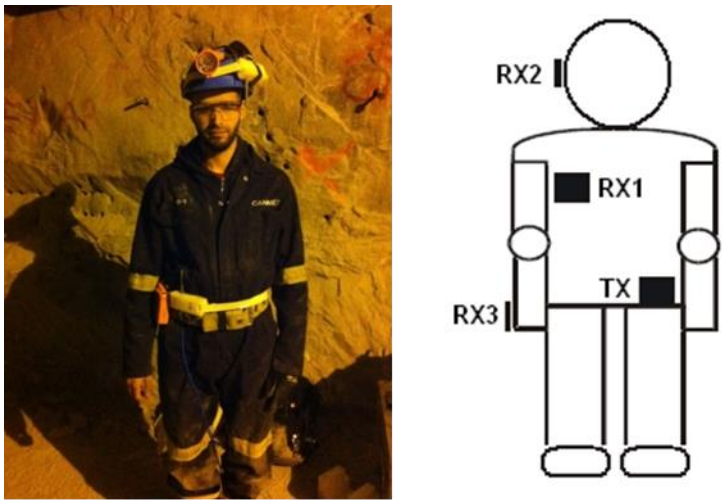

Fig. 7.2. Antenna positions for On-body measurements

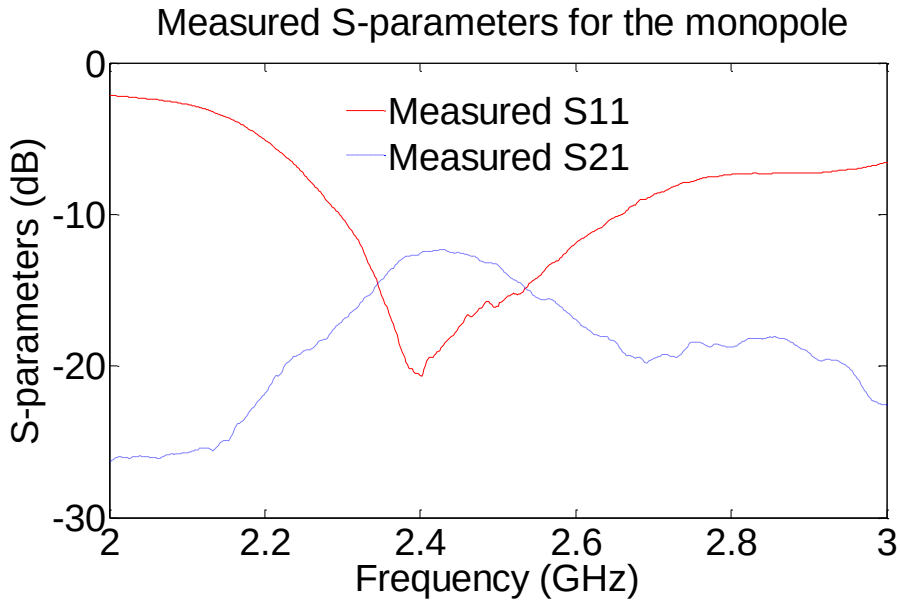

Fig. 7.3. Measured S-parameters for the monopole setup

7.2 Channel impulse response

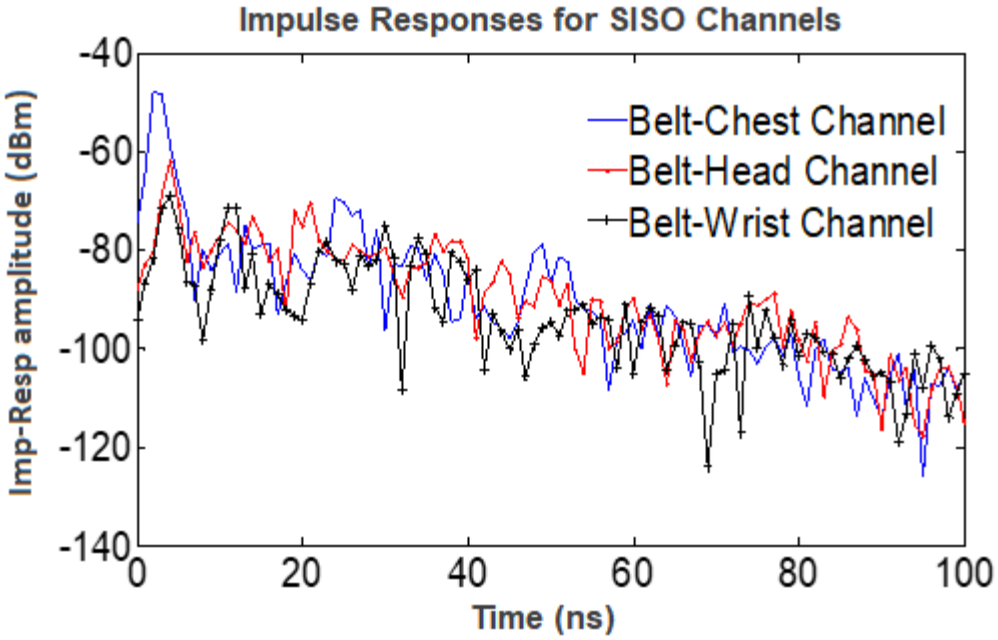

Fig. 7.4. Impulse responses for the three On-body SISO channels.

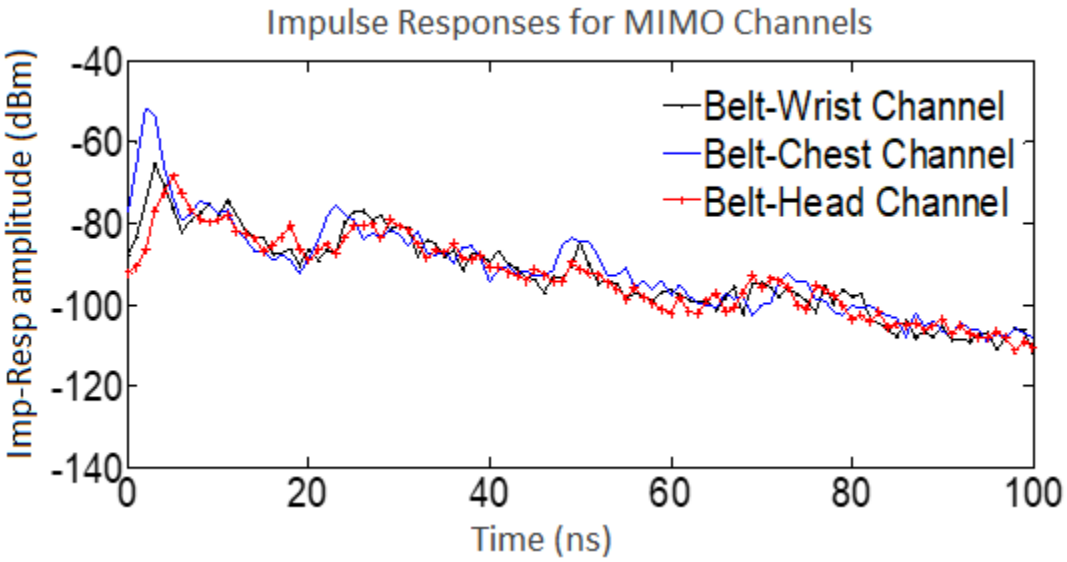

Fig. 7.5. Impulse responses for the three On-body MIMO channels

By applying an inverse Fourier transform to the measured frequency response (S_{21}) values, the channel impulse response is determined for the SISO channels and the MIMO sub-channels. In the MIMO configuration, the impulse responses were determined as the arithmetic mean of the four sub-channels impulse responses. From graphs presented in

Fig. 7.4, the SISO impulse responses exhibit a stronger line of sight (LOS) component for the belt-chest channel (-48 dBm) compared to the belt-wrist channel (-61 dBm) and the belt head channel (-53 dBm), when -10dBm is allocated to the transmitter power. This is mainly due to the direct visibility provided by the belt-chest channel. In the MIMO configuration, the belt-chest channel remains the strongest link with a -51 dBm received power, as illustrated in Fig. 7.5. It is observed that the deep fade is reduced in the MIMO results.

7.3 Rican K-Factor

The K-factor was calculated for each On-body channel and antenna setup. Table 7.1 denotes the Rican K-factor statistics for the three measurements channels in the SISO and MIMO configurations. It can be seen that MIMO setup exhibits slightly higher K-factor results than the SISO setup for the belt-chest and belt-wrist channels. This is due to the fact that the MIMO multipath (derived by averaging of MIMO branch multipath signals) powers are generally smaller than their SISO counterparts [3]. Moreover, the standard deviation of the MIMO K-factor results is smaller than their corresponding SISO K-factor standard deviations. In fact, the averaging property of MIMO reflects smaller fluctuations of the received signal at the different snap shot, which explains the standard deviation results. Moreover, the results suggest a correlation between the K-factor and the Tx-Rx separation distance combined with a strong LOS component availability. Hence, the K-factor is higher for the belt-chest channel which is characterized by the smallest Tx-Rx separation and the strongest LOS component.

7.4 RMS delay spread and Coherence bandwidth

Results show values of the RMS delay spread for the SISO channels in the rage of 15 ns to 59 ns, which correspond to coherence bandwidth (at 50% correlation) in the range of 3 MHz to 13 MHz as shown in Table 7.1. The MIMO RMS delay spread results, denoted in Table 7.1, are a little higher than the corresponding SISO results. This is due to the fact that the MIMO setup is able to collect more multipath components than the SISO setup.

7.5 Channel Capacity at a Constant Transmission Power

The channel capacity for a channel with a strong line of sight (LOS) component (belt-chest channel) is higher than the other channels with less strong LOS components. This result is valid for the average channel capacity (in Table 7.1) and for the CDF plots at a certain probability level (in Fig.7.6 and Fig.7.7). This is expected since a strong LOS component would result in a higher received power magnitude, and hence a higher SNR value. Detailed results for the average channel capacities of the SISO and MIMO channels are listed in Table 7.1.

Table 7.1. Parameters values for each channel

Parameters	On-Body measurement channels					
	Belt-chest		Belt-head		Belt-wrist	
	SISO	MIMO	SISO	MIMO	SISO	MIMO
Average channel Capacity (bps/Hz)	9.02	16.6	5.62	7.56	4.65	7.78
Coherence bandwidth at 50% correlation (MHz)	13.4	10.7	7.20	2.20	3.40	2.70

Coherence bandwidth at 90% correlation (MHz)	1.34	1.07	0.72	0.22	0.34	0.27
RMS delay spread (ns)	15.75	18.7	27.8	89.4	59.0	73.7
K-factor_mean (dB)	32.3	32.4	31.5	29.7	30.7	30.9
K-factor_STD (dB)	1.21	0.140	1.47	0.638	1.70	0.386

The obtained results demonstrate a considerable improvement of the channel capacity due to the use of MIMO. This improvement depends on the number of multipath components and the strength of the LOS signal; hence, the Belt-wrist channel experienced an increase in capacity of about 3.1 bps/Hz and the Belt-chest channel capacity is improved by about 7.6 bps/Hz, due to the use of MIMO.

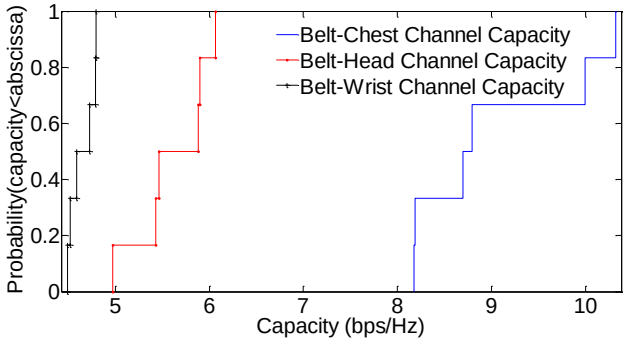

Fig.7.6. SISO capacity CDFs for the three On-body channels.

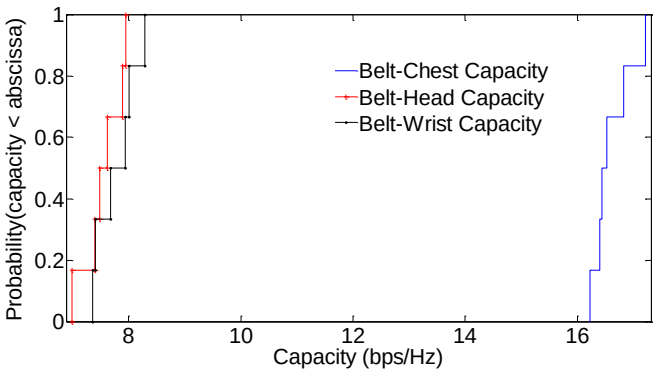

Fig.7.7. MIMO capacity CDFs for the three On-body channels assuming a fixed transmitted power

7.6 Channel Capacity for a constant SNR

This section deals with the capacity calculations assuming a constant SNR. The CDF plots in Fig.7.8 assume a SNR value of 20 dB, which was chosen large enough to guarantee that noise will not mask the results. These MIMO capacity CDFs show that at a constant SNR and for a probability level less than 80%, the belt-chest channel exhibits the highest capacity followed by the belt-head channel. Furthermore, the average MIMO capacity curves as a function of SNR emphasize this result as denoted by Fig.7.9. For a SNR of 20 dB, the belt-chest average capacity is 10.9 bps/Hz, the belt-head capacity is 9.48 bps/Hz and belt-wrist capacity is 7.95 bps/Hz. It seems that the sub-channels correlation is significantly reduced due to the creeping-wave propagation which reduces the direct ray power, as explained in [4]. Moreover, the belt-chest and the belt-head channels exhibit similar multipath phenomena because Tx and Rx are directly facing each other and the multipath powers are negligible compared to the LOS power, in both channels. The belt-chest capacity is slightly higher than the belt-head capacity, likely due to the fact that the main reflections from the walls and body parts are somewhat higher for the belt-chest channel. In the case of the belt-wrist channel, Tx and Rx main beams are pointing in different directions with the wrist-mounted Rx at a lower position than Tx due to the length of the human subject arm. Hence, the multipath propagation is mainly due to the reflections from the walls and ceiling, since the creeping wave and body reflections will likely be directed away from Rx. Moreover, the CDF curves denote less spread in capacity for the belt-chest channel. This can be explained by the minor variations of the received powers for the belt-chest channel due to the fixed Tx-Rx distance.

The improvement offered by MIMO over SISO is demonstrated through the capacity results. Ideally, for N × N MIMO channel, the capacity is increased N times for a fixed SNR level [5]. In this case, the throughput gain is less than 2 for all On-body channels due to some degree of correlation between the sub-channels. This throughput gain is found to be 1.6 for the belt-chest channel, 1.4 for the belt-head channel, and 1.2 for the belt-wrist channel. Hence, it can be concluded that the multipath richness is a significant factor in the capacity improvement.

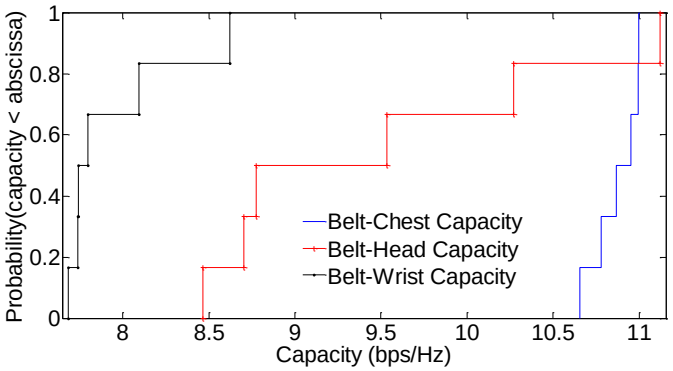

Fig.7.8. MIMO capacity CDFs for the three On-body channels assuming a fixed SNR

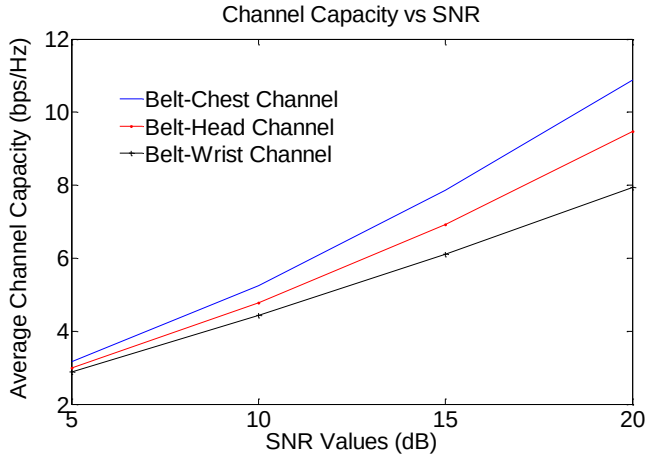

Fig.7.9. MIMO average capacity as a function of SNR for the three On-body channels

7.7 Dynamic channel parameters results

In addition to the measurement for a quasi-static channel, measurements were performed with different sets of movements for the three channels (Belt-Head, Belt-Chest, and Belt-wrist). The activity sets, and the corresponding capacity results for the three channels are given in Table 7.2. The results show that the movement of the human body has a minor effect on the capacity. This is clearly demonstrated by comparing the capacity results for a movement where the Tx-Rx length remains somewhat constant to the average SISO capacity of the corresponding Quasi-static channel. For instance, the capacity for a belt-chest channel when sitting down (at a typing posture) is 8.9 bps/Hz, which is close to 9.0 bps/Hz that is found for a quasi-static channel. The length of the link, however, has a greater impact upon the capacity values (with variations from the average capacity values of a quasi-static channel reaching up to 5bps/Hz, when the length of the Rx-Tx link endures a big change during the movement). These results are expected, since the speed at which the receiver moves with respect to the transmitter is negligible compared to the speed of light, making the observed frequency at the receiver (including the Doppler effect), effectively the same as the emitted frequency. The channels are still effectively considered quasi-static. Moreover, when the Tx-Rx are misaligned due to a certain movement (such as in the case of the Belt-Head channel when walking or when lifting things from floor), the channel capacity is reduced compared to static channel result. Table 7.2 represents the capacity values of the different On-body channels when the human subject undergoes certain typical body movements.

Table 7.2. SISO Capacity corresponding to typical states of the human body

Belt-Head Postures	**Belt-Head Capacity (bps/Hz)**	**Belt-Chest Posture**	**Belt-Chest Capacity (bps/Hz)**	**Belt-wrist Posture**	**Belt-wrist Capacity (bps/Hz)**
Shaking head-left-right	4.31	Moving arm-eating posture	9.97	Moving arm-eating posture	7.27
Shaking head-up-down	4.57	Sitting down-typing posture	8.90	Writing and typing	9.89
Moving arm while standing	5.47	Leaning down-while standing	8.46	Lifting things from floor	9.05
walking	3.82	Leaning down-while siting	9.23	Waving Bye-Bye	6.71
Lifting things from floor - stand-sit movement	3.80	Exercise-stand-sit	10.54	Clapping	5.79

7.8 Stochastic-empirical modeling for the on-body channel

Similarly to the B2B modeling (in chapter 5), a statistical-empirical model (for the on-body) channel is presented. This novel model allows generating the impulse response, which approximates the 2.4 GHz measurements based one.

The arrival times are stochastically modeled by comparing their steps distribution to different distributions used in the literature (as seen in Fig. 7.10), then generating a random vector following the optimal one. Finally, the MPCs amplitude model vector is joined to its corresponding arrival times vector in order to get the impulse response model. The

Weibull distribution (with the shape and scale parameters equaling 16.5 and 2.6 successively) was found to best describe the arrival time steps, since the supremum of the set of distances in the KS test was smallest with a value of 0.22. The minimum mean square error (MMSE) estimation of the optimal impulse response model (in Fig. 7.11) is 0.0019, which shows that the model approximates well the measurements.

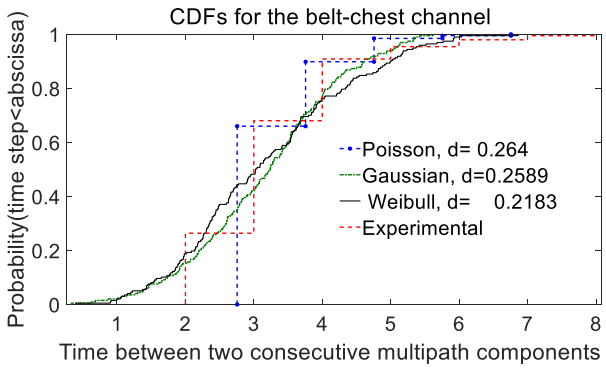

Fig. 7.10. Arrival time steps CDFs

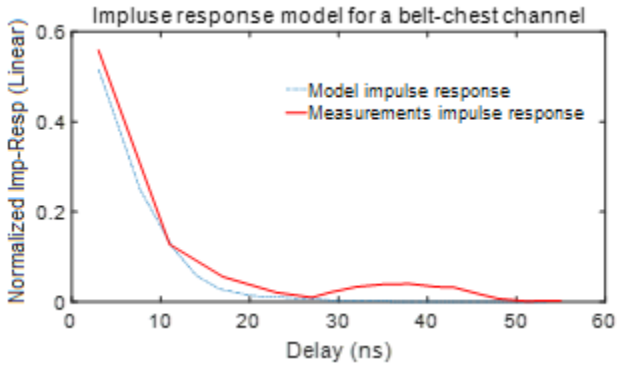

Fig. 7.11. Measured impulse response vs. model

7.9 Conclusion

The significance of using MIMO for On-body channels in underground mines has been demonstrated through measurements for a 2×2 MIMO link. Three On-body channels have been considered for 2.45 GHz measurements. When a constant transmitted power is

assumed, the channel capacity is highest for the belt-chest channel due to the small Tx-Rx separation and rich multipath phenomenon. The K-factor results are correlated to the capacity values at a constant transmitted power. These values reflect the multipath richness and the presence of a strong LOS component, which also explains the RMS delay spread results. The belt-chest channel, due to its strong direct ray, exhibits the smallest RMS delay spread value. The RMS delay spread values are higher for the MIMO setup compared to SISO because the MIMO setup is able to collect more multipath components than SISO. The capacity results for a fixed SNR suggest that the sub-channels correlation is significantly reduced due to the creeping-wave propagation which reduces the direct ray power. Furthermore, the capacity results- for certain typical body movements- reflect the Tx-Rx separation regardless of the body motions. Finally, the on-body belt-chest channel was modeled using stochastic-empirical techniques. The impulse response model show very good approximation to the underground mine on-body measurements (with an MMSE of 0.0019). This novel modeling technique is very promising and allows characterizing the on-body channel with no need for extensive measurements campaigns. Moreover, since the on-body' channel is affected mainly by the LOS propagation as well as the body parts reflections (while the reflected and diffracted signals from the mine gallery are negligible) the on-body model should apply to a wide range of underground environments.

7.10 References

[1] M. El Azhari, M. Nedil, I. B. Mabrouk, L. Talbi, K. Ghanem, and Y. S. Alj, "Performance evaluation of a MIMO-on-body system in a mine environment," Progress In Electromagnetics Research C, Vol. 61, 55-63, 2016.

[2] S. Ahsanuzzaman Md Tariq, C. Despins, S. Affes, and C. Nerguizian,“Rough surface scattering analysis at 60 GHz in an underground minegallery,” in IEEE International Conference on Communications Workshops (ICC), pp. 724–729, June 2014.

[3] I. Khan, “Diversity and MIMO for body-centric wireless communication channels”, PhD thesis report, University of Birmingham, September 2009.

[4] I. Khan, P. S. Hall, "Experimental Evaluation of MIMO Capacity and Correlation for Narrowband Body-Centric Wireless Channels," Antennas and Propagation, IEEE Transactions on , Vol.58, no.1, pp.195,202, Jan. 2010.

[5] E. Biglier, R. Calderbank, A. Constantnides, A. Goldsmith, A. Paulraj and H.V. Poor, MIMO Wireless Communications. New York: Cambridge Univ. Press, 2007.

Chapter 8 Characterization of off-body systems

As part of this work, several papers, characterizing the MIMO off-body channel inside a mine, were published. In [1], the MIMO off-body channel performance was compared to a previously studied SISO channel [2]. Moreover, since, the off-body link in a mine environment is prone to obstruction, NLOS scenarios were studied in comparison to LOS scenarios. Finally, the effect of directivity on the MIMO-off-body link was explored both for LOS [3-4] and NLOS [5-6].

8.1 Effect of human obstruction on the MIMO-off-body link

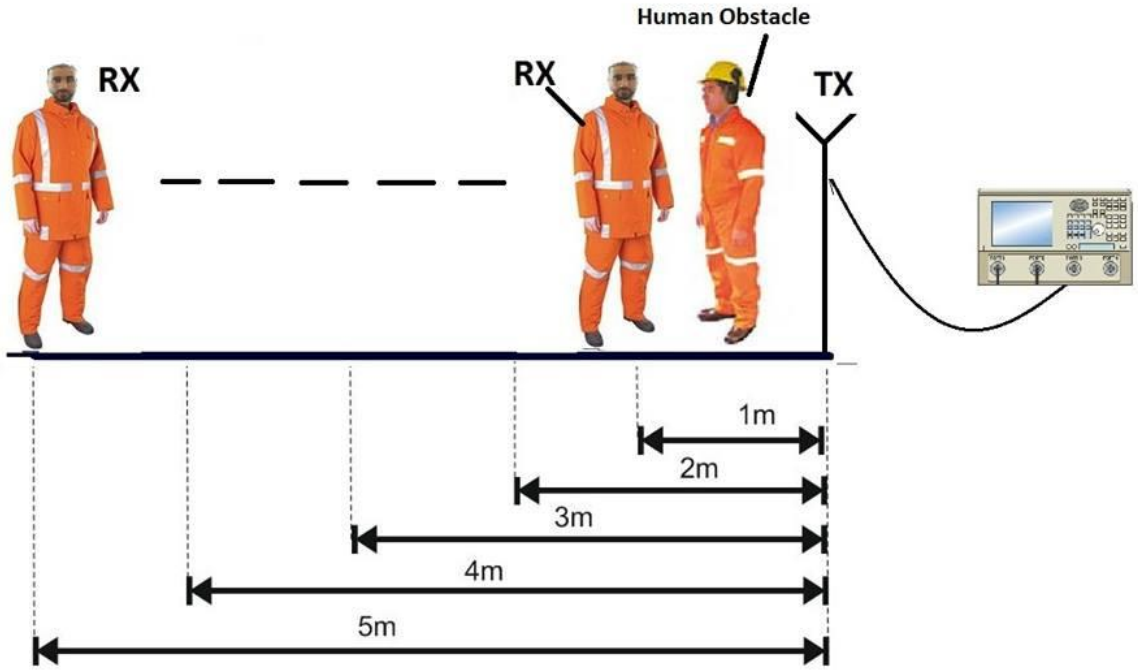

Fig. 8.1. Measurements setup inside the mine

In this contribution [1], a 2×2 MIMO Off-body channel has been characterized in a mine gallery at both LOS and NLOS scenarios using monopole antennas. It was observed that the PL exponent at NLOS is smaller than its counterpart value at LOS (1.43 vs.1.79). Path loss results are represented in Fig. 8.2. The channel capacity (at a constant transmitted power) decreases with the increase in distance and with the obstruction of the LOS signal, due to the decrease in the SNR, as denoted in Figure 8.4. An improvement of about 8.5bps/Hz is observed for MIMO compared to the SISO configurations (at a fixed SNR), which proves the significance of the multipath richness in enhancing the channel capacity.

Compared to LOS, MIMO capacity at a fixed SNR, the NLOS capacity is generally higher due to a lower correlation. Comparing MIMO to SISO channel capacity results (both at a constant transmitted power and at a fixed SNR), we conclude that the PL has a greater effect on capacity than the multipath richness. It is clear from the results (in Figure 8.4 and Fig. 8.5) that MIMO topologies provide a remarkable capacity improvement compared to the SISO topologies [7].

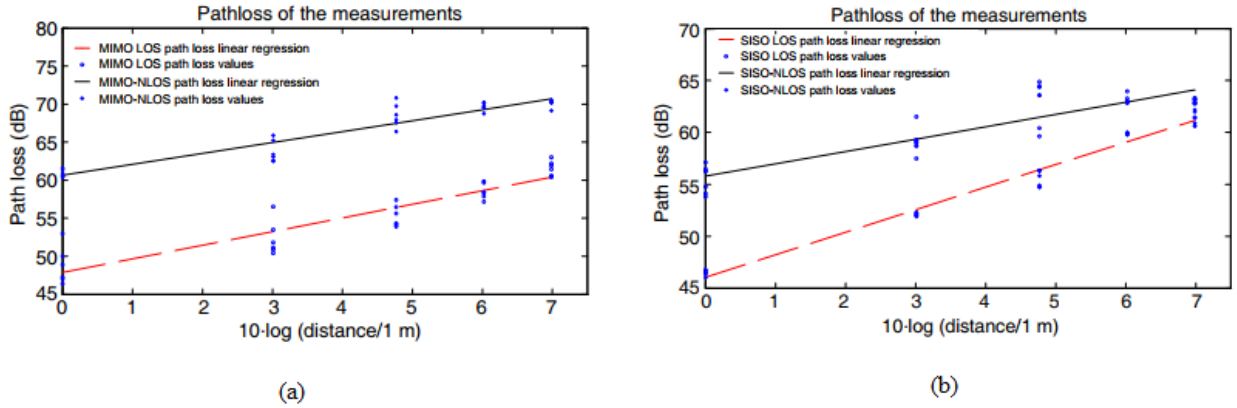

Fig. 8.2. MIMO (a) vs. SISO (b) path loss results

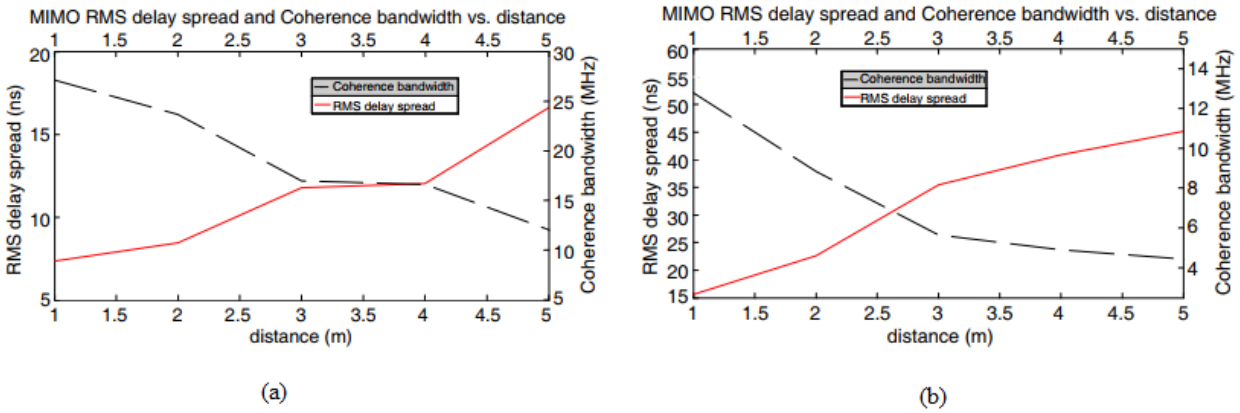

Fig. 8.3. MIMO RMS delay spread and coherence bandwidth vs. distance for LOS (a) and NLOS (b)

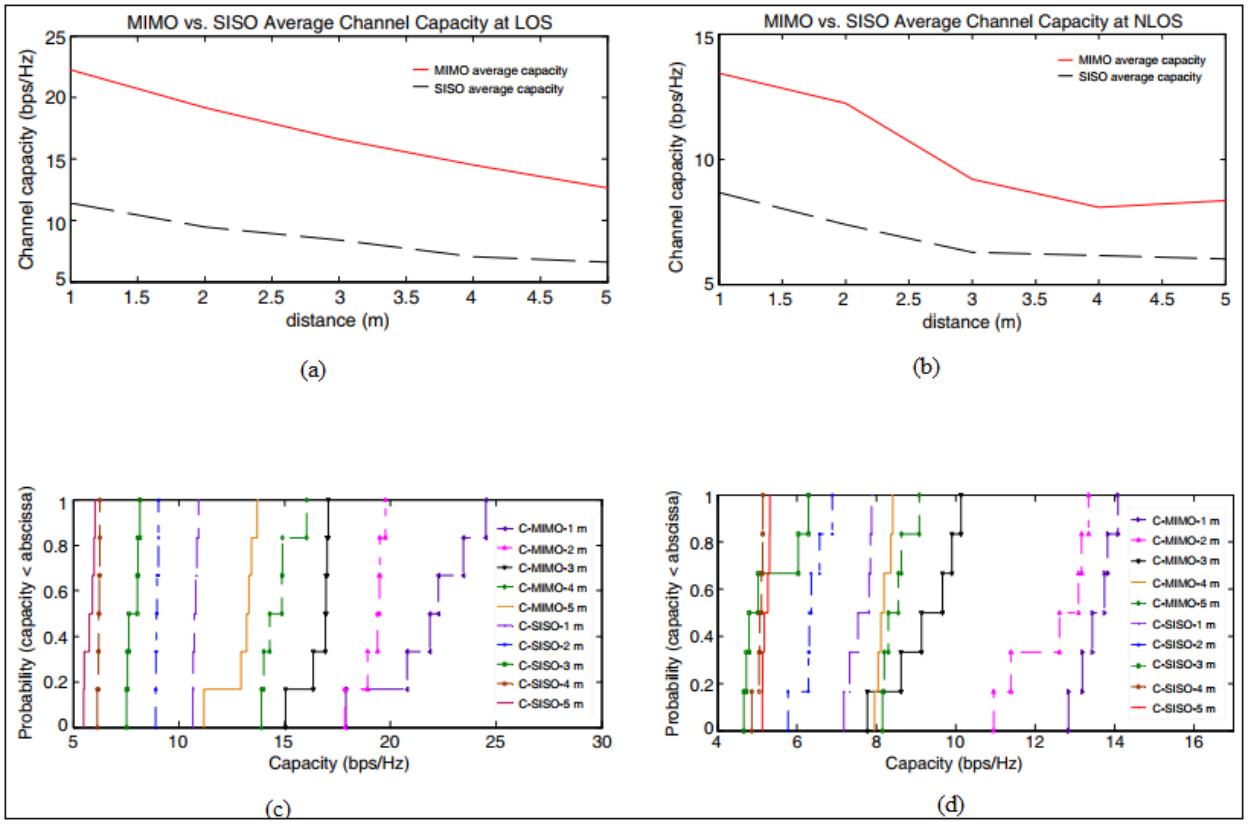

Figure 8.4. MIMO and SISO average capacities (a, b) and capacity CDFs (c,d) of the off-body channel assuming a constant transmitted power at LOS (a,c) and NLOS (b,d)

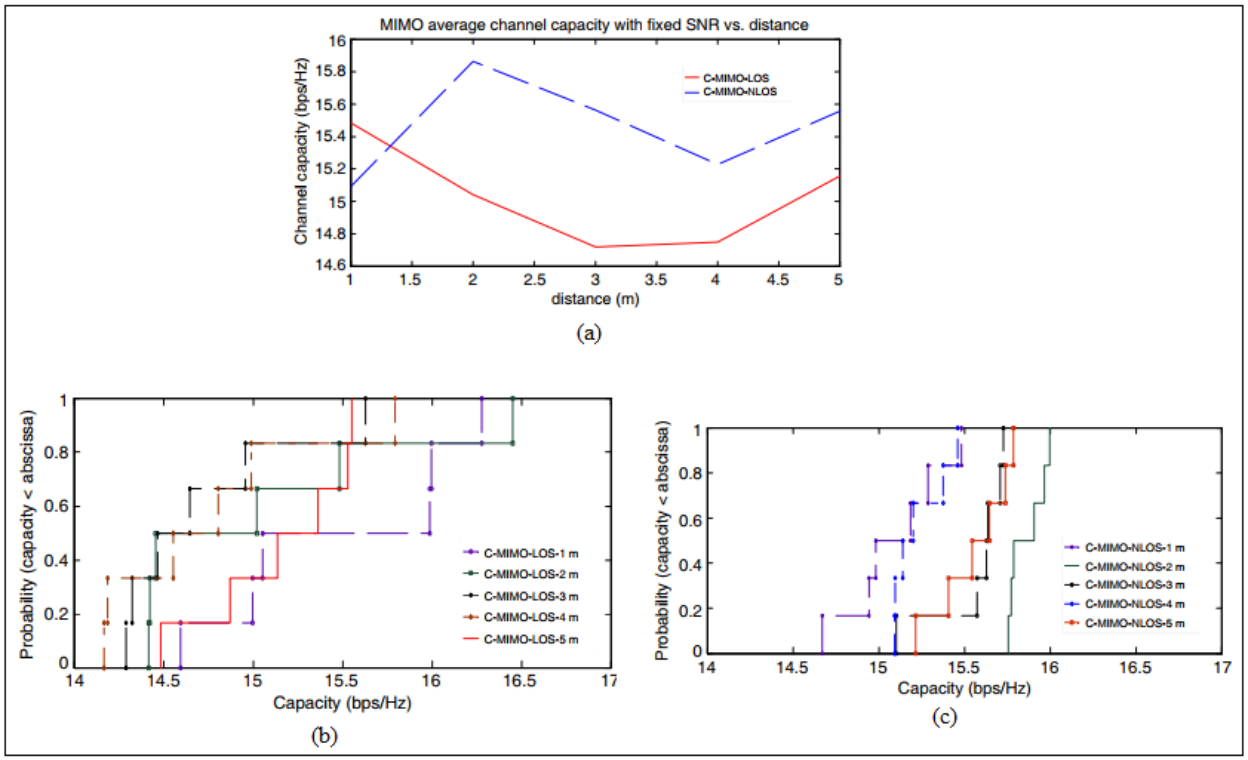

Fig. 8.5. MIMO-monopole LOS vs. NLOS average capacities (a) and capacity CDFs of the off-body channel at LOS (b) and NLOS (c), assuming a constant transmitted power

8.2 Effect of directivity on the MIMO-off-body link

In this contribution, four conference articles were published. The effect of multipath on the channel capacity for a MIMO-patch (MIMO-p) setup compared to a MIMO-monopole (MIMO-m) system was studied at LOS [3] and NLOS [5]. Moreover, the PL effect on channel capacity has been reported for MIMO-p compared to MIMO-m at LOS [4] and NLOS [6].

The multipath was confirmed to increase both channel capacity and the RMS delay spread at both LOS and NLOS. The K-factor is found to be highly correlated to the channel capacity at constant SNR (for both LOS and NLOS). The capacity and RMS delay spread values using directive antennas are generally worse than those of a comparable monopole

setup at NLOS [1]. This is due to the fact that the monopole antenna is more capable to catch multipath signals than the directive patch antenna. For a variable SNR and a constant transmitted power, the effect of increasing multipath with the distance was not able to counter the effect of the path loss. It was found that directivity did not improve capacity due to the high PL. compared to the monopole results (presented in the previous sub-section) [1], the channel capacity and the path loss exponents of MIMO-p are worse than those of the MIMO-m due to a worse signal degradation of the MIMO-p compared to MIMO-m. This result is explained by the fact that the monopole setup captures a greater number of multipath components, which causes the MIMO-m to have a greater contribution to the total received power (than MIMO-p) from the multipath signals.

The results for the MIMO-p antennas are represented in the bellow figures (Fig. 8.6 and Fig. 8.7).

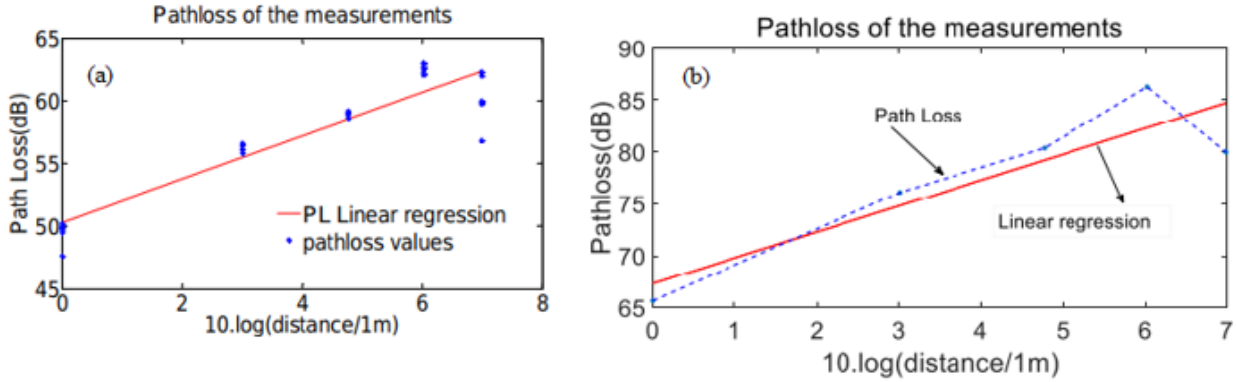

Fig. 8.6. Path loss of the MIMO-p setup for LOS (a) and NLOS (b)

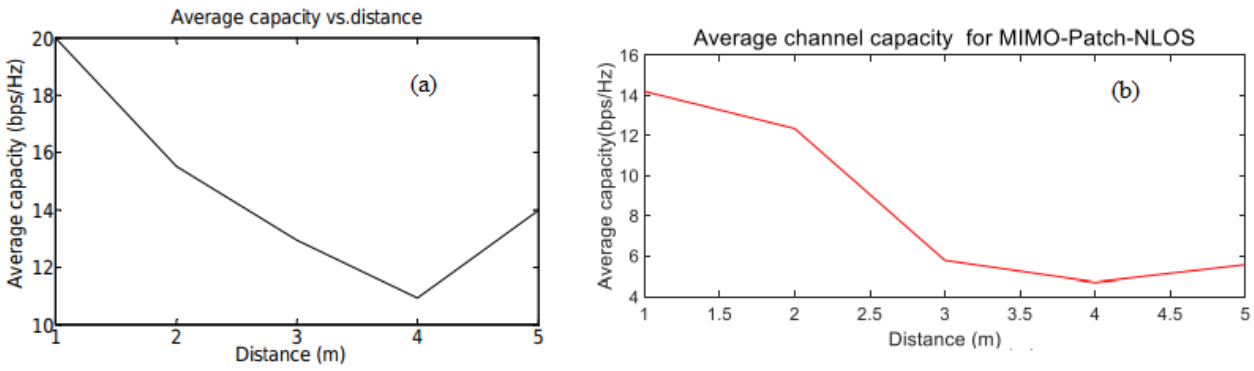

Fig. 8.7. Average capacity at a constant transmit power of the MIMO-p setup for LOS (a) and NLOS (b)

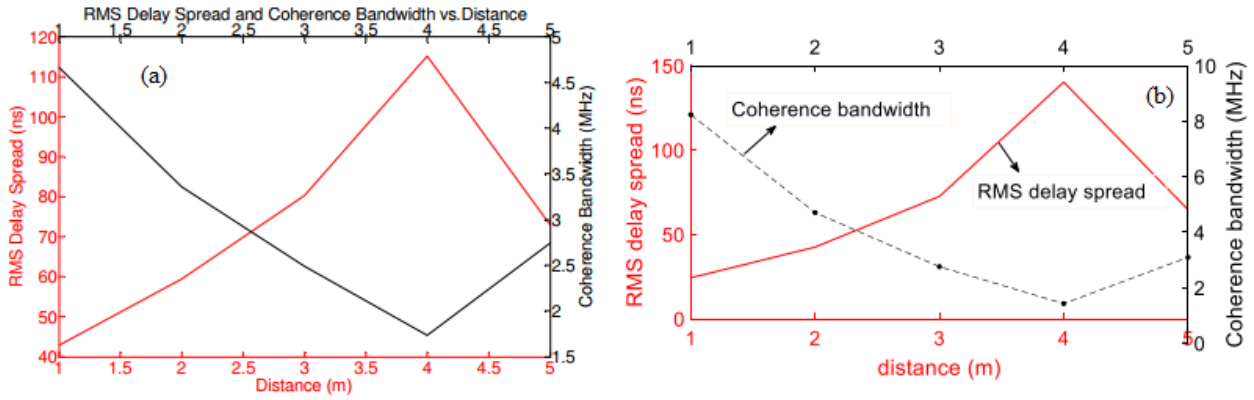

Fig. 8.8. MIMO-p RMS delay spread and coherence bandwidth for LOS (a) and NLOS (b)

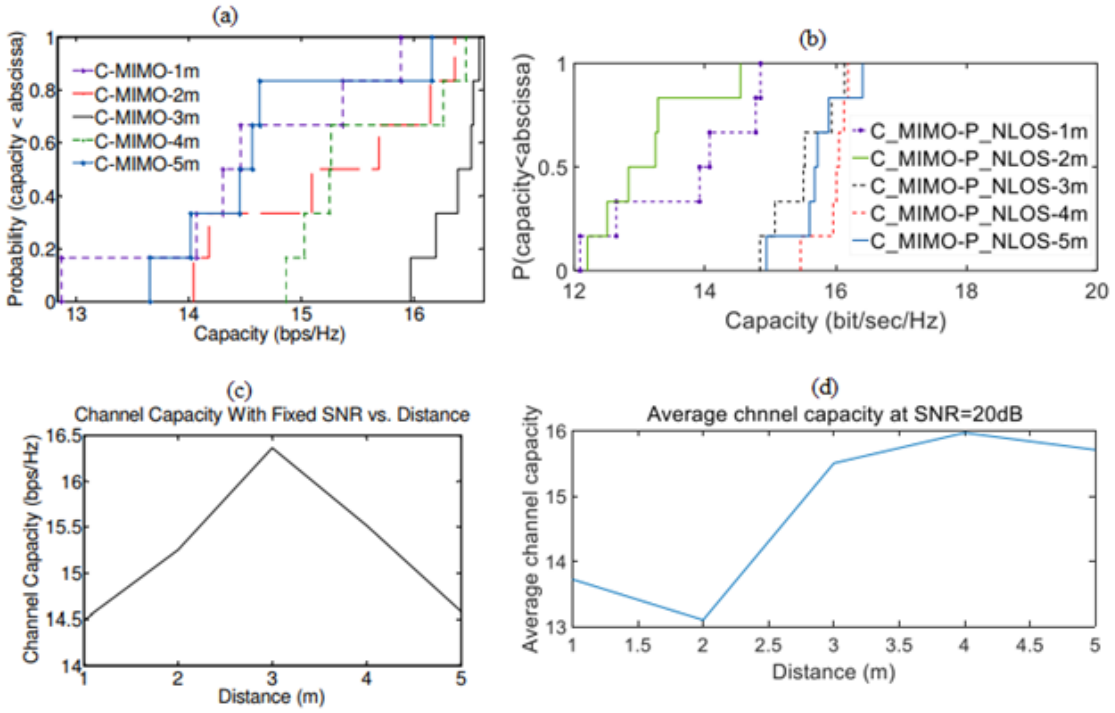

Fig. 8.9. Outage and average capacities at a fixed SNR (20 dB) of the MIMO-p setup for LOS (a, c) and NLOS (b, d)

8.3 UWB measurements results for an off-body channel inside a mine

UWB measurements (from 3.1 to 10.6 GHz) were performed at a 90 m deep mine gallery. The procedure consisted in taking S parameter measurement for 8097 frequency points. 10 snap shots were considered for each of the 10 considered distances. The SISO results were published in [8].

8.3.1 Impulse response and path loss

The channel impulse responses are represented for three distances in Fig. 8.10 for LOS and NLOS configurations.

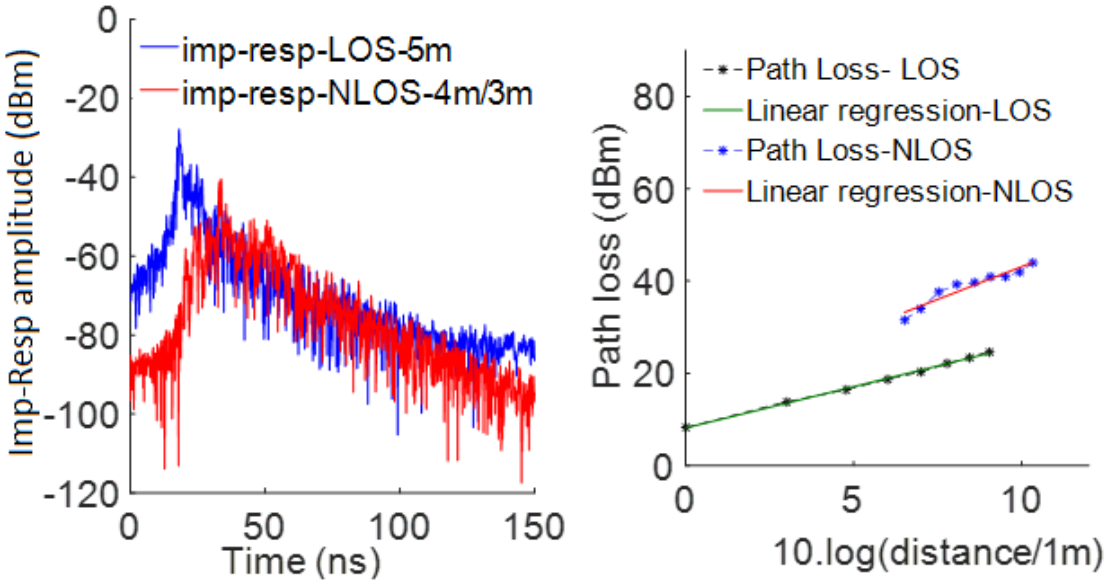

Fig. 8.10. Impulse responses and Path loss results

It is clear from the impulse response results that the NLOS signal suffer from a considerable degradation with regards to the strength of the received signal and the deep fades.

The PL results in Fig. 8.10 exhibit the expected degradation of the NLOS signal compared to the LOS one. As for the rate of this degradation, The PL exponent is determined to be 2.8 at NLOS; expectedly, it is higher than the LOS PL exponent (which is 1.79) and that of the free space.

8.3.2 RMS delay spread

The RMS delay spread was determined using (2.6). The Coherence bandwidth was also calculated (for 50% correlation) as expressed in (2.7).

Results show that RMS delay spread values are between 9.2 ns and 13.5 ns at NLOS, and between 3.2 ns and 5.9 ns at LOS, as illustrated in Figure 8.11. The increase of the RMS delay spread at NLOS is due to the increase in multipath richness. Moreover, due to the narrow UWB impulse response, a better time dispersion is achieved compared to the 2.4 GHz results for both LOS and NLOS.

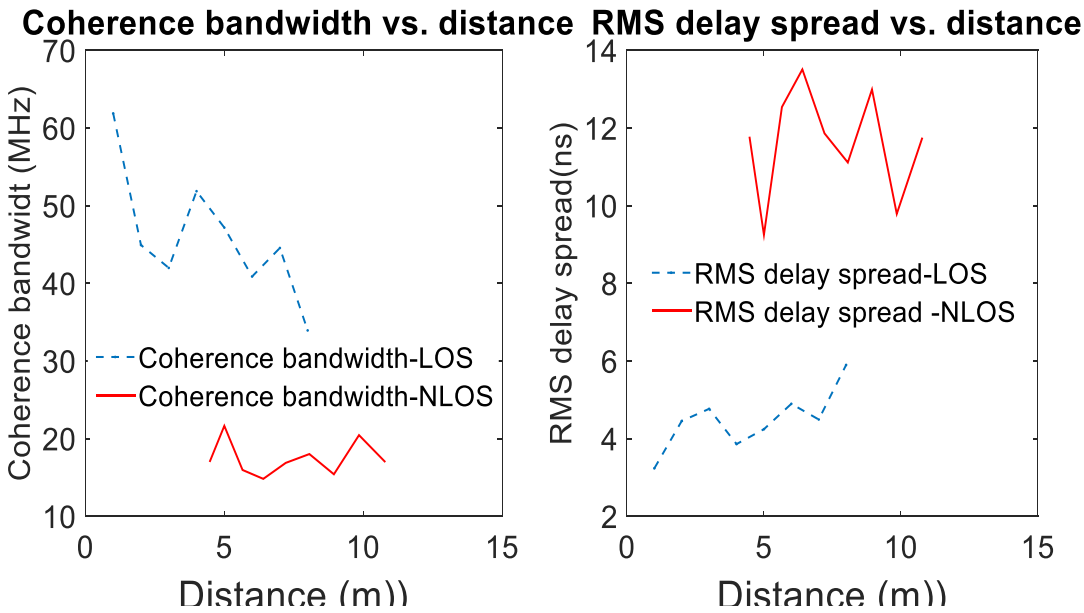

Figure 8.11. RMS delay spread and coherence bandwidth

8.3.3 Channel Capacity

SISO channel capacity (shown in Fig. 8.12) is extracted from measurements using the usual Shannon formula (3.5).

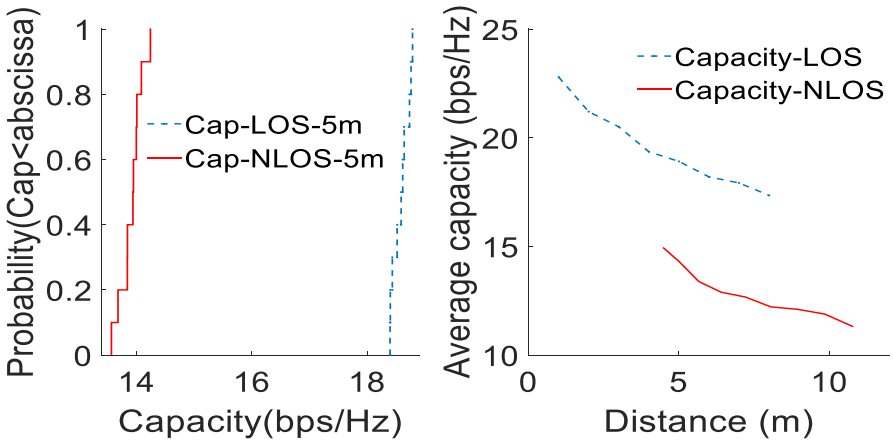

Fig. 8.12. SISO Average channel capacity and capacity CDFs

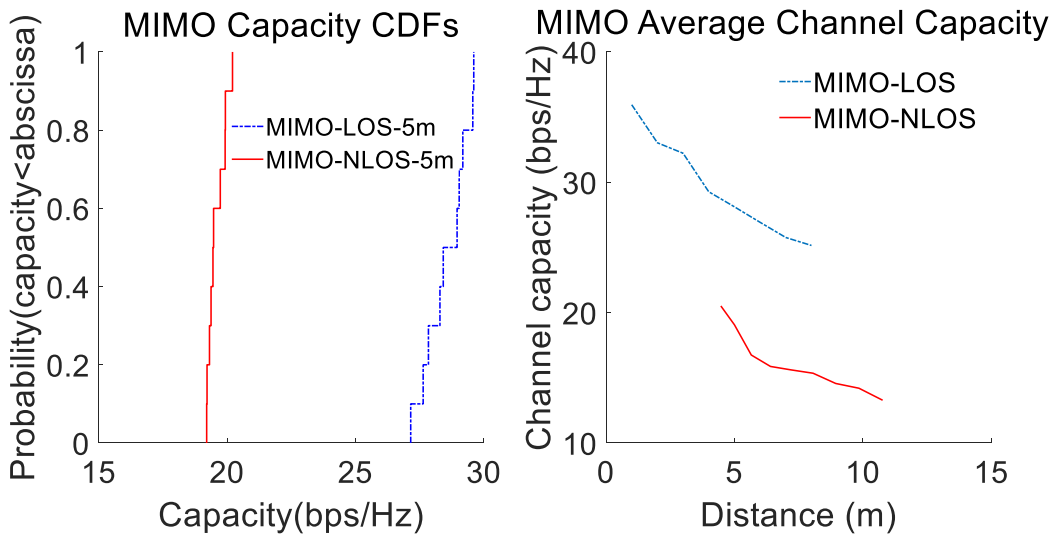

Fig. 8.13. Average channel capacity and capacity CDFs for the MIMO WBAN channel at constant transmitted power

The average capacity and the capacity at a certain probability level decrease with distance. This is due to the fact that the smaller distances correspond to higher received powers and hence a higher SNR. It can be noted that the capacity results are correlated to the PL results. Expectedly, the LOS capacity is higher than that of NLOS due to the higher SNR at LOS.

8.4 References

[1] M.E. El Azhari, M. Nedil, I. Benmabrouk, K. Ghanem, and L. Talbi, "Characterization of an off-body channel at 2.45 GHz in an underground mine environment," Progress In Electromagnetics Research M, Vol. 43, 91-100, 2015.

[2] M.E. El Azhari, M. Nedil, I. Benmabrouk, K. Ghanem, and L. Talbi, “Off-body channel characterization at 2.45 GHz in underground mine environment,” Proc. IEEE Antennas and Propagation Society Int. Symp. (APSURSI), 251–252, Jul. 6–11, 2014.

[3] M. E. Azhari, M. Nedil, I. Ben Mabrouk and L. Talbi, "Multipath effect on off-body channel parametters of a MIMO system using patch antennas inside a mine," 2016 IEEE International Symposium on Antennas and Propagation (APSURSI), Fajardo, 2016, pp. 1693-1694

[4] M. E. Azhari, M. Nedil, I. Ben Mabrouk and L. Talbi, "Path loss effect on off-body channel capacity of a MIMO system using patch antennas inside a mine," 2016 IEEE International Symposium on Antennas and Propagation (APSURSI), Fajardo, 2016, pp. 1697-1698.

[5] M. E. Azhari, L. Talbi, M. Nedil and I. Ben Mabrouk, "NLOS Capacity and Time dispersion of a Multipath Fading MIMO Channel Using Directive Antennas in an Underground WBAN Application" IEEE/APS2017

[6] M. E. Azhari, L. Talbi, M. Nedil and I. Benmabrouk, "Impact of NLOS on the Path Loss and Channel Capacity of a MIMO Off-body System Inside a Mine " IEEE/APS2017

[7] M.E. El Azhari, M. Nedil, I. Benmabrouk, K. Ghanem, and L. Talbi, “Off-body channel characterization at 2.45 GHz in underground mine environment,” Proc. IEEE Antennas and Propagation Society Int. Symp. (APSURSI), 251–252, Jul. 6–11, 2014.

[8] M. E. Azhari, L. TaIbi and M. Nedil, "UWB Off-Body Channel Characterization in a Mine Environment," 2018 IEEE International Symposium on Antennas and Propagation & USNC/URSI National Radio Science Meeting, Boston, MA, 2018, pp. 559-560.

Chapter 9 Discussion and conclusion

9.1 Application based discussion

This thesis is intended to be as a contribution to the design and optimization of in-mine communications destined to prevent the mining accidents and improve rescue operations if a mine accident actually occurs. From an application point of view, wireless body area networks (WBAN) represent an important field for improving the underground mining safety [1]. Vital signs, acceleration and proximity sensors as well as tracking tags (attached to the miners) could be used to improve the miners safety and help coordinate mine rescue efforts following a mining accident [1]. Moreover, collision awareness systems (CAS) involving body-attached tags could help prevent mining accidents, especially in narrow galleries with hidden pathways. A CAS module installed on the mine vehicles would be able to detect nearby miners (and vehicles), estimate their distance and warn both the conductor and incoming miner of a possible danger. While some companies already invested in developing such systems, the lack of telecommunication expertise sometimes

lead to poor technology choices, which compromises performance or significantly increases the equipment cost. This is the core of this PhD thesis.

Our project provides the necessary measurements results for the usual off-body channel (which could correspond to a channel between miners attached tags and a stationary access point) as well a B2B channel (which could correspond to a channel between two miners attached tags). These channels are of great importance to the mining companies which implement tracking and collision awareness systems destined to the safety of their personnel. The on-body reported results provide a reference for on-body system designers, such as those systems intended to monitor the miners vital signs. Channel capacity and other parameters (such as the RMS delay spread and Rican K-factor) are readily derived. Hence, a complete estimation of the underground channel is made available (to designers) for different WBAN schemes and frequency ranges (2.4 GHz and UWB). The published results would enable the design engineers to make important decisions. For instance, the PL graphs would help determine the number of needed access points (that would receive and transmit information from and to different human and vehicle tags). Comparison of MIMO to SISO results allows having a rough idea of weather to use sparsely spaced MIMO transceivers or content of using closely spaced SISO access ones. In fact, from an application point of view, the body worn tags should talk to each other in a peer-to-peer fashion (in order to minimize the cost). If, however, the peer-to-peer communication could not be established, the body worn tags (that are limited in the transmission power) would need to talk to each other via a fixed access point. If the required bit rate is not achieved by a SISO system at a certain distance, this means that using the SISO system will require to also use additional access points to ensure a successful communication at the required bit

rate. Hence, an important consideration (for the design engineer) is to compare the cost increase (of a certain WBAN system) when using MIMO to that of using SISO (with additional fixed access points). Moreover, since a WBAN communication system would also require point-to-point communication to transfer the data to a far away human attached transceiver, a study of such channel was also performed. Polarization and antennas directivity effects on the channel performance were studied and reported (at both LOS and NLOS scenarios).

In this thesis, a model for the B2B channel was presented. The model takes into consideration the complexity of the mine structure and quickly generates the impulse response of the channel, when an estimate of the RMS delay spread of the environment is provided. Since, the values of this parameter are reported in the open literature, the simplicity of this model indeed justify its suitability to the underground channels uses.

To summarize, in WBAN, the aim of the design engineer should be to primarily use peer-to peer communication, and use miner-to-access point communication only when this peer-to-peer one is not possible. Hence, the cost of deploying MIMO access points (that are sparsely spaced in the mine) could be significantly lower than increasing the density of SISO access points. In other words, the cost gain could be due to the reduction in the number of required access points for the case of MIMO deployment. This thesis provides the necessary information to take such design decisions without doing extensive field measurements. This include the PL results (to estimate the signal degradation) and the channel capacities (to estimate the maximum achievable bit rate) which would compare both SISO and MIMO topologies.

9.2 Conclusion

9.2.1 Summary

In this thesis, we presented the results for MIMO-off-body, MIMO-on-body and MIMO-B2B WBAN systems deployed in a mine gallery at the 2.4 GHz and UWB. The on-body results demonstrated the effectiveness of using MIMO systems for on-body applications. This was clearly demonstrated by an improvement in the MIMO channel capacity between 3.1 bps/Hz and 7.6 bps/Hz (corresponding to throughput gain between 1.3 and 1.8). The off-body channel performance was also described through its measurement derived parameters at the 2.4 GHz band. In fact, the advantage of using circular polarization combined with MIMO configurations is clearly demonstrated through comparison with linear systems. When two circular MIMO antennas are deployed at the Tx and Rx ends, the first refection is not suppressed efficiently due to the surface roughness of the mine. Moreover, it is observed that the B2B time dispersion parameters are higher and the capacity is lower than the point-to-point configuration. This is due to the effect of the human body which provides additional paths increasing the multipath richness and degrading the quality of the received signal affected by creeping waves. The UWB signal, due to its narrower impulse response exhibits less MPC and higher channel capacities than the 2.4 GHz signal. The NLOS system was compared to the LOS one, in terms of channel parameters and capacity. The degradation of the signal due to the LOS obstruction was mitigated by the NLOS multipath richness, which helped achieve acceptable channel capacities for the MIMO systems (between 20.5 bps/Hz and 13.3 bps/Hz). The time dispersion, path loss and capacity results demonstrate that the UWB channel is better suited for the in-mine WBAN communications than the 2.4 GHz band at LOS and NLOS

scenarios (due to the higher channel capacities and lower RMS delay spread). With regards to the channel modeling, models of the impulse response were determined through a statistical-empirical approach. The path amplitudes were modeled as an exponentially decaying signal with the channel delay. Additionally, the difference between two successive amplitudes, being random, allow to use a statistical approach to find out which distribution best describes this difference. The distribution of the arrival times steps is compared to the different random distributions from the literature, namely, Poisson, Gaussian, and Weibull. The K -S test was used for each distribution to find out the parameters for the distribution that approaches that of the measurement. In fact, for the B2B measurements, the Poisson distribution offers the best fit for these time steps. By generating a random vector (following the optimal distribution) of these time steps, then adding them to their corresponding arrival times (starting from the known LOS time of arrival) the arrival times vector is generated. The final step consisted in matching the time of arrivals to the path amplitudes to generate the impulse response.

9.2.2 Future work

WBAN technology, for underground applications, is currently a vast research topic. There exist many topic areas, which were not covered by this PhD work. For instance, while the different WBAN scenarios were thoroughly investigated, with different scenarios and antenna characteristics, the important millimetre wave band was not yet examined. Hence, an open problem that future research work needs to consider is the exploration of mm bands such the 60 GHz band, which would allow exploiting a considerably larger bandwidth. Moreover, other diversity schemes (such as time and frequency diversities) should be investigated as a way improve performance. Finally, future work should consider the use

of flexible antennas, which would be more suitable for WBAN systems (such as to incorporate in a mining suit).

Regarding WBAN channel modeling, the future work should improve the existing model to address the NLOS topology. The statistical-empirical model should generate the channel parameters, which then needs to be compared to the ones derived from measurements. Other modeling techniques should be investigated for WBAN application inside the mine. This include the deterministic techniques using the uniform theory of diffraction and approximating the mine walls roughness to some reasonably close geometrical shapes. Image processing techniques could be adopted to study the wall roughness and determine its effect on the propagation characteristics of the WBAN signals.

9.3 References

[1] M. E. ElAzhari, L. Talbi, M. Nedil, “Body- to-Body Channel Characterization and Modeling Inside an Underground Mine”, IEEE *Antennas and Propagation Trans.*, Vol. 68, NO. 6, pp. 4799-4809, June 2020.

Appendix: Stochastic processes

Stochastic processes are generally described either by a probability density function or by a cumulative distribution function. The probability density function, here denoted by $p(x)$ for the variable x, is such that the probability of x taking a value in the infinitesimal interval x to $x+dx$ is $p(x)\,dx$. The cumulative distribution function, denoted by $F(x)$, gives the probability that the variable takes a value less than x. The functions are related as follows:

$$p(x) = \frac{d}{dx}[F(x)] \tag{A.1}$$

or:

$$F(x) = \int_c^x p(t)\,dt \tag{A.2}$$

Where c is the lowest limit of the values which t can take.

The following distributions are the most important:

– Normal or Gaussian distribution,

– Log-normal distribution,

– Rayleigh distribution,

– Rice distribution,

– Nakagami distribution,

Below are explanations of these widely used distributions.

Rayleigh distribution

A well accepted model for rapid fluctuations in the amplitude (small scale fading) in the absence of a strong received multipath component is the Rayleigh fading model [1] characterized by:

$$f(x) = \frac{x}{\sigma^2}\exp(-\frac{x^2}{2\sigma^2}),\ \sigma > 0, x > 0, \quad \text{(A.3)}$$

$$F(x) = 1 - \exp\left(-\frac{x^2}{2\sigma^2}\right), \quad \text{(A.4)}$$

$$E[x] = \sigma\sqrt{\frac{\pi}{2}}, \quad \text{(A.5)}$$

$$Var[x] = \frac{(2-\pi/2)}{\sigma^2}, \quad \text{(A.6)}$$

$$\sigma = \frac{m_1}{\sqrt{\pi/2}}. \quad \text{(A.7)}$$

Conveniently, its unique σ parameter only requires knowing the first moment to be estimated. The Rayleigh distribution is widely used to describe the multipath fading given its elegant theoretical explanation and occasional empirical justification. [2]

Rice distribution

This distribution may be used when a strong multipath exist along with scattered components (having considerably lower power values). This dominant component can be a direct line of sight (LOS) component or a component that has undergone a considerably

lower attenuation compared to the other multipath components [2], [3]. The Rice distribution is defined by [4-6]:

$$f(x) = \frac{x}{\sigma^2}\exp\left(-\frac{(x^2+\sigma^2)}{2\sigma^2}\right) I_0(\frac{xv}{\sigma^2}), x > 0, \quad \text{(A.8)}$$

$$F(x) = 1 - \mathrm{Q}_1\left(\frac{v}{\sigma}, \frac{x}{\sigma}\right), \quad \text{(A.9)}$$

$$E[x] = \frac{\sqrt{\frac{1}{2}}\sigma^2 L_{\frac{1}{2}}(-\frac{v^2}{2\sigma^2})}{|\sigma|}, \quad \text{(A.10)}$$

$$Var[x] = v^2 + 2\sigma^2 - \frac{0.5\sigma^4 L_{\frac{1}{2}}^2(-\frac{v^2}{2\sigma^2})}{|\sigma|^2}, \quad \text{(A.11)}$$

$$v = \sqrt{\frac{Km_2}{K+1}}, \quad \text{(A.12)}$$

$$\sigma = \sqrt{\frac{m_2}{2(K+1)}}, \quad \text{(A.13)}$$

Where

$Q1\ (x,y)$ is the Marcum-Q function;

$L_n(x)$ is the Laguerre function satisfying the following equation:

$$\mathrm{x}\frac{\mathrm{d}^2\mathrm{y}}{\mathrm{dx}^2} + (1-\mathrm{x})\frac{\mathrm{dy}}{\mathrm{dx}} + \mathrm{ny} = 0 \quad \text{(A.14)}$$

$\mathrm{I_n(x)}$ is the modified Bessel function of order n of the first kind;

K is a parameter serving to estimate the parameters v and σ using a table established from the following equation:

$$\frac{m_1}{\sqrt{m_2}} = \frac{\sqrt{\pi}}{2\sqrt{K+1}}\exp\left(-\frac{K}{2}\right)\left[(K+1)I_0\left(\frac{K}{2}\right) + KI_1(K/2)\right] \quad \text{(A.15)}$$

Nakagami distribution

The Nakagami distribution has two parameters: a shape parameter m and a second parameter controlling spread, Ω. This distribution is a general distributionfading being reduced to a Rayleigh distribution when m = 1 and to a unilateral Gaussian distribution for m = 1/2. It also approximates with a high precision, the Rice distribution, and approaches the Log-normal distribution under certain conditions [2]. It is defined as [7], [8]:

$$f(x) = \frac{2m^m x^{2m-1}}{\Gamma(m)\Omega^m}\exp\left(-\frac{mx^2}{\Omega}\right), m = \frac{\{E[x^2]\}^2}{Var[x^2]} \geq \frac{1}{2}, x > 0, \quad \text{(A.16)}$$

$$F(x) = P(m, \frac{m}{\Omega}x^2), \quad \text{(A.17)}$$

$$E[x] = \frac{\Gamma(m+1/2)}{\Gamma(m)}\sqrt{\frac{\Omega}{m}} \quad \text{(A.18)}$$

$$Var[x] = \Omega(\,1 - \frac{1}{m}(\frac{\Gamma(m+1/2)}{\Gamma(m)})^2), \quad \text{(A.19)}$$

$$\Omega = m_2, \quad \text{(A.20)}$$

$$\frac{m_2}{{m_1}^2} = \frac{m\Gamma(m)^2}{\Gamma(m+1/2)^2} \quad \text{(A.21)}$$

Where m is the Nakagami parameter, m_1 and m_2 are the first and the second moments, Γ(*x*) is the gamma function, and *P*(*x*, *y*) is the incomplete gamma function.

Weibull distribution

Several studies have demonstrated that this distribution may provide good modeling performance [2]. This distribution could be used to model the times of arrival of the different paths within the impulse responses. The Weibull distribution is defined as [9]:

$$f(x) = abx^{b-1}\exp(-ax^b),\ a>0\ ,\ b>0\ ,\ x\geq 0\ , \tag{A.22}$$

$$F(x) = 1-\exp(-ax^b), \tag{A.23}$$

$$E[x] = (a^{-1/b}).\Gamma(1+1/b), \tag{A.24}$$

$$Var[x] = (a^{-1/b})^2[\ \Gamma(1+2/b)-\Gamma^2(1+1/b)], \tag{A.25}$$

$$\sqrt{\frac{m_2-m_1^2}{m_1^2}} = \frac{\sqrt{\Gamma\left(1+\frac{2}{b}\right)-\Gamma^2(1+1/b)}}{\Gamma\left(1+\frac{1}{b}\right)} \tag{A.26}$$

B is found using a table based on the following equality:

$$a = \{m_1/\Gamma(1+1/b)\}^{-b} \tag{A.27}$$

The Weibull distribution is reduced to a Rayleigh distribution for b=1/2 and reduces to an exponential distribution for b=1.

Gaussian or normal distribution

This distribution is applied to a continuous variable of any sign. The probability density, having a mean μ and the standard deviation σ, f(x) is written in the usual way:

$$f(x) = \frac{1}{\sigma\sqrt{2\pi}}exp\left[-\frac{1}{2}\left(\frac{x-\mu}{\sigma}\right)^2\right] \tag{A.28}$$

The cumulative distribution function is:

$$F(x) = \frac{1}{\sigma\sqrt{2\pi}} t \int_{-\infty}^{x} exp\left[-\frac{1}{2}\left(\frac{t-\mu}{\sigma}\right)^2\right] dt = \frac{1}{2}\left[1 + \text{erf}\left(\frac{x-\mu}{\sigma\sqrt{2}}\right)\right] \quad \text{(A.29)}$$

with:

$$erf(z) = \frac{2}{\sqrt{\pi}} \int_0^z e^{-t^2} dt \quad \text{(A.30)}$$

Lognormal distribution

The Lognormal distribution is the distribution of a positive variable whose logarithm has a Gaussian distribution. It has often been used to explain large-scale variations of the amplitudes of a signal in a multipath fading environment [2]. It is defined by [10]:

$$f(x) = \frac{1}{\sigma\sqrt{2\pi}} \frac{1}{x} exp\left[-\frac{1}{2}\left(\frac{ln\, x-\mu}{\sigma}\right)^2\right] \quad \text{(A.31)}$$

$$F(x) = \frac{1}{\sigma\sqrt{2\pi}} \int_0^x \frac{1}{t} exp\left[-\frac{1}{2}\left(\frac{ln\, t-\mu}{\sigma}\right)^2\right] dt = \frac{1}{2}\left[1 + \text{erf}\left(\frac{ln\, x-\mu}{\sigma\sqrt{2}}\right)\right] \quad \text{(A.32)}$$

Where erf(x) is the error function. In these relations μ and σ are the mean and the standard deviation not of the variable x but of the logarithm of this variable. The characteristic quantities of the variable x can be derived without difficulty. We find:

– most probable value: $\exp(\mu - \sigma^2)$ (A.33)

– median value: $\exp(\mu)$ (A.34)

– mean value: $exp\left(\mu + \frac{\sigma^2}{2}\right)$ (A.35)

– root mean square value: $exp(\mu + \sigma^2)$ (A.36)

– standard deviation: $exp\left(\mu + \frac{\sigma^2}{2}\right)\sqrt{exp(\sigma^2) - 1}$ (A.37)

– $\sigma = \sqrt{\ln(\frac{m_2}{m_1})}$ (A.38)

– $\mu = \ln(m_1) - \frac{1}{2}\ln(\frac{m_2}{m_1})$ (A.39)

where m_1 and m_2 are the first and second moments.

Unlike the Gaussian distribution, a log-normal distribution is extremely asymmetrical. In particular, the mean value, the median value and the most probable value (often called the mode) are not identical.

References

[1] Boutin, M.; Benzakour, A.; Despins, C.L.; Affes, S., "Radio Wave Characterization and Modeling in Underground Mine Tunnels," in Antennas and Propagation, IEEE Transactions on , vol.56, no.2, pp.540-549, Feb. 2008

[2] Rappaport T. S. et Seidel S. Y. "Multipath propagation models for in-building communications". Mobile Radio and Personal Communications, 1989, Fifth International Conference on, (11-14 December), pp. 69-74. 1989.

[3] Rayleigh L. "On the resultant of a large number of vibrations of the same pitch and of arbitrary phases". Phil. Mag., vol. 10, pp. 73-78, et vol. 27, pp. 460-469 (June). 1889.

[4] Rice S. O. "Mathematical analysis of random noise". Bell syst. Tech. J., vol. 23, pp. 282-332, 1944, et vol. 24, pp. 46-156, 1954.

[5] Abdi A., Tepedelenioglu C., Kaveh M. etGiannakis G. "On the estimation of the K parameter for the rice fading distribution". Communications Letters, IEEE, vol. 5, no. 3 (march), pp. 92-94. 2001.

[6] Dong Xiaofei, Beaulieu N. C. "Average level crossing rate and average fade duration of selection diversity". Communications Letters, IEEE, vol. 5, no. 10 (octobre), pp. 396-398. 2001

[7] Proakis J. G. Digital Communications. McGraw-Hill Series in Electrical Engineering. McGraw-Hill Book Company, second edition. 1989.

[8] Nakagami M. The m-distribution-A general formula of intensity distribution of rapid fading. In Statistical Methods of Radio Wave Propagation. Pergammon Press. 1960.

[9] Flannery B. P., Teukolsky S. A. etVetterling W. T. Numerical Recipies in Pascal. W. H. Press, Cambridge University Press, Cambridge. 1989.

[10] Engelhardt M. "On simple estimation of the parameters of the Weibull or extreme-value distribution". Technometrics, vol. 17, no. 3 (août). 1975.